ETIOLOGY OF PERCEIVED STRENGTH CHANGES IN THE MUSCLES OF THE LEGS FOLLOWING LOCOMOTION UNDER SIMULATED LOW GRAVITY

by

Karl Ulrich Schultz
Ensign, United States Navy

SUBMITTED TO THE DEPARTMENT OF AERONAUTICS AND ASTRONAUTICS IN PARTIAL FULFILLMENT OF THE REQUIREMENTS FOR THE DEGREE OF

MASTER OF SCIENCE

at the

MASSACHUSETTS INSTITUTE OF TECHNOLOGY

June 1995

Signature of Author_____
Department of Aeronautics and Astronautics
May 22, 1995

Certified by _____
Professor Dava J. Newman
Thesis Supervisor

Accepted by_____
Professor Harold Y. Wachman
Chairman, Department Graduate Committee

ABSTRACT

This thesis investigates changes in human leg muscles following exposure to simulated Martian and lunar gravity, specifically, the hypothesis that muscular gains are lowered during reduced gravity exposure and a period of readaptation is necessary upon return to a 1 g environment. Three research aspects are included in this thesis: gait analysis, energetics, and posturography. This thesis also presents an analytical model of posture using modern control theory techniques. The model attempts to replicate the changes observed, thus providing some analytical insight into the underlying causes of post-exposure changes. The gait analysis measurements include ground reaction forces in all three axes during walking as well as joint positions via video. Experimental results show that peak forces increase following brief exposure to simulated low gravity ($p<0.02$). Contact time is slightly shortened after exposure. No changes were noted in joint angles or limb positions while walking. Results of the energetics experiment reveal that oxygen consumption decreases significantly in Martian and lunar gravity levels and that for gravity levels below 0.3 g, running is a more efficient means of locomotion than walking ($p<0.05$). The trajectory of the center of pressure (CoP) was measured for the posturography protocol. These data were analyzed spatially and temporally. Spatial variables include the root mean square (rms) position of the CoP in the x and y axes. Temporal analysis yields the diffusion coefficient measuring stochastic activity, and the correlation coefficient measuring trends in the trajectory of the center of pressure. Results of the posture study show that rms values increase significantly ($p<0.01$) in both axes following simulated reduced gravity exposure. Temporal analysis reveals that human posture can be divided into a short term and a long term period. The short term exhibits higher stochastic activity and persistent trends, while the long term period shows relatively low stochastic activity and anti-persistent trends. The estimator based model succeeds in replicating temporal characteristics of human posture and spatial characteristics by lowering the variable muscle gain in the model, validating the theory that muscular gains are lowered during low gravity exposure.

Thesis Advisor: Dr. Dava J. Newman

Title: C.S. Draper Assistant Professor of Aeronautics and Astronautics

Acknowledgments

I would like to start by apologizing to anyone who is reading this in hopes that it will be funny or even clever. It is now 1:30 on May 22 (The due date) and I'm not done. My original desire to amuse the reader has now been replaced by a panicked desire to finish. Also, my page numbers are already figured out so there is no way this stuff goes over 1 page. With that said, on with the acknowledgments.

First of all, I would like to list the people who I'm not thanking. The guy who stole my credit cards is absolutely not getting thanked. And if you're reading this, you'd better not take this copy of my thesis. Whoever bought that really uncomfortable couch in the lab that I've been sleeping on for a week is not getting thanked, except maybe by my chiropractor. I would also not like to thank Major League Baseball Player's Association representative Donald Fehr. Thanks for ruining my last full season of Boston Baseball, JERK. Finally, I would not like to thank John Denver. No reason really, I just don't like him.

My first real thank you has to go to Jen. If theses had co-authors, your name would definitely be on the cover of this thing. Thanks for all the help over the last few months. I don't think I can tell you enough how much I appreciated it. By the way, if you show me one more crossword puzzle, I'll kill you.

Big, huge, gigantic, steroid-enhanced thanks to Prof. Dava (not Dave) Newman whose support and Bar-B-Q helped me to finish this masterpiece. Not many people could have helped me put this thing together as quickly as you did. Thanks (Hi Gui) :)

To my Mom, and Dad, and the rest of my family your ghost son/brother says 'thanks'. Sorry I haven't had more time to spend at home. Love ya.

Thanks to the Hertz Fellowship people who were nice enough to pay my bills for the last two years.

I'd like to thank CDR Angus Rupert for presenting me with a thesis topic, almost. Oh well, everything worked out.

To Rob and Jason, my understanding roommates: If you think I made a lot of noise before, wait 'til I get this thing signed. It's been a great 2 years. I couldn't have asked for better roommates. Thanks.

To Grant 'U-boat', Keoki, and Dave, my lifting, drinking, spring break, scamming partners. Boston wouldn't have been the same without you. Neither would Newport, or Key West, or Houston, or New Orleans, 'the Happiest Place On Earth', or Preakness. Come to think of it, this whole 2 years would have sucked. Thanks. Hopefully the beginning of my Navy life isn't the end of my Boston life. (Huh-Huh Shut up, Dumas)

To Deb and Andrea, the other two angels. Your help was much more appreciated than you know. Good luck and take care.

To all of the co-dependent borderline psychotic women who I was unfortunate enough to date during the past two years and did their best to make my life in Boston a living hell, 'Hello!'. (By the way, if any of you are reading this, I'm talking about everyone else, not you. XOXOXO).

To "Daisy Buchannan's": if I had spent half as much time on this thesis as I have there, this would be a Ph.D thesis.

I'd like to thanks Calvin Klein underwear model Christy Turlington just for being her. I'd like to thank Steve Jobs for inventing this computer and Bill Gates for writing this program. I'd like to thank Pete the Pete's wicked ale guy and Jim Cook, the boring guy on the Sam Adams commercials. I'd like to thank his holiness Pope John Paul for his divine intervention in helping me complete this thesis. My final thanks goes to the U.S. Navy who bought that story about me coming to Boston to go to school. I guess what they don't know won't hurt em.

To everyone who helped me during my two years here at the MIT. Thanks Peace and I'm outta here!!!!

ETIOLOGY OF PERCEIVED STRENGTH CHANGES IN THE MUSCLES OF THE LEGS FOLLOWING LOCOMOTION UNDER SIMULATED LOW GRAVITY

TABLE OF CONTENTS

ABSTRACT 2
ACKNOWLEDGMENTS 3
TABLE OF CONTENTS 4
LIST OF FIGURES 6
LIST OF TABLES 8

Chapter 1 Introduction 9

1.1 Motivation 10
1.2 Contribution 12
1.3 Hypotheses / Objectives 13
1.4 Thesis Outline 14
1.5 Conventions 16
1.5.1 Verbal Conventions 16
1.5.2 Axes Definition Conventions 18

Chapter 2 Background 20

2.1 Muscles and Reflexes 20
2.1.1 General Muscle Characteristics 20
2.1.2 Muscle Proprioceptors 21
2.1.3 Neurons 22
2.1.4 Stretch Reflex 22
2.1.5 Hill Muscle Model 24
2.2 Locomotion 26
2.2.1 Anatomy of a Step 26
2.2.2 Difference Between Walking and Running 33
2.2.3 Inverted Pendulum Model for Walking 35
2.2.5 Reduced Gravity Locomotion 36
2.3 Energetics and Workload 37
2.3.1 Energetics 37
2.3.2 Reduced Gravity Energetics 39
2.3.3 Workload Measurements 40
2.4 Estimator Based Model of Posture 40

Chapter 3 Partial Gravity Simulation Techniques 50

3.1 Parabolic Flight 50
3.2 Water Immersion 52
3.3 Suspension Systems 53
3.3.1 Overhead Suspension Systems with Counterweights 53
3.3.2 Body Inclination Systems 54
3.3.3 Overhead Suspension Systems with Springs 54

Chapter 4 Methods 57

4.1 Subjects 57
4.2 Equipment 58
4.2.1 Reduced Gravity Simulator 59
4.2.2 Treadmill 59
4.2.3 Force Platform and Amplifier/Conditioner 62
4.2.4 Accelerometer/Reflex Hammer 63
4.2.5 EMG 63
4.2.6 Video System 65
4.2.7 Metabolic Measurement System 65
4.3 Experimental Protocol 66
4.3.1 Metabolic Experiment 66
4.3.2 Musculoskeletal Experiments 67
4.4 Data Analysis 69
4.4.1 Metabolic Data Analysis 69
4.4.2 Reflex Latency Analysis 70
4.4.3 Posturography Analysis 72
4.4.4 Gait Analysis 77

Chapter 5 Results and Discussion 80

5.1 Results 80
5.1.1 Metabolic Analysis 80
5.1.2 Gait Analysis 86
5.1.3 Posture 97
5.1.3a Subject Posture Data 97
5.1.3b Model Posture Data 103
5.2 Discussion 106
5.2.1 Limitation of Experimental Design 106
5.2.2 Workload 106
5.2.3 Gait and Stretch Reflex 107
5.2.4 Posture Data 107

Chapter 6 Summary and Conclusion 111

References 115
APPENDIX A OPTIMAL CONTROL BACKGROUND 119
APPENDIX B EXPERIMENTAL SUBJECT CONSENT FORM 121
APPENDIX C LABVIEW™ SCRIPTS 125
HammerAccel.vi 126
Forceplate.vi 128
Posture.vi 131
Write To Spreadsheet File.vi 134
APPENDIX D MATLAB™ SCRIPTS 136
REFLEX_ANALYZE.M 137
POSTURE_ANALYZE.M 139
POSTURE_ANALYZE_STEP2.M 141
FORCEPLATE_ANALYSIS.M 144
VIDEO_SCALE.M 148
CARTTOPOLAR.M 152
POLARTOCART.M 152
MUSCLE_PENDULUM_MODEL.M 153
APPENDIX E POSTUROGRAPHY COEFFICIENT DATA SUMMARY 158

LIST OF FIGURES

Chapter One

Figure 1.1 Body Centered Directional Conventions 18

Chapter Two

Figure 2.1 Muscle Spindle Structure 23
Figure 2.2 Stretch Reflex 23
Figure 2.3 A.V. Hill Muscle Model 25
Figure 2.4 Compass Gait 28
Figure 2.5 Pelvic Rotation 28
Figure 2.6 Pelvic Tilt 29
Figure 2.7 Stance Knee Flexion 30
Figure 2.8 Plantar Flexion 30
Figure 2.9 Lateral Shift of Pelvis 32
Figure 2.10 Lateral Displacement of Pelvis 32
Figure 2.11 Potential and Kinetic Energy of Walking 34
Figure 2.12 Three Dimensional Model of Posture 42
Figure 2.13 Model Plant State Space Block Diagram 46
Figure 2.14 Reflex Feedback Block Diagram 46
Figure 2.15 Estimator Model Block Diagram 47
Figure 2.16 Complete Posture Model Block Diagram 49

Chapter Three

Figure 3.1 KC-135 in parabolic flight 51
Figure 3.2 Water Environment Training Facility (WETF) 51
Figure 3.3 Overhead Suspension System 55
Figure 3.4 Inclined Suspension System 55

Chapter Four

Figure 4.1 Partial g Simulator and Treadmill 61
Figure 4.2 Experiment Hardware 64
Figure 4.3 Reflex Latency Analysis 71
Figure 4.4 CoP Time Course Plot 73
Figure 4.5 Temporal Analysis Technique 75
Figure 4.6 Stabilogram Diffusion Plot 76
Figure 4.7 Determination of Landmark Positions 79
Figure 4.8 Definition of Angles Measured 79

Chapter Five

Figure 5.1 Metabolic Cost versus Gravity Level 82
Figure 5.2 Cost of Transport versus Gravity Level 82
Figure 5.3 CoT versus Gravity Level - All Subjects 84
Figure 5.4 Stretch Reflex Latency Results 87
Figure 5.5 Ground Reaction Forces Description 89
Figure 5.6 Ground Reaction Force Comparisons 89
Figure 5.7 Maximum Normal Forces versus Condition 91

Figure 5.8 Maximum Total Forces versus Condition 91
Figure 5.9 Maximum and Minimum Antereoposterior Forces 91
Figure 5.10 Maximum Shear Forces versus Condition 91
Figure 5.11 Contact Time versus Condition 92
Figure 5.12 Time to Peak versus Condition 92
Figure 5.13 Video Data o f a Single Step 94
Figure 5.14 Comparison of Video Variables 95
Figure 5.15 Synchronized Video and Forceplate Data 96
Figure 5.16 Center of Pressure Trace Comparison Subject J 98
Figure 5.18 X Axis Root Mean Square versus Condition 99
Figure 5.19 Y Axis Root Mean Square versus Condition 99
Figure 5.20 Diffusion Stabilogram Plot-Subject J 101
Figure 5.21 Diffusion Coefficient versus Condition 101
Figure 5.22 Correlation Coefficient versus Condition 101
Figure 5.23 Critical Distance versus Critical Time 102
Figure 5.24 Center of Pressure Trace Comparison - Model 104
Figure 5.25 Diffusion Stabilogram Plot - Model 105
Figure 5.26 Temporal Variable Comparison - Model versus Subjects 105
Figure 5.27 Complete Model of Posture with Activation Gain 110

LIST OF TABLES

Chapter Two

Table 2.1 Block Diagram Legend 46

Chapter Four

Table 4.1 Subject Database-Metabolic Experiment 58
Table 4.2 Subject Database-Musculoskeletal Experiment 58
Table 4.3 Post Exposure Exercise Order 68

Appendix E

Table E1 Short Term Diffusion Coefficients 159
Table E2 Long Term Diffusion Coefficients 159
Table E3 Short Term Correlation Coefficients 160
Table E4 Long Term Correlation Coefficients 160

Chapter 1 Introduction

The scientific study of walking and running began over a century ago when Eadward Muybridge placed several cameras in series in order to determine whether or not all four feet of a galloping horse were off of the ground at the same time. Since that time, the study of locomotion has advanced human understanding of the way animals, including humans, are able to move about. The vast majority of locomotion studies have investigated gait in the normal 1 g Earth environment (one times Earth gravity, or $9.8 m/s^2$). This is not surprising since, until 30 years ago, locomotion by any animal had never taken place in a non-1 g environment.

The Apollo missions to the moon placed man in an entirely novel environment. The lunar surface not only possesses different atmospheric properties, but also provides only one sixth the gravity (1/6 g) present on Earth. Astronauts were forced to adopt new, unfamiliar gaits which were not used on Earth. Two legged jumping and loping, which is similar to one legged hopping, became the easiest ways for the astronauts to move around. Locomotion on the moon was strikingly different than on Earth.

A future mission to Mars will present similar problems upon reaching the planet's surface. However, such a mission would be additionally confounded by degradation in human performance following extended absence of gravitational stimulus. The trip to the moon took only a few days, but the trip to Mars is expected to take nearly a year, during which time the astronauts will suffer all of the deleterious effects of micro gravity including bone loss, muscle atrophy, and blood volume decrease. Add to this the difficulty involved with walking in a unique environment and the mission success may be questioned. Before attempting another planetary mission, the changes that take place in gait must be more fully understood.

Recent experiments have attempted to identify changes that occur during and immediately following exposure to reduced gravity environments. These experiments have noted many interesting changes concerning low g locomotion including the reduction of energy consumption, change in the speed at which people stop walking and begin running, and the changes in strategies of locomotion in low g, but despite these findings, many questions still linger. What underlying characteristics are causing the observed changes? What is the time course of these changes? Can countermeasures be

developed to exacerbate the presence of these changes? This thesis provides possible answers to some of these questions.

The experiments detailed in this thesis are targeted at exploring the existence of a 'heavy legs' syndrome. Heavy legs has been reported by numerous participants in low g locomotion studies. Subjects reported that their legs felt weaker than normal, but that this sensation eventually went away after returning to 1 g. It is theorized that the sensation experienced is caused by reduced muscle gains in the muscles of the legs which, in turn, cause decreased activation levels in the muscles. Lower than normal reaction forces when running or walking in reduced gravity convince the central nervous system (CNS) that lower muscular activation levels are needed for normal locomotion and, as a result, the gains in the legs are reduced. Immediately upon return to the normal 1 g environment, the lowered gains are poorly suited for locomotion, producing the 'heavy legs' sensation.

Changes in locomotion after partial gravity simulation are investigated through video and ground reaction force analysis of gait. Such analysis reveals changes in the forces exerted as well as changes in walking strategies, such as increased leg compliance, or variation in touch-down or take-off angles. The changes could verify the 'heavy legs' theory and allow more effective countermeasures to be developed

Postural stability changes have been witnessed following prolonged exposure to micro gravity. These changes are investigated in this study by observing changes in the spatial and temporal (time domain) characteristics of standing. Also, this thesis presents a model of posture using modern control theory techniques. The model attempts to replicate the changes observed, thus providing some analytical insight into the underlying causes of post-exposure changes.

1.1 Motivation

There exist several reasons for conducting this experiment. The first is to identify the neuromuscular changes that take place during acute exposure to hypogravity. A related goal is to characterize the transient behavior of the changes upon return to a normal 1 g environment. A third goal is to develop and evaluate effective aids in accelerating neuromuscular recovery in a 1 g environment. An incidental benefit of this research

effort is that it provides energetics and workload data in reduced gravity, enhancing the currently limited partial gravity database.

The utility of this research is most clearly realized in the context of a lunar or Martian mission. By better understanding how the central nervous system adapts to reduced gravity environments, a safer, and more realistic mission can be planned, thus dramatically increasing the possibility for a successful mission. Also, the countermeasures developed in this research could accelerate full recovery once terrestrial operations have begun.

The role of gravity on human locomotion is still a relatively poorly understood phenomenon. Although the presence of gravity's effect on human gait is undeniable, exactly how that effect is realized is still largely debated. Understandably, the bulk of information about human locomotion has been gathered from 1 g studies. This fact makes sense since most humans spend their entire lives on Earth. However, a great deal can be learned through the analysis of gait across the spectrum of gravity level. Given the possibility of another lunar mission, and eventually a Martian mission, the need for partial gravity locomotion research becomes even more evident.

Changes in gravity level also change the energy required for normal activities. In reduced gravity simulations, increases have been noted in activities that require upper body effort [Prescott, 1966]. The increase in cost is attributed to decrease in traction [Wortz, 1969]. In a partial g environment, the reaction forces produced during running and walking are lowered proportionally to the g-level. As a result of the reduction in forces, less energy is required to produce motion [Hewes, 1969], [Sanborn, 1967], [Robertson, 1968], [Newman, 1992], and [Farley, 1992]. On Earth, walking is roughly twice as efficient as running. As gravity is reduced, this difference becomes less pronounced. At low enough gravity levels (below 0.5 g's) running becomes more efficient than walking. The data gathered during this experiment attempts to verify the earlier findings of Hewes, Sanborn, Robertson, Newman and Farley and, at the same time, demonstrate the validity of the reduced gravity simulator.

Short and long range exposure to reduced gravity environments produces numerous negative effects on the human body. Loss of muscle mass, size and strength all occurs in low gravity environments. Such loss produces changes in gait strategy. Touchdown angle, or the angle of the leg when the heel strikes the ground, is slightly reduced in

partial gravity, creating the appearance of a more upright step [Margaria, 1964]. The vertical stiffness of the leg increases in reduced gravity. This means that the leg flexes less with similar applied loads [McMahon, 1990]. Postural stability is diminished upon return from space. Many astronauts report sensations of swaying, dizziness, and even complete inability to stand up [Paloski, 1993]. Muscular changes, along with vestibular changes and orthostatic intolerance, are a major cause of the change in postural performance.

This experiment attempts to determine how gravity affects the gait of humans, specifically, how the central nervous system adapts to changes in the gravity vector and how quickly this adaptation occurs. By isolating the effect of muscle activation levels, muscle strength, and reflexive properties of muscles, the central nervous system changes that occur in the new environment can be better understood. Through understanding of the changes that occur and the time course of those changes, deterioration of human performance following reduced gravity exposure can be predicted allowing better and safer mission planning.

1.2 Contribution

The purpose of this research is to study the effects of brief exposure to low gravity locomotion on lower leg musculature. To that end, a great deal of energy went into the development of a partial gravity simulator. The suspension harness constructed for this experiment is similar to the apparatus used at the Harvard Field Station [Farley, 1992], [He, 1991]. The harness provides a constant unloading force, and with the addition of a treadmill, allows locomotion to be simulated at any gravity level between 0.1 and 1.0 times normal Earth gravity.

The section describing metabolic measurement is a continuation of earlier work by Newman and Farley [Newman, 1993], [Farley, 1992]. This thesis will provide additional energy consumption data and verify the harness as a viable simulation technique. By measuring energy consumption at various speeds and across the g-level spectrum, a clearer picture of the relationship between gravity level and energy consumption can be attained.

The musculoskeletal experiments conducted reveal changes in human gait strategies and performance following exposure to reduced gravity. By recording force traces and video

position data, dynamic and kinematic characteristics of walking can be determined. Any changes in gait appearance or reaction forces could reveal altered walking control strategies or differences in leg muscle performance following partial g locomotion.

The primary contribution of this thesis is the development of a multi-variate, inverted pendulum, estimator based model of human standing. The model uses modern control theory, optimal control strategies, and realistic system characteristics to capture the important aspects of quiet standing. The model assumes the human to be an inverted pendulum with the mass of the subject concentrated at the top of the pendulum. The plant is controlled at the ankles with muscle actuators that are simple Hill muscle models. This plant is controlled through two optimal feedback paths, the inner path representing reflexive feedback, and the outer loop representing the addition of vestibular feedback into the closed loop system. This analytical model helps to explain some of the changes that occur in lower leg musculature following brief exposure to reduced gravity.

1.3 Hypotheses / Objectives

The central hypothesis of this thesis is that changes in perceived gait following hypo-gravity exposure are the result of changes in central nervous system processing rather than changes in the mechanical properties of the muscles, or sub-cortical neural changes. Changes in muscle mass or strength cannot occur during the limited, acute exposure provided in this experiment (up to intervals of 6 minutes). As the protocols reveal, the stretch reflex latency remains unchanged following partial gravity exposure. Therefore, any change in motor function, perceived or otherwise, must be due to the effect of CNS gain changes brought about by exposure to reduced forces in the legs during walking or running.

It is hypothesized that, following hypogravity exposure, normal muscle activation is decreased due to a reduction in neuromuscular gain directed by the central nervous system. This phenomenon is what actually causes the subject to experience 'heavy legs'. This feeling subsides naturally with time as the muscle gains are reset to normal 1 g values. It is also believed that this recovery can be accelerated through exercise intervention. The ability of different exercises to speed recovery of 'heavy legs' is evaluated.

The change in muscle activation levels is revealed through the use of posturography. Once adapted to low gravity locomotion, upon returning to a 1 g environment, a person responds with one of two possible strategies for maintenance of postural sway. The natural response of the subject is an increase in the magnitude of the excursion from upright. Due to the lower activation levels in the musculature of the legs, the natural sway of the subject increases, causing an expansion in the trajectory of the center of pressure of the subject. A second possibility occurs because of the cognition of the subject. Recognizing that he is less stable than before, the subject hyper-activates his muscles, keeping as far away from the stability boundary as possible. This results in a much smaller center of pressure trajectory than noted before exposure.

1.4 Thesis Outline

Chapter two of this thesis provides background information on the three principal topics: locomotion, energetics, and posturography. Section 2.1, Muscles and Reflexes, explains muscle behavior, reflex characteristics, and presents a simple model of muscular behavior. Section 2.2, Locomotion, familiarizes the reader with basic characteristics of human gait, the differences between running and walking, and presents a basic model for running and walking. Section 2.3, Energetics and Workload, orients the reader with the fundamental concepts of human energy expenditure and the process of oxygen uptake measurement, or $\dot{V}_{O_2}$, measurements Finally, Section 2.4, Posturography, introduces the technique of posturography and presents a control theory estimator based model of postural behavior during quiet standing.

Chapter three introduces some of the methods currently being used for partial g simulation including parabolic flight, submersion, and several suspension techniques, which are discussed in Sections 3.1.1, 3.1.2, and 3.1.3 respectively. The advantages and disadvantages of each method are noted. The simulation apparatus designed for this experiment is introduced in Section 3.4, Partial Gravity Simulator.

The experimental methods and hardware used to conduct this experiment are detailed in Chapter 4. The subjects who participated in this study are described in Section 4.1. Section 4.2 describes all of the hardware used during this study. Finally, the experimental protocols are revealed in Section 4.3.

Chapter 5 presents the results of this experiment and provides a detailed discussion of these results. Section 5.1, Results, details the findings of the metabolic, gait, and posture protocols of this experiment. This section also evaluates the ability of the estimator model to capture the important attributes of quiet standing. Section 5.2, Discussion, begins by outlining the limitations of the experimental design. The impact of the workload results is then discussed, followed by a discussion of the gait analysis and posture techniques, and finally, the utility of the estimator model is discussed.

Chapter six presents the summary and conclusions of this experiment. Potential applicability of these results to current and future study in this field is suggested as well as potential areas of focus for related future experiments. Chapter six also points out relevance these findings may have on the design of a future lunar or Martian landing mission.

1.5 Conventions

This section outlines all of the terms and arbitrary sign values used in this thesis. Many of the terms here are universally accepted as defined in this section. Other terms or conventions may be specific to this research. A clear distinction is made to avoid confusion.

1.5.1 Verbal Conventions

Many words found in this thesis are not used in every day life. To avoid confusion, a brief glossary is included.

Algebraic Ricatti Equation (ARE) - Tool used in solving optimal feedback equations through least squares minimization techniques - See Appendix A.

CoM- center of mass

CoP- center of pressure

CoT-Cost of Transport - The amount of energy needed to move 1 unit mass 1 unit distance.

Cost minimization - Finding the least costly way of accomplishing a task, given certain system parameters or limitations.

Cost Function - An equation that defines the relative costs of states or controls during the operation of a system.

d.o.f.- degrees of freedom

EMG- electromyogram - A device used for measuring activation levels of the muscles.

Extensors - muscles that extend joints when activated

Feedback - using the past performance of a system to determine future inputs to the system to achieve the desired output

Flexors - muscles which contract joints when activated

g- gravity

'Heavy Legs' syndrome - A sensation of being heavier than normal caused by brief exposure to a reduced gravity environment.

Linear Quadratic Regulator (LQR) - An optimal feedback method which attempts to drive all state variables to zero.

Low gravity - See Reduced gravity

Optimization - see Cost minimization

Partial gravity - See Reduced gravity

Proprioceptive - pertaining to signals responding to stimuli that originates within the body.

Reduced gravity - An environment in which the vertical forces experienced are less than on Earth (between 0 and 1g).

1.5.2 Axes Definition Conventions

Body Related

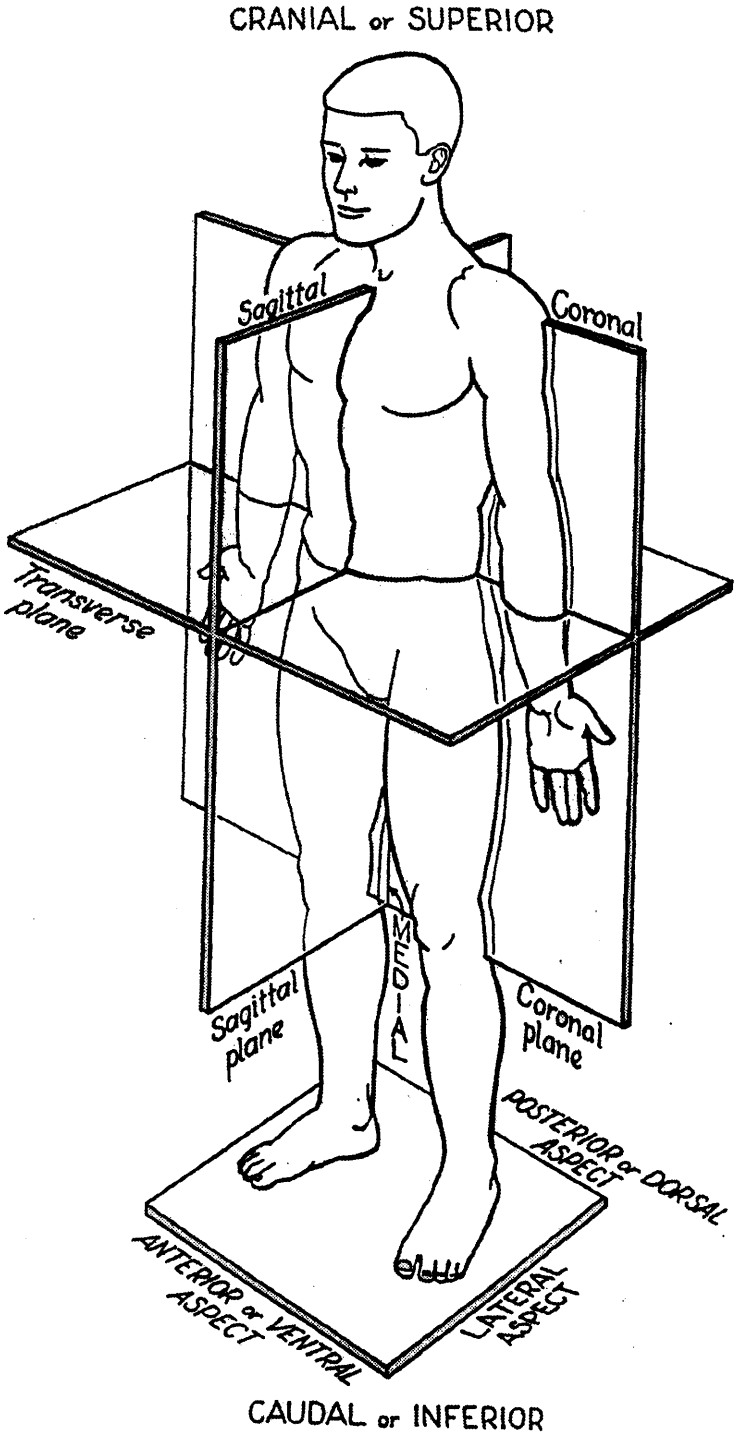

Figure 1.1 shows all of the body related conventions used in this thesis.

Forceplate

These conventions are specific only to this thesis, but are consistent throughout. The axes are valid for both the posture and kinematics protocols

X axis-perpendicular to the coronal plane, ventral side positive

Y axis-perpendicular to the sagittal plane, subject's right side positive

Z axis-perpendicular to the transverse plane, down is positive

Other Conventions

All matrices are denoted as underlined capital letters. Variables are denoted as letter, or characters, with no identifying features. Velocity terms, or single derivatives, are symbolized by a single dot over the variable. A double dot over the variable represents a double derivative (acceleration). A hat over any variable denotes an estimate of the variable. A delta term represents a change in a variable.

Matrices	$\underline{A}, \underline{L}, \text{or } \underline{K}$
Variables	$x, y, \text{or } \theta$
Derivatives	$\dot{x}, \dot{y}, \text{or } \dot{\theta}$
Double Derivatives	$\ddot{x}, \ddot{y}, \text{or } \ddot{\theta}$
Estimate	$\hat{x}$, or $\hat{y}$
Change	Δx or Δy.

Chapter 2 Background

This chapter provides background on all the major experimental measurement topics of this thesis, including locomotion, energetics and workload, and posturography. Section 2.1 explains muscle behavior and reflex characteristics, and presents a simple muscle model. Section 2.2 introduces the key concepts of human gait and locomotion. The difference between walking and running as pertaining to energy and dynamics is discussed, and a simple, inverted-pendulum model for walking is introduced. Section 2.3 highlights the fundamentals of metabolic costs and energetic processes and concludes by discussing workload measurement techniques. The technique of posturography is outlined in Section 2.4. This section introduces the basic principles involved in postural control and sway stability. An estimator model of postural control based on theoretical control engineering is introduced here and used for analysis in Chapter 5, Results.

2.1 Muscles and Reflexes

The following section outlines the muscle characteristics that are important to understand as background for this thesis. Relevant topics include the gross characteristics of muscle activity mechanisms, the use of feedback for control of muscles, and reflex characteristics of muscles which are important for the reflex protocol of this experiment. It also introduces a simple muscle model which will be used later in this chapter to develop a complete postural control model.

2.1.1 General Muscle Characteristics

The human body contains three types of muscle: cardiac, or heart muscle; smooth muscle that control involuntary actions such as blood pressure, digestion, and urinary excretion; and skeletal muscle, that control voluntary movement of body parts. Only skeletal muscle will be discussed in this thesis. The basic mechanisms for muscular activation are important, therefore, the gross characteristics of muscle activity will be discussed. Muscle mechanics on a cellular level are beyond the scope of this research effort.

A muscle is activated when it receives a signal from a motor neuron originating in the motor cortex (or from reflexive sources). The signal is delivered to individual muscle fibers that actively contract when a strong enough signal is received. All muscles contain both fast twitch and slow twitch fibers. Muscles which contain primarily fast twitch

fibers, or white muscle, provide a quick, explosive contraction. These muscles, while very fast, heavily rely upon glycolytic processes for energy. This fuel is rapidly depleted, limiting the duration which and individual muscle can activate. Slow twitch, or red muscle, contain a large amount of mitochondria that facilitate energy release through aerobic processes. This fuel is constantly replenished, giving red muscle high endurance characteristics [Newman, 1993].

Prolonged exposure to microgravity causes severe deterioration of muscular performance. Atrophy begins almost immediately upon entering space. Although primarily in the extensors, flexor atrophy is also seen. Loss of muscle mass, cross sectional area, and strength are all direct results of extended periods spent in space [Keller, 1991], [Cavanagh, 1992]. For this experiment, exposure to simulated reduced gravity is limited to 6 minute intervals. As a result, no such deterioration is expected.

2.1.2 Muscle Proprioceptors

Muscle control of movement is a closed loop system. Limb position and muscle tension are constantly fed back to neural centers and adjustments in motor neuron signals are made. Groups of neurons called central pattern generators (CPGs) aid in the generation of coordinated limb movement. Neural pattern generators can be located in either the brain or spinal cord [Getting, 1985], [Houk, 1989]. While CPGs control gross movements, fine tuning is accomplished through proprioceptive feedback. The primary proprioceptors for muscles are spindle organs and golgi tendon organs (GTO).

The spindle organs act in parallel with the muscle to determine the change in muscle length. The spindle is made up of two types of fibers, nuclear bags and nuclear chains. The spindle is attached in parallel to the main muscle at both ends of a muscle fiber, allowing the spindle to experience the same relative length changes as the muscle [Boyd, 1985]. Figure 2.1 shows the muscle spindle and accompanying neurons. The spindles are responsible for the stretch reflex that is discussed in Section 2.1.4, Stretch Reflex. The golgi tendon organs are located in the tendons and operate in series with the muscle. The GTOs are analogous to a force transducer in a mechanical system. Since the GTOs are not instrumental in reflex mechanics, they are discussed not in further detail.

2.1.3 Neurons

All muscles are innervated with two basic types of neurons, efferents and afferents. Efferent neurons carry signals away from the spinal cord to the muscles while afferent, or sensing, neurons carry signals from the muscles to the spinal cord. In most cases the two neurons work in cooperation to achieve the desired limb motion. As shown in Figure 2.1, the afferent fibers of the muscle spindle are broken up into two sub-groups, Group I primary afferents, and Group II secondary afferents. Group I neurons are large neurons with high conductivity and resultant high signal velocities. Group Ia neurons carry information from the spindles while Ib neurons carry signals from the GTO to the spinal cord. Group II neurons are smaller and slower than the primary neurons. These typically innervate the nuclear chain of the muscle spindle. The efferent fibers of the muscle spindle are called gamma (γ) neurons. Gamma motor neurons innervate the muscle fibers of the spindle and coordinate contraction of the spindle with its attached muscle.

2.1.4 Stretch Reflex

When an active muscle is stretched by an external force, the muscle undergoes an active contraction in an effort to maintain its original length. This phenomenon is known as the *stretch reflex*, and can be easily induced in the quadriceps by striking the patellar tendon (as often experienced during a routine physical exam)[McMahon, 1984].

The steps involved in the reflex are as follows and are shown in Figure 2.2:

1) The muscle and connected spindle are stretched.

2) The stretch is sensed by the spindle which send a signal to the spinal cord via type Ia afferents.

3) The signal is received, scaled, and is sent back out of the spinal cord to the muscles.

4) Receipt of the returned signal by the muscle causes contraction of the muscle resulting in reflex motion.

The stretch reflex is fast because it involves only one synapse, the one between the Ia afferent and a γ efferent neuron. Experiments have shown this total lag time between strike and muscle activation to be approximately 24 milliseconds [Kroonenberg, 1995]. All of the signals and processing take place in sub-cortical pathways (the signal remains in the spinal column, and does not enter the brain), resulting in rapid

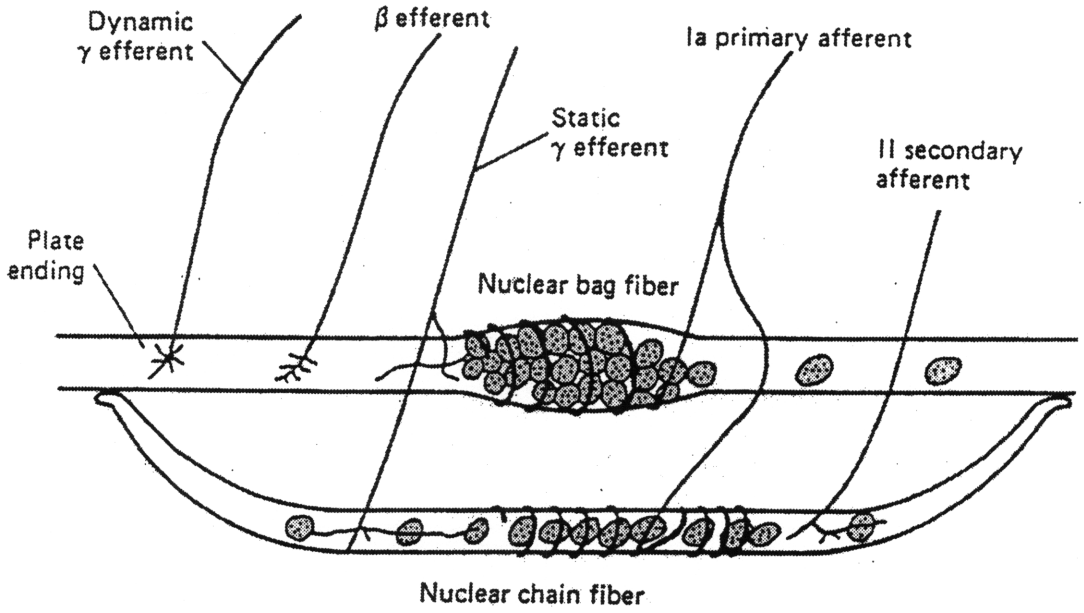

Figure 2.1 Muscle Spindle and Corresponding Efferent and Afferent Neurons

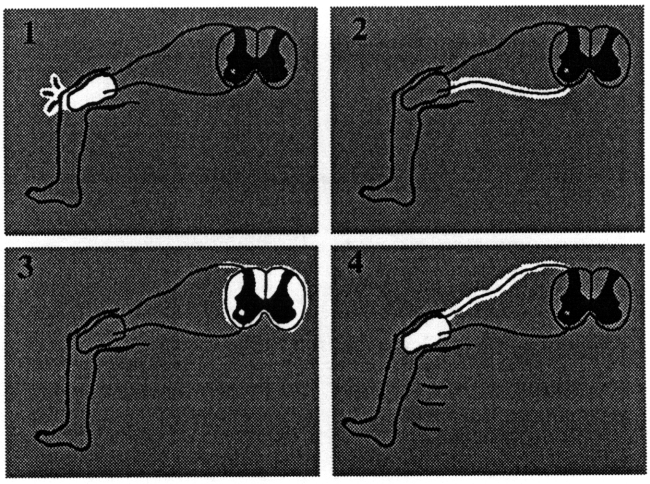

Figure 2.2 Stretch Reflex Sequence. 1) Tendon and spindles are stretched. 2) Spindle sends signal to spinal cord. 3) Signal is received by spinal cord and sent out to muscles. 4) Muscles receives signal and contracts.

completion of the control loop. This is the simplest example of closed loop control of muscle activity.

It is not expected that acute exposure to a reduced gravity environment will alter the sub-cortical pathways used during the reflex. Any change in muscle behavior is expected to be due to changes at the cortical level (the brain). Therefore, the reflex latency is hypothesized to remain invariant following exposure to reduced gravity.

2.1.5 Hill Muscle Model

Many analytical models attempt to adequately predict or replicate physiological muscle behavior. The one chosen for this experiment was developed by A.V. Hill in the early twentieth century [McMahon, 1984]. The Hill model assumes that there are active and passive characteristics of muscle. The muscle itself is modeled as a damped force generator placed in parallel with an elastic component, modeling the contraction and lengthening characteristics of the isolated muscle. This lumped element is placed in series with a second elastic element, to account for the elasticity of tendons and ligaments at the end of the muscle. Figure 2.3 shows the Hill Model. The relationship between the tension generated, the contraction of the muscle, and the external tension of the muscle can be expressed as:

$$T\left(\frac{B}{K_{PE}+K_{SE}}s+1\right)=\frac{K_{PE}K_{SE}}{K_{PE}+K_{SE}}\Delta x+\frac{K_{SE}B}{K_{PE}+K_{SE}}\dot{x}+\frac{K_{SE}}{K_{PE}+K_{SE}}T_O \qquad \text{Eq. 2.1}$$

where K_{SE} is the series elastic component
K_{PE} is the parallel elastic component
B is the damping component
and T_o is the force generation component.

s denotes a derivative in the LaPlace domain.

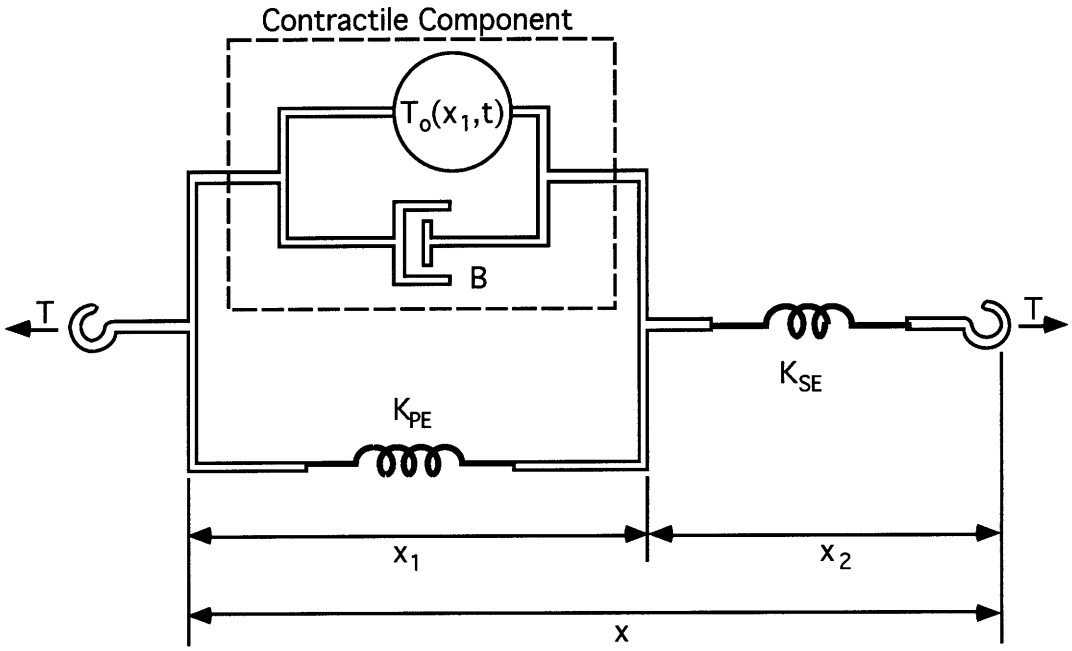

Figure 2.3 A.V Hill Muscle Model represents the muscle as a force generator (T_o) in parallel with a viscous damper (B) and an elastic element (K_{PE}),. and in series with a second elastic element called the series elastic element (K_{SE}).

2.2 Locomotion

Locomotion is defined as the act of moving or the ability to move from place to place. It is the way that all living things get from one place to another. Locomotion is one of the most basic activities performed by all animals, including humans. This section introduces the reader to the basic determinants of human locomotion, points out some important differences between various human gaits, and presents a simple model of human gait.

2.2.1 Anatomy of a Step

The act of walking is much more than simply putting one foot in front of the other. While that may be the walking style of toddlers or stiff robots, the gait of adult humans is far more complicated than simply lifting and placing the feet alternately in a single plane. McMahon lists 6 separate determinants of normal gait [McMahon, 1984]. Each of these involves the addition of 1 degree of freedom (d.o.f.) in a lower extremity joint. The addition of each d.o.f. flattens the trajectory of the center of mass (CoM) resulting in a smoother and more comfortable stride.

The six determinants of gait are:

1) compass gait
2) pelvic rotation
3) pelvic tilt
4) stance knee flexion
5) plantar flexion of the stance ankle
6) lateral displacement of the pelvis.

The first distinguishable determinant of gait, **compass gait,** involves walking in two dimensions. Each hip pivots in the sagittal plane, swinging the leg forward. The leg is planted and the hip swings over the stance foot. During compass gait, the leg length does not change. This causes the center of mass of the body to travel in an arc-like trajectory with a radius equal to the leg length. As a side note, this gait as defined is not possible since in order for the swing leg to get back in place for the next support phase, it would have to become shorter to avoid hitting the ground, breaking a basic conditions of this gait. An illustration of compass gait is shown in Figure 2.4. Notice the jerky transition when body support transfers from one leg to the other.

The addition of **pelvic rotation** extends the effective length of the legs, smoothing the trajectory of the CoM. During pelvic rotation, the pelvis is turned about the vertical axis. The hip of the swing leg shifts forward approximately 3° just before the foot is placed. A normal stance phase then takes place and the process is repeated with the other leg. Figure 2.5a shows what pelvic rotation looks like while walking and Figure 2.5b shows the magnitude of the rotation of the pelvis as the step is carried out.

In addition to rotating, the pelvis also tilts. **Pelvic tilt** occurs during the swing phase. Just before toe off, the hip on the swing side abruptly falls slightly lower than the support hip, with the line between the hips creating about a 5° angle with the horizontal plane. Pelvic tilt smoothes the CoM trajectory even further, and is shown visually in three dimensions in Figure 2.6. As an incidental fact, this necessitates the inclusion of another action, *knee flexion.* Without bending the knee of the swing leg, the leg would scrape the ground during the swing phase.

Without bending the knee, the CoM trajectory rises a great deal in the middle of the stance phase. This problem is alleviated by introducing **stance knee flexion** to human gait. By bending the knee slightly, the peak in the trajectory at the center of the step is slightly flattened, resulting in a much smoother path for the CoM. Figure 2.7 shows the appearance of the step with the addition of stance knee flexion.

The first four gait determinants all deal with pivots at the hip and knee joints. Trajectory-smoothing motion also occurs at the ankle joint. **Plantar flexion of the stance ankle** further helps smooth the CoM path and also imparts angular velocity to the shank and thigh for the following swing phase. Just before toe off, the ankle of the stance leg extends the foot, pushing the sole (plantar surface) of the foot down. Figure 2.8 shows the side view of plantar flexion.

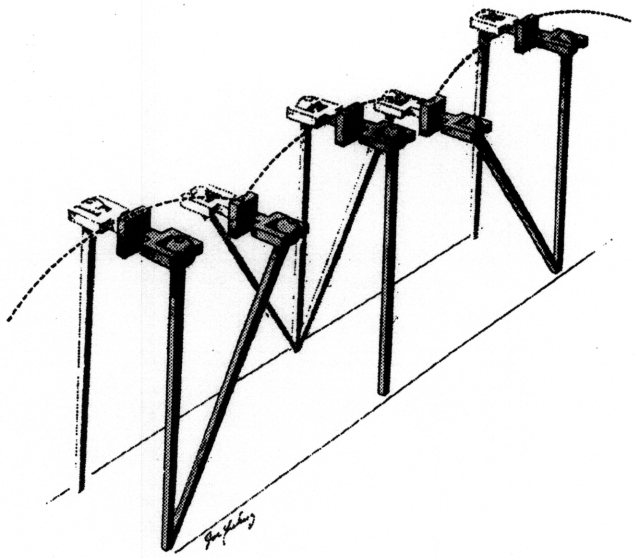

Figure 2.4 Compass Gait. The stance leg remains stiff as the trunk moves in an arc for each step. From McMahon, 1984.

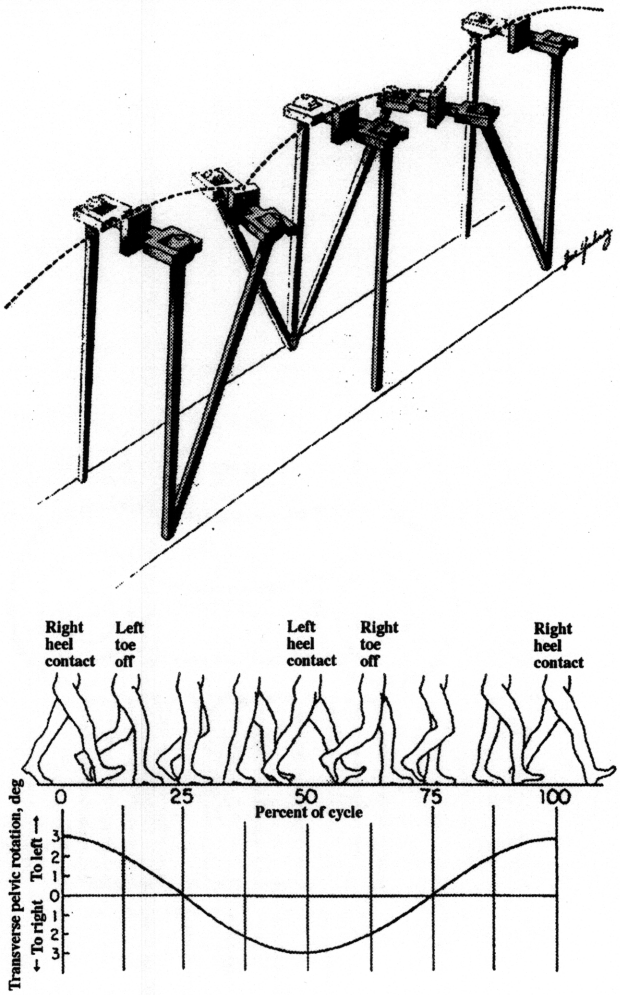

Figure 2.5 Pelvic Rotation. The pelvis turns about the vertical axis, increasing the effective leg length and flattening the arc. From McMahon, 1984.

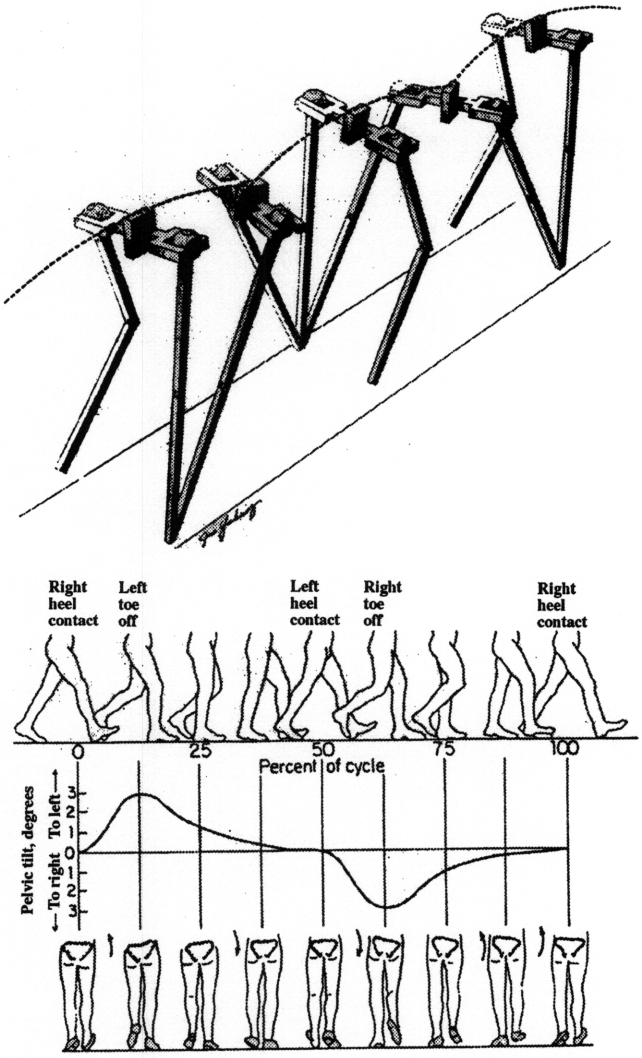

Figure 2.6 Pelvic Tilt. The pelvis is lowered at toe off and raised slowly until heel strike. The addition of pelvic tilt flattens the trajectory arc even further. From McMahon, 1984.

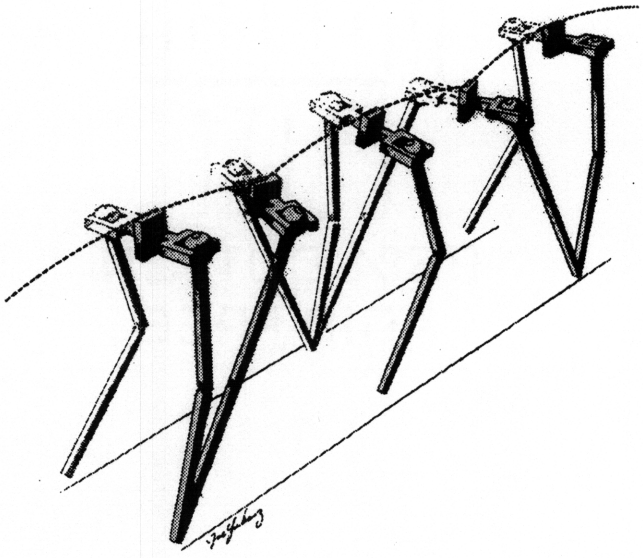

Figure 2.7 Stance Knee Flexion. Flexing the stance knee succeeds in flattening the CoM trajectory. From McMahon, 1984.

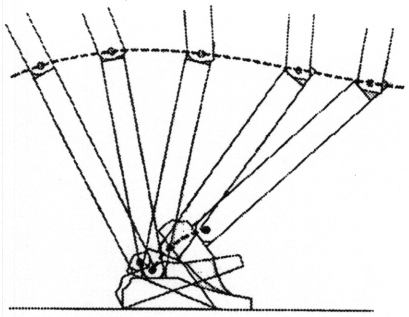

Figure 2.8 Plantar Flexion. A smooth transition from double support phase to swing phase is accomplished through plantar flexion of the stance ankle. From McMahon, 1984.

The final determinant in human gait mentioned by McMahon is the **lateral displacement of the pelvis.** As a person steps forward, support is constantly being transferred from one foot to the other. When the foot is placed, the CoM shifts approximately 2 cm (0.8 in) toward the weight bearing leg. As Newman points out, this shift is minimized by the fact that the femoral shafts are not sagittally aligned (See Figure 2.9) [Newman, 1992]. The knees are, in fact, medial to the hips in the sagital plane. Lateral shift keeps the center of mass over a stable column enabling humans to walk without falling over. This is shown in Figure 2.10.

The importance of these gait determinants becomes apparent in Section 5.1.2, Gait Analysis. Knee flexion, plantar flexion, and pelvic tilt are all easily observable during locomotion when viewed from the profile perspective.

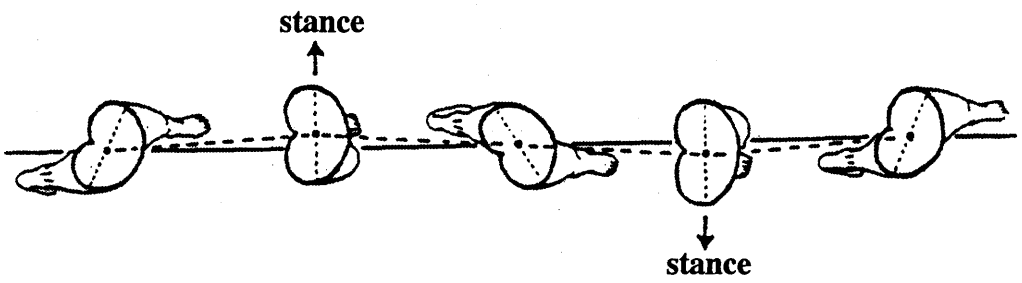

Figure 2.9 Lateral Shift of the Pelvis. Twice during each step, the pelvis shifts 2 cm toward the stance leg. Lateral shift aids in maintenance of a stable platform while walking.

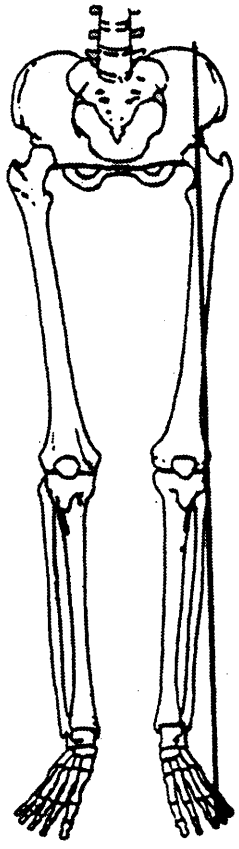

Figure 2.10 Alignment of Hips and Knees. The lateral shift is minimized by the fact that the hips are outside of the knees with respect to the sagittal plane.

2.2.2 Difference Between Walking and Running

In a normal, 1 g Earth environment human beings primarily rely upon two gaits for locomotion: walking and running. In reduced gravity, either loping or jumping may be used as an alternative, but walking and running still provide very interesting comparisons. The differences between the mechanics of locomotion are important and are discussed below.

Some of the differences between walking and running can be easily observed. The easiest difference to notice is that in walking, at least one foot is in constant contact with the ground at all times while running includes and aerial phase in which neither foot is touching the ground. One slightly less obvious difference between walking and running is that in walking, the center of mass of the subject is at its highest point at midstep while in running, midstep marks the lowest point of the center of mass.

Walking involves a swing phase, a double support phase, and a stance phase. During the swing phase one leg provides support for the body while the other leg swings forward to support the body during the next phase. Once the swing leg makes contact with the ground, there is a brief period of double support in which both feet are touching the ground at the same time. Following this, the former stance leg lifts and becomes the swing leg, with the weight of the body supported by the stance new leg.

During normal running, only one leg at a time touches the ground. The stance phase involves recoiling of the support leg followed by an explosive release of energy. This release is followed by a short period in which neither leg touches the ground. This aerial phase makes running easily distinguishable from walking. During the aerial phase, the other leg swings in front of the CoM and the cycle is repeated.

From an energy standpoint, the two main human gaits are just as different as they are from a mechanical standpoint. During normal walking, the change in gravitational potential energy and forward kinetic energy are almost exactly out of phase (See Figure 2.11). This is analogous to the behavior of an inverted pendulum as it swings through its zenith. This fact results in very little change in total external energy during walking. This natural exchange of energy makes walking a very efficient means of locomotion, accounting for between 65 and 70% of total energy recovery. This means that only 30 to 35% of the energy for walking needs to be supplied by the muscles [Cavagna, 1977].

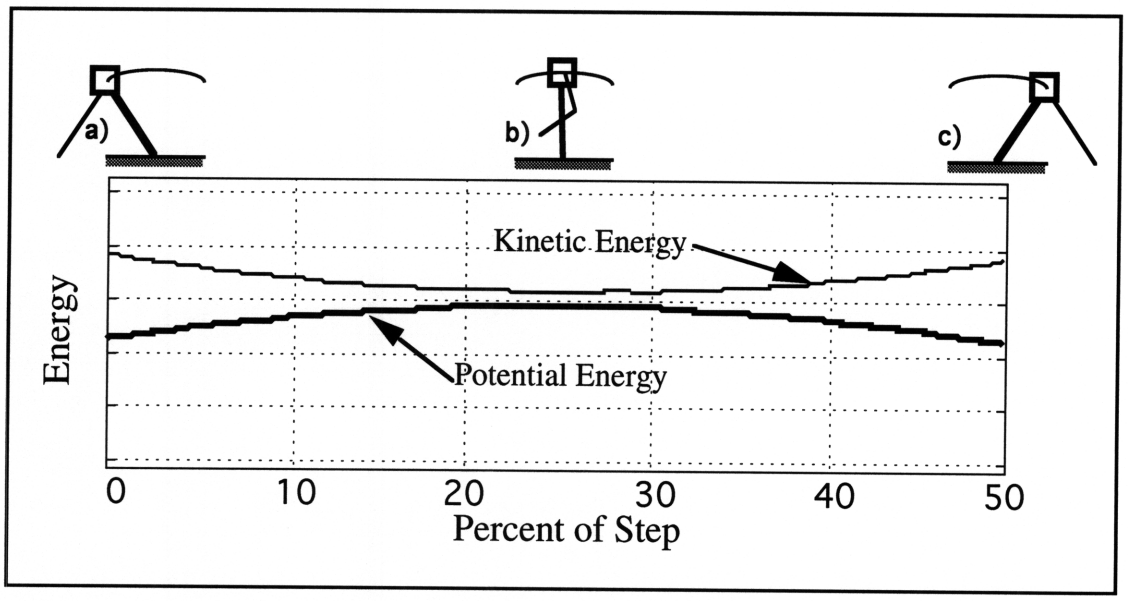

Figure 2.11 While walking, the potential and kinetic energy are exactly 180° out of phase, resulting in an efficient exchange of energy and the high energy efficiency found in walking. Potential energy reaches a maximum at midstep and a minimum at the beginning/end of the stride. Kinetic energy reaches its maximum at the end of the stride, and is at a minimum at midstride.

A similar energetic efficiency is absent in running. Running involves a change in potential energy and forward kinetic energy almost simultaneously, causing large changes in total energy during each step. Consequently, according to the external energy model, nearly all of the energy for running must be supplied by the muscles. In fact, it was found that only between 0-4% of the energy necessary for motion is recovered through pendular means. Of course, this method has ignored the storage of energy via elastic means that is key to efficient locomotion at higher speeds and can account for almost 40% energy recovery during running, requiring that the muscles supply 60% of the energy necessary for normal running [Margaria, 1976].

There exists a *transition velocity* at which a human will switch from walking to running. While walking is the most efficient way to travel at low speeds, at a certain speed, the changes in kinetic energy during a stride cycle are too large to be sustained by the changes in potential energy during a stride. For a normal 1 g environment, this speed is about 2.36 m/s [Margaria, 1964]. To attain higher speeds, additional energy must be supplied to achieve the necessary higher acceleration levels. This addition results in a simultaneous increase in both kinetic and potential energy and nearly no energy exchange between the two.

2.2.3 Inverted Pendulum Model for Walking

The simplest model of a walking human is the inverted pendulum model [Blickhan, 1987], [Cavagna, 1977], [Heglund, 1982]. As its name implies, this model assumes that the subject is a point mass which is affixed atop a leg of constant length l_o. The leg swings through angle 2θ at which point the opposite leg becomes the support leg.

The energy equations for this model are relatively simple. The gravitational potential energy is defined as:

$$\dot{W}_v = PE = mgh \qquad \text{Eq. 2.2}$$

Where $\dot{W}_v$ is the gravitational potential energy, m is the mass of the body, g is gravity, and h is the vertical displacement of the center of mass of the body. Figure 2.11 shows that PE reaches a maximum at the center of the support phase and a minimum when the leg angle is at a maximum.

The kinetic energy of the mass is almost exactly 180 degrees out of phase with the potential energy. The horizontal kinetic energy is defined as:

$$\dot{W}_h = KE = \frac{1}{2}mv^2 \qquad \text{Eq. 2.3}$$

where $\dot{W}_h$ is the horizontal kinetic energy and v is the horizontal velocity of the body. By assuming that the system is 100% efficient, a reasonable assumption in this case, the two energy terms can be equated.

$$\dot{W} = mgh = \frac{1}{2}mv^2 \qquad \text{Eq. 2.4}$$

Although there is some energy loss, this equation is a good first order approximation. This equation makes it obvious that as g level decreases, so does the maximum attainable walking speed.

2.2.5 Reduced Gravity Locomotion

The way in which a human locomotes in reduced gravity is, by necessity, fundamentally different than locomotion on Earth. This is true of both walking and running. Limits to walking are still related to PE limits, but low gravity exacerbates this problem. Running is limited by the normal forces produced by a runner in low gravity.

When in a low gravity environment, a human's weight is reduced a factor proportional to the gravity level with a proportional reduction in potential energy change during a normal stride cycle. As shown by Equation 2.4, this reduction in change in potential energy (ΔPE) severely limits the range of acceptable velocities for walking. Even at low walking speeds, the forward kinetic energy exceeds the total change in potential energy. The *transition velocity* mentioned before is much lower in reduced g. The theoretical limit for walking on the moon has been calculated to be 0.3 m/s [Margaria, 1964]. Beyond this speed, alternate gaits such as loping must be adopted.

Running also changes in reduced gravity environments. During running, the force produced by the muscles has both a vertical and a horizontal component. Vertical force determines the duration of the aerial phase, while horizontal force dictates the forward velocity of the subject. The friction necessary for horizontal acceleration is proportional to the normal (vertical) force produced. The maximum running speed in low gravity conditions is limited by the fact that the vertical component of the force may not be high enough to maintain the friction necessary for proper traction, causing slipping. Theoretically, this fact was determined to limit running speeds to about 1.4 m/s [Margaria, 1964]. This limit has not been found to be a barrier in experimental simulations [Newman, 1992], [Farley, 1992].

Reduced gravity running is different from normal 1 g running in several other ways. The touchdown angle is slightly lower in reduced gravity which may result from an attempt to increase the normal forces and prevent slipping. For lunar running at 2.6 m/s, the touchdown angle varies from 20° experimentally, and 14° theoretically from one model [He, 1991], to 38° from another model [Margaria, 1964]. Also, the vertical stiffness of the leg, K_{vert}, increases slightly in reduced gravity. This may allow for slightly higher vertical forces without changing vertical excursion of the body.

Other characteristics of running do not change during reduced gravity locomotion. First, the spring stiffness of the leg is invariant with respect to gravity. This means that the leg flexes less in a low gravity environment. Second, the vertical excursions of the center of mass during flight phase do not significantly change with either forward speed or gravity, signifying that as gravity is reduced, the vertical force undergoes a concomitant reduction, keeping the overall vertical excursion the same. Also, as the gravity level is decreased, the ground reaction forces undergo a related decrease in magnitude. This means that during low gravity locomotion, the forces provided by the muscles are smaller and a lower energetic cost of transport can be expected [He, 1991].

2.3 Energetics and Workload

The basic operation of the muscles of the body has already been outlined. However, the source of energy for muscular activity has not yet been discussed. The basic means of energy production and conversion are given in Section 2.3.1. An outline of energy consumption measurement techniques is provided in Section 2.3.2. The technique outlined in Section 2.3.2 is used for workload measurement in this experiment.

2.3.1 Energetics

The human body produces energy via three basic mechanisms: phosphagen split, creating adenosine triphosphate(ATP); combustion of food; and glycolysis, producing energy and lactic acid as by products. By measuring these three processes the rate of metabolic energy consumption can be easily determined.

The fuel that is actually used by the muscles for contractile motion is called ATP. This fuel is stored in the muscles for quick release of energy upon contraction. However, the ATP stores in the muscles are rapidly depleted and must be resynthesized at the same rate they are depleted in order to sustain muscular contraction. The primary source of ATP synthesis is a group of substances containing high-energy phosphates called phosphagens. The phosphagens themselves must then be resynthesized. The energy for resynthesis must come from external sources, either energy stores of the body (glycogen) or consumed energy (food) [Margaria, 1976].

The amount of energy released or absorbed by each of the reactions can be determined through chemical measurements of the phosphagen and lactic acid contents of the body

and by measurement of the consumption of oxygen. These measurements can then be coupled with known energy levels involved with each process to determine total energy consumption.

A schematic diagram of the three main engines for energy production and use in the body is shown in the equations below.

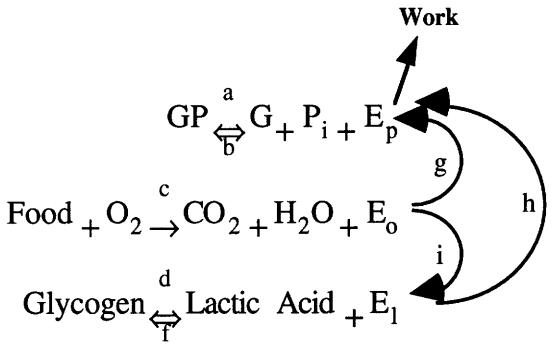

where GP is phosphagen, P_i is inorganic phosphate, E is energy (subscripts p-phosphagen, o-oxygen, and l-glycogen), O_2 is molecular oxygen, CO_2 is carbon dioxide, and H_2O is water.

The overall equation for energy consumed is expressed as:

$$E = A - B + C + D - F \qquad \text{Eq. 2.8}$$

with B and F representing energy consuming processes and A, C and D all representing energy producing reactions. Notice that, ultimately, metabolism of food is the single source of energy to the system, the other two equations are merely energy storage and transformation processes [Margaria, 1976].

The equation above is useful but limited, since measurement of glycogen and phosphagen in the body are difficult without using intrusive measuring techniques or sacrificing the subject. Therefore, a simpler method of energy measurement must be devised. Fortunately, Equation 2.8 can be greatly simplified in two ways. The first is that Equation 2.5 can be effectively eliminated. After 1 minute or less of exercise, phosphagen production reaches equilibrium. The amount of phosphagen produced (A) exactly equals the amount of phosphagen being consumed (B), eliminating both A and B from Equation 2.5. Also, for submaximal exercise, there is no lactic acid production or

glycogen synthesis. Therefore, D and F are both zero, re-writing equation 2.8 as:

$$E = C \qquad \text{Eq. 2.9}$$

By measuring the amount of oxygen consumed, the amount of energy can be determined by a simple equation:

$$E = C = MV_{O_2} \qquad \text{Eq. 2.10}$$

where M is the energy equivalent of one milliliter of oxygen and V_{O_2} is the volume of oxygen consumed in milliliters. The energy equivalent of 1 ml of oxygen used in the combustion of food is known to be 5 calories. The power, P, is the time derivative of the energy consumed and is written as:

$$P = \dot{E} = M\dot{V}_{O_2} \qquad \text{Eq. 2.11}$$

where $\dot{E}$ is the energy consumed per unit time and $\dot{V}_{O_2}$ is the volume of oxygen used per unit time. By measuring the $\dot{V}_{O_2}$ (oxygen uptake) of an individual, an accurate measurement of total metabolic rate can be attained. Such measurements allow the energetic cost of transport at various gravity levels to be determined.

2.3.2 Reduced Gravity Energetics

During the past 30 years, interest has been shown in identifying the relative metabolic costs of locomotion and other activities in reduced g environments. Experiments have consistently shown that locomotion in reduced gravity is less costly than 1 g locomotion [Shavelson, 1968] and [Newman, 1991], however, upper torso tasks require more energy in reduced g simulations than in a normal 1 g environment [Wortz, 1969], particularly tasks requiring a great deal of upper body torque. Resting energy needs were found to be unchanged [Prescott, 1966]. Also, Robertson found that as degrees of freedom (d.o.f.) in a simulator increase, the energetic cost decreases [Robertson, 1968]. These results conflict with Sanborn's findings that the number of d.o.f. does not effect the energy cost [Sanborn, 1967]. It is apparent from these studies that energy consumption in reduced gravity environments is a very task specific phenomenon. Therefore, one must be careful not to overgeneralize any results obtained for a specific task.

One very interesting finding is that a simulated 75% reduction in gravity level (1/4 g) produces a 72% reduction in cost of transport for running, but only a 33% reduction in the energy needed for walking. As a result, at gravity levels below 0.5 g's, walking is no longer the most efficient means of travel. From an energetics standpoint, running or loping is the cheapest way to locomote in very low g environments [Farley, 1992], [Newman, 1992]. The next logical question is "How can the energy consumption be measured?"

2.3.3 Workload Measurements

The amount of work performed by a human during a given task can be measured in a variety of ways. Subjective reports can be used, although these reports are often inconsistent, non-repeatable, and of little value. Descriptions like 'easier' or 'harder' are difficult to base broad conclusions on, or to use for comparison between subjects. A more objective measure of workload performance was outlined in Section 2.3.1, Energetics.

By measuring oxygen uptake, the amount of metabolic activity can be measured, assuming that a few conditions are true. The same can be said for heart rate measurements, as is shown in the following sections. Both measurement techniques are used during this experiment.

Oxygen Uptake Analysis

Oxygen uptake ($\dot{V}_{O_2}$) is measured by an off-the-shelf system, whose basic operation is as follows. The normal composition of air is approximately 79% Nitrogen, and 21% Oxygen, with small trace elements ignored. It is assumed that inspired air is composed this way. By measuring the relative concentrations of O_2 and CO_2 of the expired air, oxygen consumption and carbon dioxide production can be determined. The system used for this experiment measures the total respiratory volume by metering the expired air. Samples of expired air are routed through an analysis chamber where oxygen and carbon dioxide levels are measured. Although most systems require differential nitrogen calibration, this system is self calibrating. It also determines heart rate, energy consumed, and respiratory quotient. This system will be discussed further in depth in Section 4.2.7, Metabolic Measurement System.

2.4 Estimator Based Model of Posture

Initially, this section provides background on the theory and strategies of maintaining upright human posture. It also introduces current analysis techniques of postural performance. Then the estimator based model used to verify experimental results is described.

The task of standing upright involves a complex and not fully understood sensorimotor control system. The basic analogy is that of controlling an unstable, inverted pendulum by maintaining the center of pressure (CoP) within the bounds of stability (the feet) at all times. The CoP is the point directly below the center of mass of the subject, and is the point at which the resultant force exerted on the ground by the subject is located. If the CoP travels outside the stability bounds, the subject cannot maintain an upright posture without moving his feet and will fall.

By tracking the CoP of a standing subject, objective measurements regarding sway stability can be attained. It has been shown that humans use a variety of sensory inputs in a feedback manner to maintain upright posture. Visual, vestibular, and proprioceptive cues are all used, although the removal of the visual cue did not significantly change subject performance [Dietz, 1991]. Upon return from space, investigators found an increased reliance on visual cues in subjects in addition to the appearance of some postural instabilities due either to orthostatic intolerance, or vestibular conflict upon return to a 1 g environment [Paloski, 1992].

Through spatial and temporal analysis of CoP trajectories, changes in sway stability strategies and performance can be objectively evaluated and compared between conditions as well as among subjects. Spatial analysis includes computation of the mean and rms (root mean square) position of the CoP in the x and y axes, as well as the resultant rms. Temporal analysis notes the position and change in position of the CoP as a function of time, allowing stochastic activity and self correlation factors to be determined. By using this data, and adding a control strategy to the inverted pendulum model mentioned earlier, a useful, and realistic model can be developed.

A human standing erect can be modeled as an inverted pendulum with length l equal to leg length and the mass of the subject concentrated at the hips. Figure 2.12 shows the model and its projections onto the x and y axis.

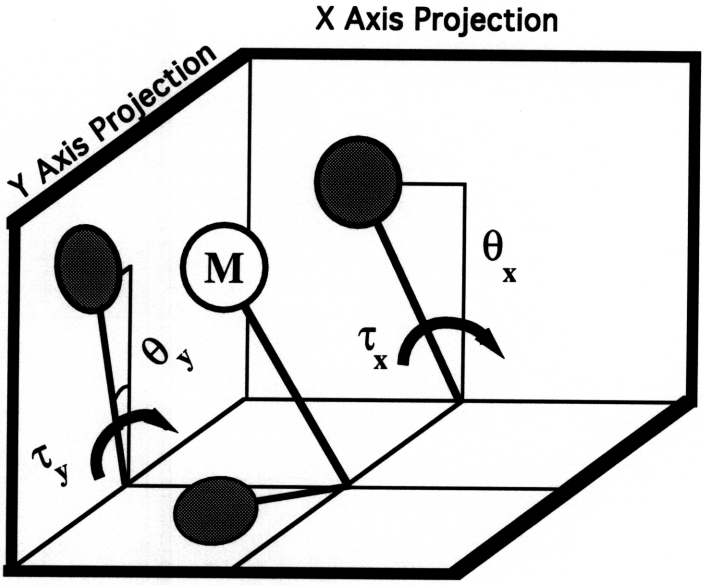

Figure 2.12 Human standing can be modeled as an inverted pendulum with length equal to leg length and the mass of the subject concentrated at the hip. This model is free to move in either the x or y axis and is controlled by torques applied at the ground contact points (in this case the ankles).

The pendulum is controlled by two torques applied at the ankles, one in each axis. The 3-dimensional model can be simplified into 2 uncoupled, linear models, each with the following governing equation:

$$\ddot{\theta}_x = \frac{-mg\sin\theta_x}{I} + \frac{\tau_x}{I} \qquad \text{Eq 2.13}$$

where θ_x is the angle in the x axis, m is body mass, τ_x is ankle torque and I is moment of inertia (an analogous equation exists for the y-axis). The moment of inertia for a point mass at the end of a rigid bar is ml^2 where l is the leg length.

The entire system can be modeled using matrices and the following equations.

$$\dot{x} = \underline{A}x + \underline{B}u \qquad \text{Eq. 2.14}$$

$$y = \underline{C}x + \underline{D}u \qquad \text{Eq. 2.15}$$

where

$$x = \begin{bmatrix} \dot{\theta}_x \\ \theta_x \\ \dot{\theta}_y \\ \theta_y \end{bmatrix} \quad y = \begin{bmatrix} \theta_x \\ \theta_y \end{bmatrix} \quad \text{and } u = \begin{bmatrix} \tau_x & \tau_y \end{bmatrix}$$

The matrices are defined as:

$$\underline{A}_{ip} = \begin{bmatrix} 0 & \frac{g}{l} & 0 & 0 \\ 1 & 0 & 0 & 0 \\ 0 & 0 & 0 & \frac{g}{l} \\ 0 & 0 & 1 & 0 \end{bmatrix} \quad \underline{B}_{ip} = \begin{bmatrix} \frac{-1}{ml^2} & 0 \\ 0 & 0 \\ 0 & \frac{-1}{ml^2} \\ 0 & 0 \end{bmatrix} \quad \underline{C}_{ip} = \begin{bmatrix} 0 & 1 & 0 & 0 \\ 0 & 0 & 0 & 1 \end{bmatrix} \quad \underline{D}_{ip} = \begin{bmatrix} 0 & 0 \\ 0 & 0 \end{bmatrix}$$

Where the ip subscript denotes the plant state space matrices.

To account for the characteristics of the muscular actuators in this system, a model of the muscle is placed in series with the pendulum model. The Hill model is used in this system. If it is assumed that there is no muscular length change during quiet standing, therefore, the first and second terms of Eq. 2.1 can be eliminated, leaving the relationship between T_O and T to be:

$$T = \left(\frac{K_{SE}}{Bs + K_{PE} + K_{SE}} \right) T_o \qquad \text{Eq. 2.16}$$

This relationship can be converted into single input single output (SISO) state space format by creating an intermediate state x. The state space matrices for the model are:

$$\underline{A}_m = \frac{-(K_{PE} + K_{SE})}{B} \quad \underline{B}_m = 1 \quad \underline{C}_m = \frac{-K_{SE}}{B} \quad \underline{D}_m = 0$$

where the m subscript denotes muscle plant state space characteristics.

The constants in this model are assigned as:

$$B = 41710 \frac{Ns}{m}$$

$$K_{PE} = 200 \frac{N}{m}$$

$$\text{and } K_{SE} = 97190 \frac{N}{m}$$

These numbers can vary greatly from depending upon subject, muscle type, muscle size, and muscle activation level. These numbers represent realistic values for a young person with an activated muscle [Kroonenberg, 1995]. The K_{PE} value can almost be ignored, but was given a nominal value of 200 Newtons per meter.

Table 2.1 provides a key for all subscripts used in the block diagrams of this section. Additionally, the table details the inputs, outputs, and states of each plant.

The plant model encompassing both the inverted pendulum and the muscle model is shown in Figure 2.13

Although the plant is unstable (an inverted pendulum will fall over if let go), through reflexive feedback, the system can be stabilized. The stretch reflex is the primary engine for reflexive stability. By responding to changes in the angles and time rates of change in the angles, the stretch reflex keeps the person standing upright. This mode of stability is crude and results in swift jerky motion back and forth, but it does stabilize the system. The stretch reflex is modeled as a full state feedback loop. By using the Algebraic Ricatti Equation, described further in Appendix A, an optimal *feedback gain* , $\underline{K}_r$ can be determined, where the subscript r denotes reflexive feedback gain. Based on the current states of the system this gain matrix produces the best control strategy to be followed through a linear combination of the system states. A pure time delay is then placed in the feedback loop to model the delays present in the stretch reflex. For this model, a delay of 30 milliseconds was used for reflexive feedback.

The delay is actually modeled as the Pade approximation of a pure time delay, which uses a non-minimum phase zero (zero in the right half plane) and a stable pole to create

additional lag without changing the gain of the system. With a time delay of τ, the SISO state space equations look like:

$$\underline{A}_r = \frac{-2}{\tau} \quad \underline{B}_r = 1 \quad \underline{C}_r = \frac{4}{\tau} \quad \underline{D}_r = -1$$

where the r subscript denotes the reflexive time delay.

Noise was added before the time delay to account for uncertainties in the states of the system. A value of $\underline{N}_r$=0.01 represents a random, zero mean, normally distributed error with a variance of approximately 2° in the estimated states of the system.

The plant with the reflexive feedback is shown in Figure 2.14

Table 2.1 Block Diagram Legend

Plant	Subscript	Input	States	Output
Muscle Model	m	T_O	x_m	T
Inverted Pendulum	ip	T	$x_{ip}(\theta, \dot{\theta})$	θ
Combined Plant	P (m + ip)	T_O	x_{ip}, x_m	θ
Reflex Feeback	r	T(x) + noise	t_r	delayed T_O
Vestibular Feedback	v	$T(\hat{x})$+ noise	t_V	delayed T_O
Estimator	E	T_O and θ	$\hat{x}$	$\hat{x}$

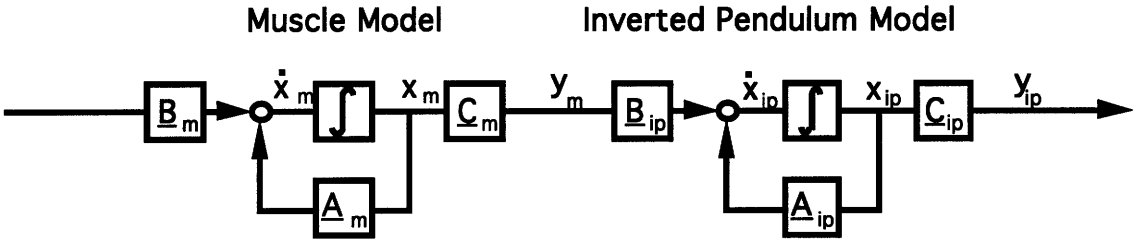

Figure 2.13 Model State Space Block Diagram. The block diagram in this figure represents the two physical plants which govern the behavior of the model: the Hill muscle model, and the inverted pendulum model for posture. The pendulum represents the human standing erect and the muscle plant models the characteristics of the muscular force generators used for control.

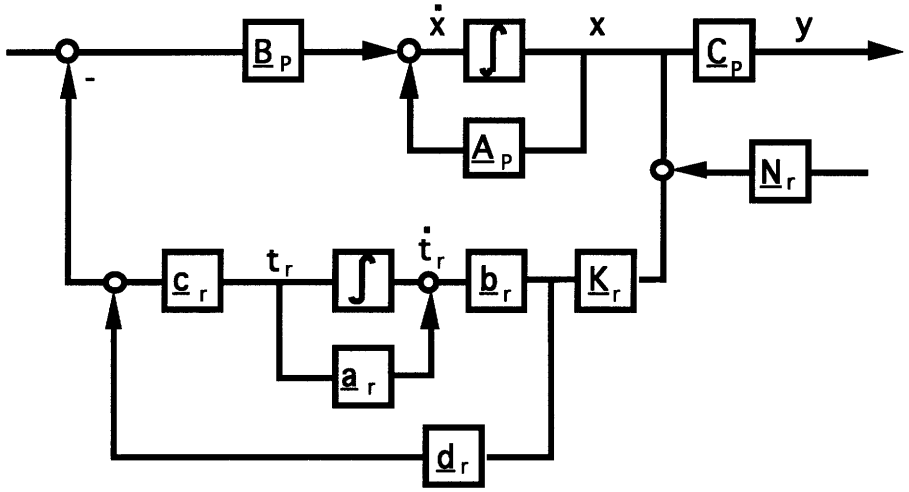

Figure 2.14 Reflex Feedback. This diagram shows how a negative feedback loop is modeled in the state space environment. $\underline{K}_r$ is an optimal feedback gain. $\underline{N}_r$ is the noise shaping matrix. This scales unit magnitude white noise to the proper level. The system modeled in the feedback path represents a time delay of 30 milliseconds, a realistic estimate of reflexive delays. The inclusion of this feedback loop succeeds in stabilizing the system, although the system response is very jerky.

Of course, reflex is not the only stabilizing feedback involved in posture. The brain becomes involved by integrating signals from various sources, determining the position of the body, and determining the appropriate response. However, instead of simply feeding the state values to the brain, this model is made more realistic by assuming that the brain cannot instantly determine the angle that the body makes with the vertical. Instead, the brain *estimates* the angles using an internal representation of the plant. The brain then compares its estimate to reality and compensates for any differences. The equations for the **estimator** are as follows.

$$\dot{\hat{x}} = \underline{A}_p\hat{x} + \underline{B}_p u - \underline{L}(y - \hat{y}) \qquad \text{Eq. 2.17}$$

$$\hat{y} = \underline{C}_p\hat{x} + \underline{D}_p u \qquad \text{Eq. 2.18}$$

where $\underline{A}_p$, $\underline{B}_p$, $\underline{C}_p$, and $\underline{D}_p$ are all identical to the actual plant matrices and $\underline{L}$ is the optimal estimator gain, that is found using the Algebraic Ricatti Equation. The hat over any variable represents an estimate of the original variable. The estimator model is shown in Figure 2.15.

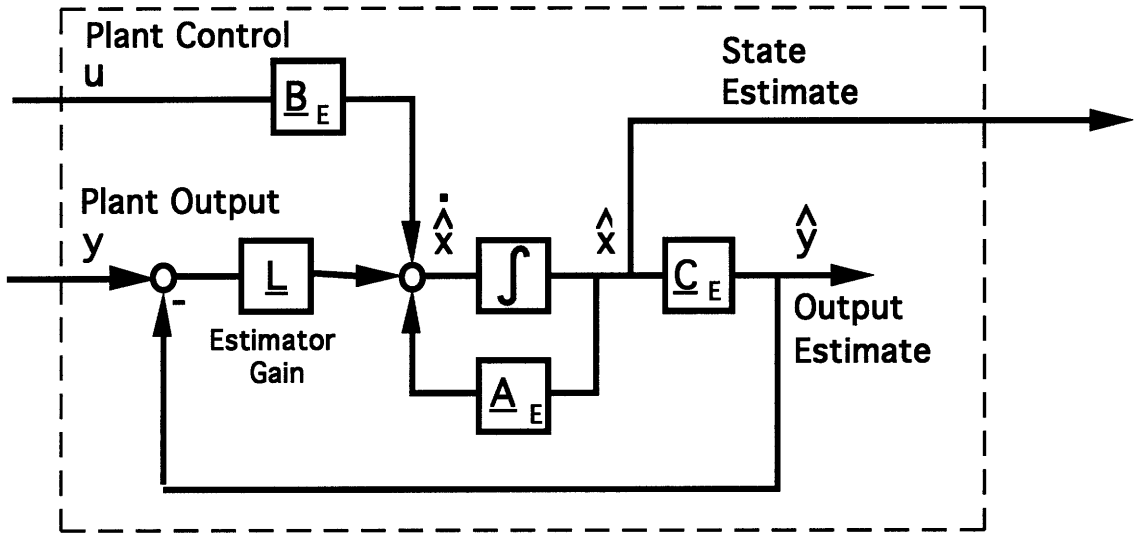

Figure 2.15 shows the block diagram of the estimator which is used in this model. Using an internal representation of the plant, the estimator reconstructs the states of the plant. The estimator then checks its estimated output against the actual output of the system and scales the difference with the optimal estimator gain $\underline{L}$. This allows use of all states for feedback.

The assumption is made that the central nervous system, using its estimates of the states of the system, determines the ankle torques which optimally returns the system to equilibrium. The model also assumes that the optimal control of the system is a linear

combination of the states. By again using the Algebraic Ricatti Equation, an optimal feedback gain , $\underline{K}_V$ can be determined, where v denotes vestibular feedback gain. This gain results in a second control input torque of:

$$u = -\underline{K}_v\hat{x} \qquad \text{Eq. 2.19}$$

A second time delay of 80 milliseconds is included in this feedback path, roughly the time delay involved with vestibular inputs. This time delay is implemented in the same way as the reflexive delay. The only difference between the reflex and vestibular feedback loops, besides the obvious difference in the delay time, is that the white noise that is input into the vestibular feedback loop is filtered by a low pass filter with a corner frequency of 10 Hz, represening the physical plant of the vestibular organs, that tends to filter out some of the higher frequency noise. The matrix $\underline{N}_V$ is set to 0.0075 which makes the variance of the vestibular state error approximately 1.5° for each estimated sway angle.

The system as described above accurately models quiet standing of a person on Earth. For this research effort, an additional variable was added to the system to account for the changes in muscle characteristics following reduced g exposure. A variable muscle gain, G is input into the plant before the muscle model. This scalar value represents the neuromuscular gains of the legs, and is applied to the control signals in both axes before the signals reach the plant. The addition of this variable allows compensation for muscular adaptation during the reduced gravity protocol The final system is shown in Figure 2.16. The model shown is used to validate the hypothesis that changes following low gravity exposure are the result of changes in the muscular activation levels.

This model fails to account for the influence of vision in postural sway. All of the trials conducted were done so with eyes open. Visual influence was not included in the model since visual input was not an independent variable. A future model could incorporate a visual feedback path by conducting half of the posture trials with eyes open and the other half with eyes closed, which would allow visual influence to be determined.

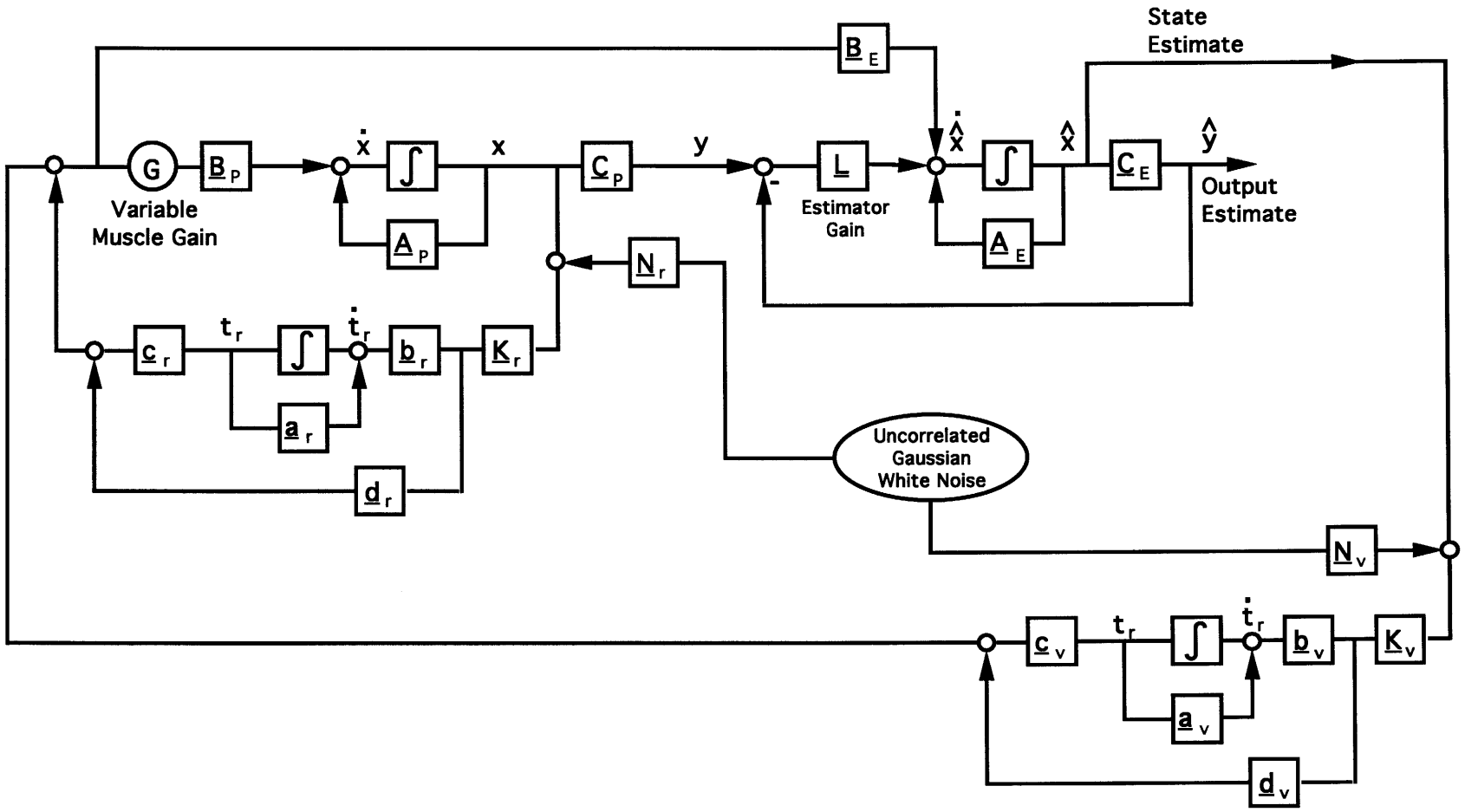

Figure 2.16 Complete Estimator-Based State-Space Model of Posture. This model uses all of the blocks previously constructed. The two plants shown in Figure 2.13 have been combined into a single plant. This plant uses reflexive feedback and estimated states in conjunction with vestibulaer feedback. Sway angle uncertainty is modeled as uncorrelated white noise and effects both the reflexive and vestibular feedback paths.

Chapter 3 Partial Gravity Simulation Techniques

Since the purpose of this thesis is to explore musculoskeletal response following acute exposure to reduced gravity, the design, construction, and evaluation of a partial gravity simulation device is a primary research objective. The main design goal is to simulate reduced gravity while still allowing the subject sufficient range of motion when walking or running. Practicality, cost, and comfort are also considered in the design. There exist three main methods for simulation of reduced gravity environments: parabolic flight, water immersion, and suspension techniques. The first three sections of this chapter explain each of these techniques, and list their advantages and disadvantages. Section 3.4 briefly describes the partial gravity simulator design for this study and discusses the advantages and disadvantages of the system.

3.1 Parabolic Flight

Brief periods of weightlessness or reduced gravity can be attained by piloting an airplane in a parabolic trajectory. This path causes the aircraft to experience a constant vertical acceleration usually ranging between 0 g and normal Earth gravity, 1 g. The true acceleration inside the aircraft is the difference between the downward acceleration of the aircraft and the acceleration due to gravity. The period of reduced gravity lasts anywhere from 25 seconds for a 0 g simulation, to 40 seconds for a Martian g level environment [Shavelson, 1968]. Usually, 40 to 50 parabolas are flown per experimental session. Figure 3.1 shows the KC-135 aircraft and path flown by the KC-135 for lunar gravity flights.

NASA's KC-135 is the aircraft most often used for reduced g simulation. The plane is capable of flying parabolas anywhere in the 0-1 g continuum, but the majority of flights simulate 0 g for astronaut training and for the validation of future space flight hardware. The KC-135 simulator is superior to other forms of reduced gravity simulation in that it replicates the gravity characteristics of space flight or planetary environments. It also allows the subject 6 degrees of freedom in which to operate during the test. However, high cost, limited duration, and limited availability are undesirable aspects of parabolic flight simulation [Newman, 1992].

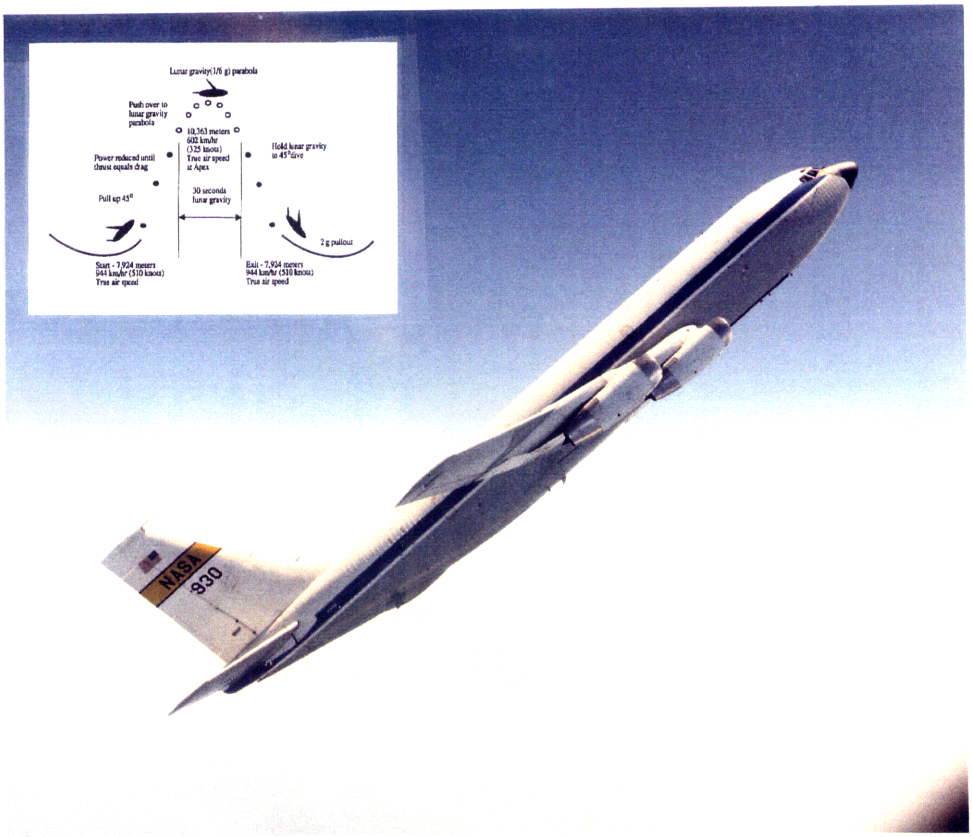

Figure 3.1 The KC-135 aircraft simulates micro-gravity by flying a parabolic trajectory.

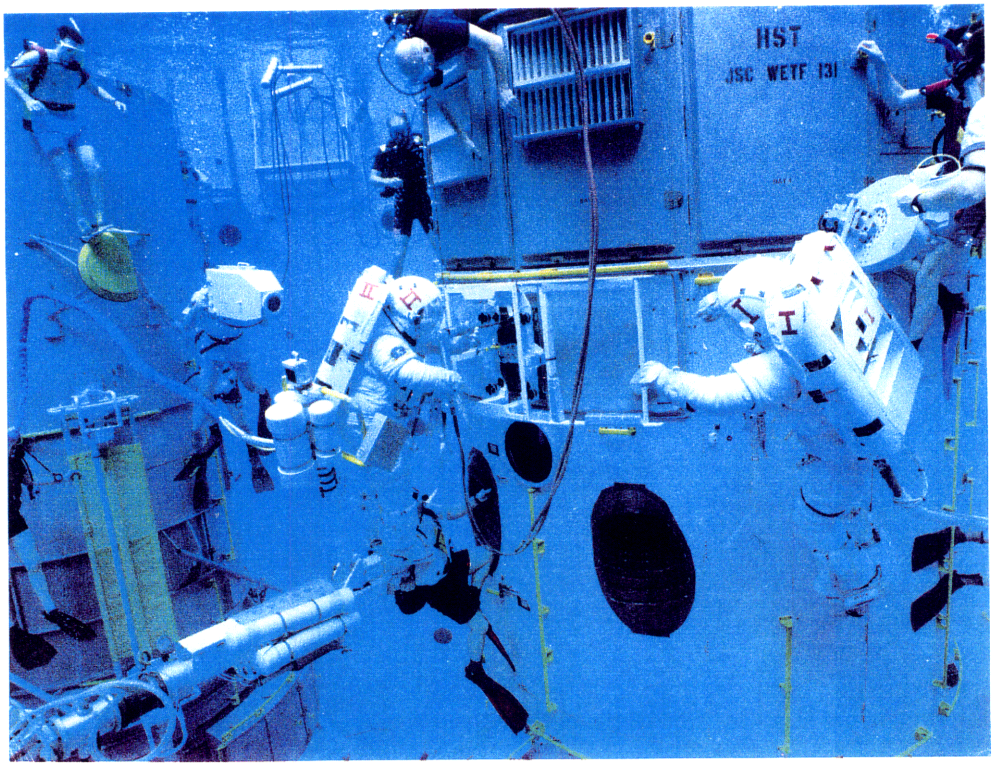

Figure 3.2 NASA's Weightless Environment Training Facility (WETF) simulates weightlessness by achieving neutral buoyancy.

3.2 Water Immersion

Water immersion techniques provide a zero gravity environment by attaining neutral buoyancy on all body segments and equipment involved in the simulation. By adding ballast or buoyancy to a submerged object, its overall density can be made to match the surrounding water; i.e., neutral buoyancy. The object neither rises nor falls, simulating the space environment. NASA's Water Environment Training Facility (WET-F) shown in Figure 3.2 is used for astronaut training at Johnson Space Center, Houston, Texas. Partial gravity is simulated by adding weight in proportion to the desired gravity level. This method was used to successfully train astronauts for Gemini XII extravehicular activities (EVAs) after failed EVAs on previous Gemini flights [Shavelson, 1968]. A human subject can be loaded on various body segments and the torso to attain partial gravity ballasting. The mass and inertial properties of each segment determine the ballast to be added.

Unlike parabolic flight, water immersion simulations can last long enough to realistically simulate most EVA or planetary activities. Water immersion also provides the subject a 6 degree of freedom simulation, like the KC-135. Motion is limited only by the dimensions of the tank and perhaps by the range of life support umbilicals. The blood volume loss that occurs in astronauts in space has also been documented during 8 hours of neutral buoyancy in water. With all of its advantages, water immersion has one major drawback. . . viscosity. The fluid-filled environment of the WET-F is sixty times more viscous than air which is, in turn, more viscous than the space environment. As long as viscosity is recognized, it can be compensated for, but this adds another degree of complexity and uncertainty to the experiment. Also, gravity is still present in this environment and still effects the otoliths in an Earth-normal manner, making the simulation less realistic. Utilizing the water environment is less expensive than parabolic flights, but still not cheap, particularly due to construction costs of the immersion tank. Water immersion also complicates the use of electrical devices which becomes much more problematic under water.

3.3 Suspension Systems

The third method for simulating reduced gravity is a suspension apparatus. By unloading a portion or all of a subject's weight, a partial loading environment can be replicated. Three types of suspension are discussed in this section: overhead suspension systems with counterbalance simulation, body inclination systems, and suspension systems with springs. They each have distinct advantages and disadvantages, but also common pros and cons.

In general, suspension systems are relatively inexpensive. They can be constructed with simple components without extensive specialization. Suspension systems are also practical in that they can be built anywhere there is room for the suspension lines and a sturdy mounting fixture. A common shortcoming of all suspension systems is the limited degrees of freedom provided for natural movement [Hewes, 1969]. This limits the realism with which a subject can train, possibly confounding experimental results. Another problem is that the internal physiological effects of reduced gravity are absent from the simulation. Although the subject may feel suspended, the force of gravity is still acting on all internal organs with the same force as it always has (1 g). A final problem that some, but not all, suspension systems have is comfort. When trying to unload a subject, where the weight is supported becomes an important issue, especially when simulating very low gravity. This can be overcome through careful design of the suspension harness.

3.3.1 Overhead Suspension Systems with Counterweights

This system operates on the normal suspension principle that reduced gravity can be simulated by unloading a portion of the subject's weight. By attaching a counterbalance equaling $(1 - g_{desired})$, the subject may then move in a simulated reduced g environment. An example is shown in Figure 3.3. One problem is that the counterbalance adds momentum to the system and tends to keep the subject moving in the direction of motion. Another problem is that keeping the force constant during vertical motion is complicated. This method has not been used extensively [Shavelson, 1968].

3.3.2 Body Inclination Systems

This suspension configuration inclines the subject on their side so that he is elevated from the horizontal 9.5° (for lunar simulation), resulting in a perpendicular gravity force vector of 1/6 normal g level. An inclined walkway is used for translation. Four cables support the subject at the head, chest, hip, and leg. The cables are attached to an overhead, low friction trolley, adding a degree of freedom to the harness (See Figure 3.4).

Body inclination systems allow relatively normal subject locomotion both forward and backward as well as normal arm and leg movements. Restricting the subject in the lateral direction does not interfere with subject performance in the other axes, although the subject cannot perform lateral jumps in this harness. The mobility problem can be solved by suspending the subject facing upward (or downward), thus allowing the subject normal lateral motion. However, since reorienting the subject now prevents motion in the sagittal plane, the important axis must be identified and the appropriate configuration implemented. Another problem associated with body inclination systems is that the trolley mounted overhead restricts subject locomotion due to friction and slow response times to movements [Sanborn, 1967] and [Hewes, 1969].

3.3.3 Overhead Suspension Systems with Springs

Overhead suspension systems with springs operate on the same basic principle as the overhead system with counterweights, using the force created by springs rather than suspended masses to unload a portion of the subject's weight. Springs are advantageous in that they add no additional inertia to the system, therefore allowing the subject more natural motion than a mass-based system [Farley, 1992].

A spring system has all of the advantages of other suspension systems. It is simple, inexpensive, safe, and effective in allowing the subject to locomote in simulated reduced gravity. However, this system can severely restrict the subject's normal motion. Since changing spring length changes the force imparted by the spring, care must be taken to minimize the vertical excursion of the harness in order to maintain a constant force.

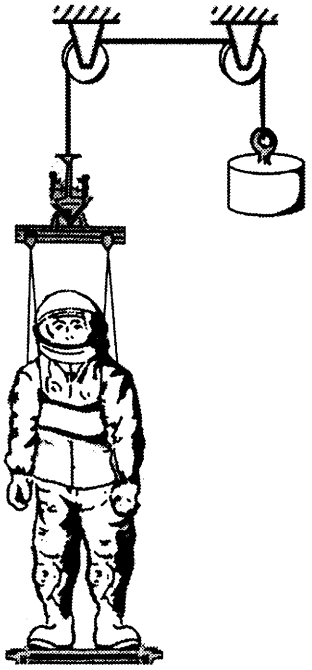

Figure 3.3 shows a generic overhead suspension system with counterweights. This system simulates reduced gravity by unloading a portion of the subject's weight with counterweight.

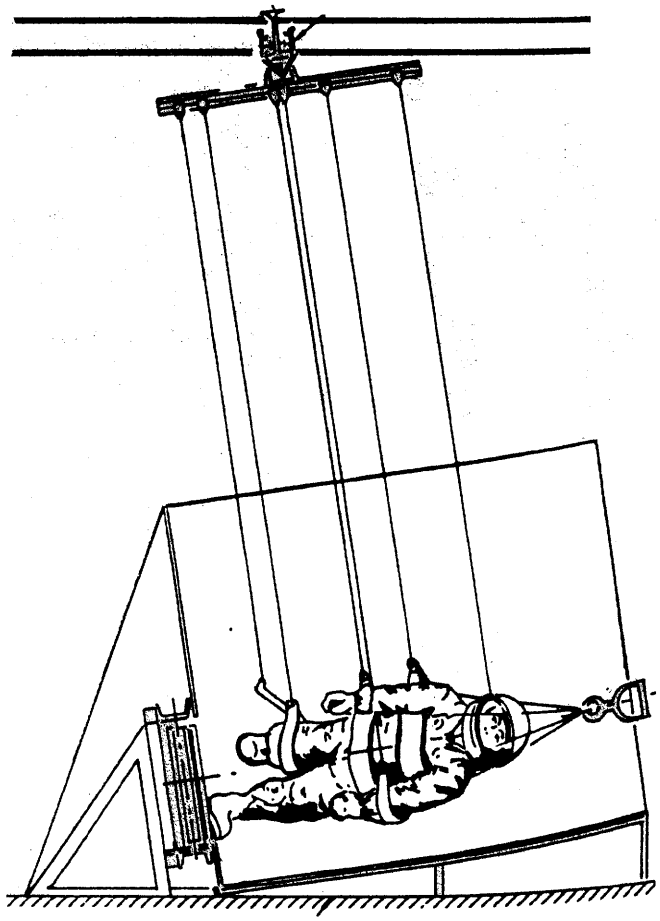

Figure 3.4 shows a body inclination low gravity simulator. The resultant normal force through the platform is one sixth of the vertical normal force.

The simulation apparatus that most successfully met the requirements of this experiment is an overhead suspension system using springs. By using a fixed, wall/ceiling mounted suspension system, a constant force is applied to the subject, allowing normal motions while walking or running on a treadmill. The design features adjustable loading, variable locomotion speeds, and ease of ingress and egress. The final configuration is further discussed in Section 4.2.1, Reduced Gravity Simulator.

Chapter 4 Methods

This chapter describes the methods of the partial gravity locomotion experiments. Section 4.1 describes the subjects who participated in the metabolic and musculoskeletal experiments. Following this, equipment designed for the experiment is described, as well as all other hardware used. Finally, the experimental protocols for each experiment are outlined, first for the metabolic experiments, then for the musculoskeletal.

4.1 Subjects

Ten healthy subjects, five men and five women, participated in the metabolic experiments. Subjects range in age from 21 to 40 years, height from 1.6 to 1.8 m, and weight from 512 to 770 N. A summary of subjects is located in Table 4.1. Subjects varied in level of physical conditioning. Weekly time spent exercising varied from 1 to 12 hours per week. All Subjects felt comfortable running at speeds up to 3.2 m/s, and were free from any orthopedic or respiratory problems. Informed consent was obtained for all experiments, and subjects were permitted to withdraw from the study at any time for any reason. Appendix B includes a copy of the informed consent form that was signed by all subjects before their participation.

For the musculoskeletal part of the experiment, five men and five women were used as subjects. These subjects range in age from 20 to 30 years, height from 1.57 to 1.95 m, and weight from 512 to 936 N. A summary of subjects is located in Table 4.2. Since this part of the experiment required a lot of running, all of the subjects were in good physical condition, felt totally comfortable running at speeds up to 3.2 m/s, and were free from any orthopedic or respiratory problems. As before, informed consent was obtained for all experiments, and subjects were permitted to withdraw from the study at any time for any reason.

Table 4.1 Subject Database-Metabolic Experiment

Subject	Gender	Age(yr)	Height(m)	Mass (kg)	Weight(N)
1	M	23	1.78	77.1	756
2	M	23	1.75	78.5	770
3	F	21	1.63	61.2	600
4	F	27	1.65	59.9	588
5	M	25	1.80	73.5	721
6	F	30	1.63	52.2	512
7	M	29	1.83	78.0	765
8	F	21	1.75	78.0	765
9	F	21	1.70	63.5	623
10	M	40	1.75	76.7	752

Table 4.2 Subject Database-Musculoskeletal Experiment

Subject	Gender	Age(yr)	Height(m)	Mass (kg)	Weight(N)
A	M	23	1.78	77.1	756
B	M	23	1.95	95.5	936
C	M	29	1.83	78.0	765
D	F	21	1.75	78.0	765
E	F	21	1.63	61.2	600
F	M	23	1.75	78.5	770
G	F	30	1.63	52.2	512
H	M	25	1.80	73.5	721
I	F	20	1.57	61.8	606
J	F	21	1.67	56.8	557

4.2 Equipment

Equipment for this experiment includes a force sensing device (forceplate), reflex measuring apparatus, metabolic measurement hardware, video equipment, and the partial gravity simulator. A suspension harness serves as the partial gravity simulator by unloading a portion of the subject's weight during walking and running. This harness is detailed in Section 4.2.1, Reduced Gravity Simulator. The treadmill used for subject locomotion while on the partial gravity simulator is described in Section 4.2.2, Treadmill. Then a description of the strain gage force platform that provides force sensing and

posturography capability is given. A reflex hammer fitted with an accelerometer and EMG electrodes to determine reflexive changes in the subject are described in sections 4.2.4 and 4.2.5, Accelerometer/Reflex Hammer and EMG. Next, the video system is described. Finally, a description of a Power Mac computer outfitted with an Input-Output (I/O) board and an Audio-Visual (A/V) board that served as a data acquisition tool is given.

4.2.1 Reduced Gravity Simulator

The design of the parital gravity simulator is based on an apparatus previously used at the Harvard Field Station [He, 1991] and [Farley, 1992]. The simulator reduces loads carried by the lower limbs, effectively treating the rest of the body as a point mass centered on the pelvic bone. The vertical unloading force is produced by stretching two garage door springs in series along the wall. The level of unloading can be controlled from an electric winch mounted to the floor, operated by a hand held controller and powered by a standard 12 volt car battery. A set of two 3 mm wires run from the top of the springs, along the ceiling, and down to a harness. The wires are supported at two points along the ceiling by pulleys affixed to 10.2x10.2 cm supports by eyebolts. The supports were in turn secured to the ceiling using pairs of Hilti brand drop-ins and 6 mm bolts. This method provides a convenient and secure means for reduced gravity simulation.

The wires connect to the harness at two support straps that are, in turn, connected to both ends of a U-shaped PVC pipe. Attached to the PVC pipe is a soft gel bicycle seat. The subject can then straddle the PVC pipe and sit securely in the bicycle seat. A mountain climbing harness is added to secure the subject to the seat and PVC pipe while running or walking. The complete harness allows up to 90% of the subject's weight to be unloaded, while still permitting normal gait for both walking and running (See Figure 4.1).

4.2.2 Treadmill

Although the harness described above provides a satisfactory reduced gravity simulation environment, it does not allow the subject to translate. This fact necessitates using a treadmill. While the harness was custom designed and constructed, a commercially manufactured treadmill was purchased. The Trotter CXT plus treadmill (Plum Treadmill, Cambridge, MA) was sturdy and reliable, with variable and, more importantly, constant speed control, allowing the subject to walk normally while suspended in the harness. The

CXT is capable of speeds ranging from approximately 0.5 to 4.5 m/s and variable grades from level to +20 degrees. The speeds are stable to ± 2% for a walking (1.0 m/s) or running (3.0 m/s) subject weighing up to 900 Newtons. The treadmill was not inclined for any part of this experiment. Figure 4.1 shows the CAD drawings of the complete reduced gravity simulator including the harness and treadmill.

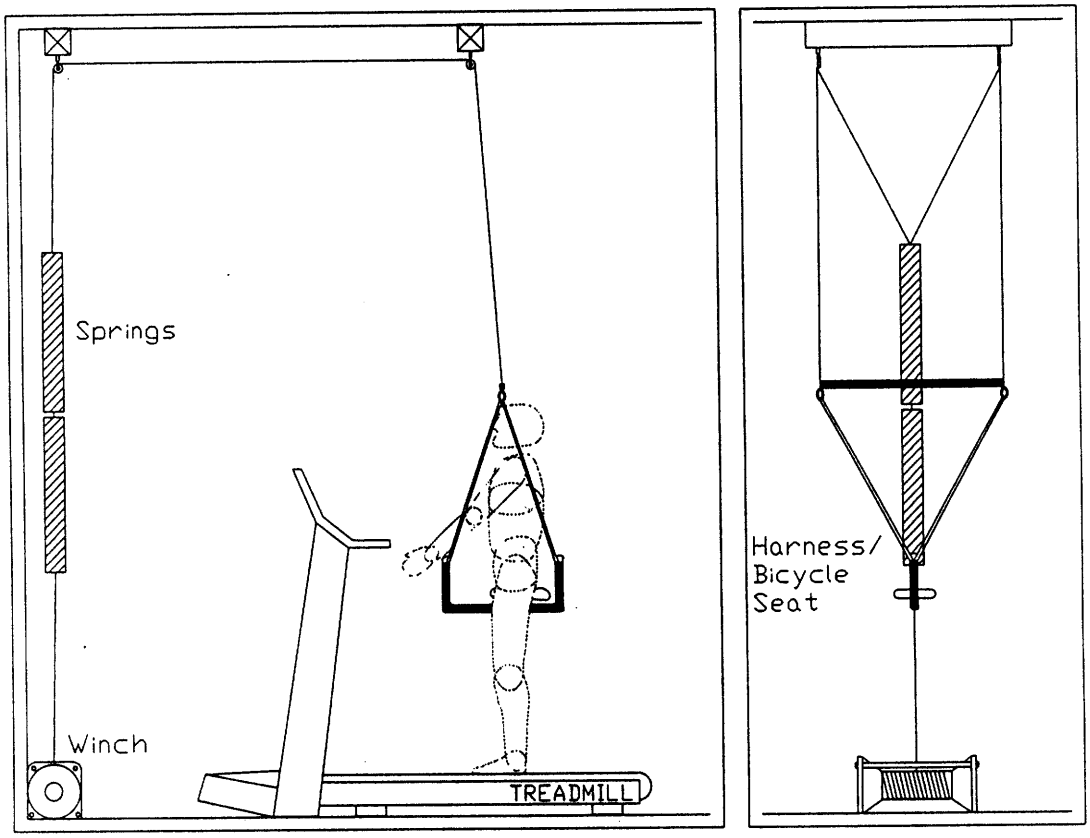

Figure 4.1 Partial g Simulator and Treadmill. The simulator and treadmill are capable of simulating environments from 5 to 90% normal Earth gravity at speeds ranging from 0.5 to 4.5 m/s.

4.2.3 Force Platform and Amplifier/Conditioner

The forceplate chosen is the Advanced Medical Technology, Inc. OR6-5 series force platform (AMTI, Newton, MA). The OR6-5 provides data for both the walking and posture protocols. Its low noise characteristics allow both ground reaction forces and center of pressure measurements to be obtained accurately. The AMTI MCA amplifier which accompanies the OR6-5 provides high gain, low noise amplification of the platform signals, facilitating acquisition by a digital computer. This platform uses full bridge strain gages mounted on four elements to measure three orthogonal force components and the moments about those three axes. The bridges use an excitation voltage of 10 V. The forceplate has a temperature sensitivity of 0.02% per degree Fahrenheit and less than 2% crosstalk on all channels. The forceplate has a maximum load capacity of 4500 Newtons and a resonant frequency of 500 Hz, well above the frequencies of interest for this experiment. The forceplate is 51 cm long by 45 cm wide, a more than adequate surface area for this experiment. The forceplate is factory calibrated in all axes in both English and metric units. The forceplate is shown in Figure 4.2.

The rack-mounted signal amplifier delivers excitation voltage to the forceplate strain gages in addition to performing high gain, low noise amplification of the 6 forceplate signals. The amplifier features easy bridge-balancing with dual LED balancing indicators to guarantee accurate signals. The amplifier also has variable gain settings of 1000, 2000, and 4000 as well as low pass filtering with variable corner frequencies of 10.5 or 1050 Hz. For the entirety of this experiment, the gain and low pass filtering were set at 4000 and 10.5 Hz, respectively. The amplifier is shown in Figure 4.2.

To facilitate natural walking motion over the forceplate, a wooden platform was constructed and placed around the OR6-5. The platform is 3.1 meters long, with a ramp at each end, and a 7.6 cm high, 1.5 m long level plateau around the forceplate. This platform can accommodate five normal steps: one on the first ramp, one before the plate, one step squarely on the surface of the plate, one after, and one step down the opposite ramp. The symmetrical design allows the subject to cross the plate naturally in either direction.

4.2.4 Accelerometer/Reflex Hammer

In order to accurately measure the latency of stretch reflex response, two variables must be recorded: muscle activation via EMG and strike hammer acceleration. By marking the time the hammer strikes the subject's patellar tendon, and the time of muscle activation, the latency can be deduced.

The hammer is a medical stretch reflex hammer from a medical supply store (Harvard Medical Coop, Cambridge, MA). The steel hammer is fixed with rubber plugs at each end. For this experiment, one of the stoppers has been removed and replaced with a machine screw which is epoxyed in place. An accelerometer is attached to the screw at the back of the hammer (See Figure 4.2). This enables the y-axis acceleration of the hammer to be measured. Upon striking the patellar tendon, a spike in the acceleration will appear, denoting that acceleration has reversed, and therefore, that the knee has been struck.

4.2.5 EMG

To record the muscle activation level, an electromyogram (EMG) is used. By measuring the ionic flow through the muscle, the EMG determines the relative levels of muscle activation. Since the signal measured by an EMG dependents upon many other things (most importantly, the placement of the electrodes), absolute activity level of the muscle cannot be determined. However, once the electrodes have been secured on the subject, relative levels of activation can be accurately obtained.

To aid in successful acquisition of this signal, an EMG preamplifier (pre-amp) is used (Iomed, Inc., Motion Control Division, Salt Lake City, UT). This pre-amp provides on-site amplification and band pass filtering to ensure that the EMG signal is uncorrupted when recorded. On-site amplification is particularly important in this case due to the fact that the voltage levels being recorded are so small they could easily be corrupted by a traveling through a long wire before amplification. This EMG enables recording to be conducted without gel or other electrode preparations. Figure 4.2 shows the EMG pre-amp.

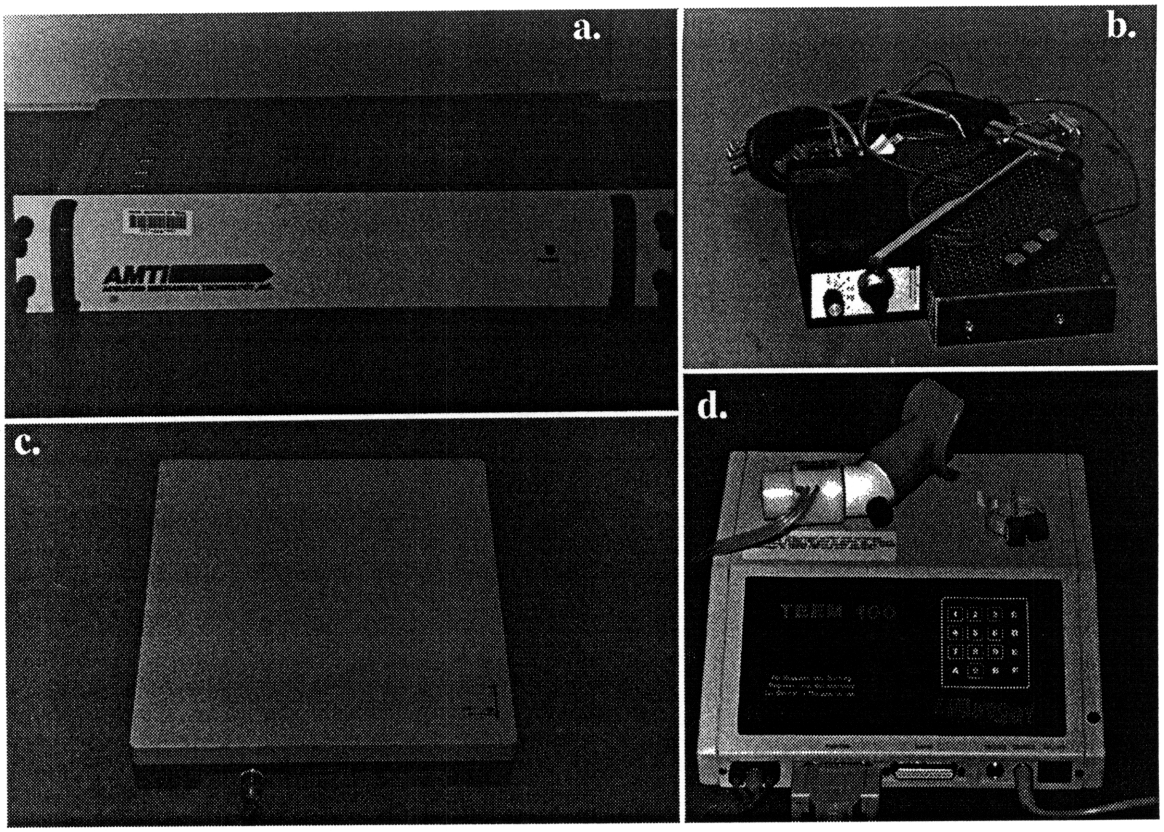

Figure 4.2 Experiment Hardware. Part a) shows the AMTI forceplate signal amplifier. The reflex hammer, and EMG pre-amp are pictured in part b). The AMTI forceplate is shown in part c). Finally, Part d) pictures the AeroSport, Inc. TEEM 100 metabolic analyzer.

4.2.6 Video System

In addition to the forceplate measurements, a video system was used during gait analysis to help determine joint angles and body mass excursions during walking. The video system consists of a Sony Handycam Video Cassette Recorder, a Power Mac 8100/80 for analysis, a Macintosh A/V Board for video acquisition, and acquisition/analysis software. The camera has Hi-8 capability, connecting to the Power Mac via an S-Video cable. The signal is then captured using Fusion Recorder™ software (Video Fusion, Inc.). The digitized frames are then analyzed using Adobe Photoshop™ graphics program (Adobe Systems, Inc.). By clicking on the reflective markers and recording, the x and y positions of each marker, joint angles and point excursions can be determined. Comparisons can then be made between pre- and post-exposure trials. Analysis of the x and y coordinates recorded was accomplished using Matlab™ Analysis software (The MathWorks, Inc., Natick, MA).

4.2.7 Metabolic Measurement System

An expired volume analyzer accurately measures the subject's energy expenditure while on the treadmill. As explained in Section 2.3, Energetics and Workload, after a short period of activity (approximately 1 minute), all energy exchange within the muscles is due to the metabolism of oxygen by the muscles. By analyzing the content of the inhaled and, more importantly, exhaled air, the amount of energy consumed can be easily determined. For this experiment, the TEEM 100 (Total Energy Expenditure Measurement) from AeroSport, Inc. is used (AeroSport, Inc., Ann Arbor, MI). The TEEM 100 was chosen because it is affordable, portable, and reliable. The TEEM 100 offers three different expirator sizes: low, medium, and high, each for the corresponding expired volume. The TEEM 100 computes, displays, and stores data every 20 seconds. The variables displayed include: volume of oxygen used, volume of carbon dioxide used, total respiratory volume, metabolic rate, heart rate and, respiratory quotient. The TEEM 100 is shown in Figure 4.2.

4.2.8 Data Acquisition Apparatus

To record the signals from all other equipment, special data acquisition hardware is necessary. The entire set up consists of a digital computer, an acquisition board to convert analog signals to digital messages, and an adapter to allow easy BNC

connections. The computer used for all acquisition and analysis is a Power Mac 8100/80 with 16 Mbytes of RAM and a 1 Gigabyte hard drive for data storage. The Power Mac is equipped with a special A/V Board to allow analysis of video signals recorded during the trials. LabView™ software was used for acquisition and analysis (National Instruments™). LabView™ offers a flexible environment for scanning, acquiring, and analyzing all data channels at once. The specific scripts written for this experiment can be found in Appendix C. The data are conditioned for the computer by a National Instruments™ NB-MIO-16L Data Acquisition board. The board allows up to 16 channels of data to be simultaneously acquired at a maximum rate of 100 kHz, which greatly exceeds the needs of this experiment. The board has other capabilities including digital output, triggering and timing functions, none of which were used for this experiment. Although the NB-MIO-16L makes it possible to input analog data into the digital computer, the input source is a 50 pin ribbon cable, which is obviously inconvenient for this experiment. To solve this problem, a BNC adapter card augments the system. Also manufactured by National Instruments™, the BNC 2080 works with the NB-MIO-16L to allow 16 input and 2 output channels to be connected to the computer via BNC connector cables. The board can operate in either 8 channel differential mode or, as is the case for this experiment, 16 channel single-ended mode. The board also allows for analog filters and conditioners to be constructed for each channel. For this experiment, no analog filtering has been used.

4.3 Experimental Protocols

This section describes the specific steps involved in each of the experiments performed. Metabolic experiments are outlined in Section 4.3.1, followed by Section 4.3.2, Musculo-skeletal Experiments which includes the reflex, gait, and posture protocols.

4.3.1 Metabolic Experiments

The purpose of the metabolic measurements was to determine the amount of energy consumed by the subject while suspended at various g-levels and moving at various speeds. A trial was begun by recording the oxygen the subject consumed while standing motionless, representing the amount of energy necessary for the subject to remain standing upright. This energy level was denoted as the subject's 'baseline' energy consumption. The subject was then placed on the treadmill at one of three gravity levels: 1 g, 3/8 g, or 1/6 g. Once a constant gravity level was achieved, the treadmill was turned

on at one of two velocities, 1 or 3 m/s. To prevent fatigue, the 1 m/s trials were always conducted first. The subject was then instructed to locomote and breathe normally for the duration of the 4 minute trial. During that time, metabolic data were sampled and recorded. The subject was then given a brief rest period before the next trial. The gravity and/or velocity condition was changed and the protocol repeated.

4.3.2 Musculoskeletal Experiments

The musculoskeletal experiments were conducted to characterize changes in lower leg musculature following brief exposure to simulated reduced g locomotion as well as to understand the transient nature of these changes. A battery of tests was run both before and after the exposure. The tests included a reflex test, postural stability evaluation, and a gait analysis test.

The stretch reflex protocol involved measuring the latency between strike of the patellar tendon and activation of the quadricep muscles in the upper leg and closely resembles the procedure followed by a doctor during a physical exam. This protocol began by securing an EMG to the quadricep of the subject, and verifying that a clean signal was received by the computer for both the EMG and the hammer accelerometer. The subject was then seated and instructed to relax, with the leg of interest crossed over the other leg. The subject was then struck on the patellar tendon several times as both the acceleration of the strike hammer and EMG signal were recorded. This was repeated several times in order to assure repeatability of the results.

The posture protocol was conducted to determine any change in postural stability following low g running. For these measurements, the subject was told to stand on the forceplate with their feet at a comfortable distance apart. They were then instructed to stand normally, with their hands at their side while fixating on a point directly in front of them. Eight (pre-exposure) or six (post-exposure) 30 second trials were then recorded while the subject stood still on the forceplate.

For the gait analysis protocol, the subject was instructed to walk normally over the forceplate several times. To aid in video analysis, reflective markers were placed on the subject's shoulder, hip, knee, and ankle joints. Since looking at the ground while walking would change the subject's gait, several practice steps were taken to ensure that the subject could walk without looking down and his foot would be on the platform during

the entire contact phase of the step. Video signals and ground reaction forces were recorded during this part of the experiment.

These nominal reflex, posture, and gait measurements were followed by the low g conditioning protocol. To induce the heavy legs phenomenon, the subject was unloaded to Martian g level. The subject then ran at 3.0 m/s (6.7 mph) for 6 minutes. Pilot studies determined that running was more effective than walking in inducing the heavy legs phenomenon, and that 5-6 minutes was a sufficient exposure duration for reaching steady state muscle gain. Heart rate, stride length, and stride frequency were recorded during the exposure period. After 6 minutes, the subject was quickly unloaded and egressed from the harness.

Following exposure, one of three heavy legs countermeasures procedures was followed. The first was a control test in which no exercise countermeasures were performed. The order in which these countermeasures were performed was randomized to avoid any order effects (See Table 4.3). For the second procedure, the subject was instructed to perform 5 low knee bends before beginning the post exposure analysis. Knee bends require a quasi-static force with a relatively high magnitude, but low rates of change of the forces involved. The performance of a series of 3 normal broad jumps determined if higher time rate of change in velocity aids in post-exposure adaptation. The forces required to execute broad jumps are large in magnitude, but also have high rates of change of forces.

Table 4.3 Post Exposure Exercise Order

Subject	Trial 1	Trial 2	Trial 3
A	None	Knee	Jump
B	None	Jump	Knee
C	Knee	None	Jump
D	Knee	Jump	None
E	Jump	Knee	None
F	Jump	None	Knee
G	None	Jump	Knee
H	Jump	Knee	None
I	Knee	Jump	None
J	None	Knee	Jump

Following performance of the post exposure exercise, each of the experiments mentioned earlier was repeated, first the reflex protocol, followed by three posture tests, then the gait analysis protocol, and finally, three more posture tests. After the analysis of four subjects, the reflex protocol was dropped due to conclusive results in agreement with the hypothesis that no change in reflex latency was incurred due to partial gravity exposure. The remainder of the tests were performed as described above.

4.4 Data Analysis

This section describes all of the analysis methods used during this experiment. Section 4.4.1 outlines the analysis of the Metabolic data acquired during the first part of this experiment. Section 4.4.2 describes the reflex protocol analysis. Section 4.4.3 describes the methods for analyzing the posturography data and is broken up into two parts, spatial and temporal analysis of posture data. Finally, Section 4.4.4 describes the analysis of the video and forceplate data for the gait protocol.

4.4.1 Metabolic Data Analysis

The means for acquiring the metabolic data have been described in Section 4.2.7, Metabolic Measurement System. The TEEM 100 outputs data at 20 second intervals. The most useful variable provided by the TEEM is the amount of oxygen consumed per minute of activity. This variable was recorded for the full partial gravity simulation at three gravity conditions, and during walking and running.

Transient data is defined as any data which occurred before phosphagen production reached steady state. Any such data was discarded. The transient time was determined for each subject individually, and was defined as the last point at which all points afterward were within one standard deviation of the mean. Although different transient times were determined between subjects, the time used was consistent for all 6 conditions within subjects. Also, the last 20 seconds of metabolic data was not used for any subject to avoid the effects of additional effort contributed by the subject at the end of the trial.

This raw data was processed and plotted in one of two ways. The first plot compared the oxygen consumption of the subject to the gravity level for both the walking (1 m/s) and the running (3 m/s) conditions. The baseline $\dot{V}_{O_2}$ output of each subject was subtracted from the consumption values of the running and walking protocols. Oxygen uptake was

then divided by the mass of the subject to yield a normalized oxygen consumption value across subjects. The milliliters of O_2 consumed per kilogram per minute were then plotted versus g-level.

The second means of metabolic data analysis incorporated an additional normalization step. By dividing the previous values by the speed of travel, oxygen consumption values that are normalized for mass and distance can be derived. The $\dot{V}_{O_2}$ was multiplied by a constant of 21 joules per milliliter of O_2 consumed, resulting in a cost of transport (CoT) in joules per kilogram-meter. Cost of transport reveals the amount of energy necessary to move a unit of mass a certain distance and allows comparison of the gaits in a different, and somewhat more pragmatic sense. CoT allows the most efficient means of locomotion to be determined, whether on Earth, the moon, or Mars.

4.4.2 Reflex Latency Analysis

The analysis of the reflex data consisted of determining the latency between the hammer strike and the activation of the muscles. Due to the inherent noise of the EMG signal, the actual magnitude of the activation level of the muscle could not be determined. However, the patellar tendon strike produced a large enough response that activation of the muscle could be perceived. The latency was determined automatically, by simply measuring the time difference between the hammer strike and muscle activation. Figure 4.3 shows a typical reflex latency plot. The accelerometer affixed to the hammer produced a large spike upon striking the leg of the subject. The point of maximum voltage was called t_0, for initial time. The analysis program then looked for an increase in the EMG signal during the next 0.5 s. It tagged the first peak in activation level and determined the time difference between the two points, Δt. Although this analysis is automated, due to the noisiness of the EMG signal, and the fact that a response was not always elicited, the analysis was double checked by a human operator. The latencies were then compared for all conditions for each subject.

The reflex data was acquired by the LabView™ script **hammer_accel.vi**. The wiring diagram summary of this script is plotted in Appendix C. The reflex data was analyzed by the Matlab™ script **reflex_analyze.m**. The text of this program can be found in Appendix D.

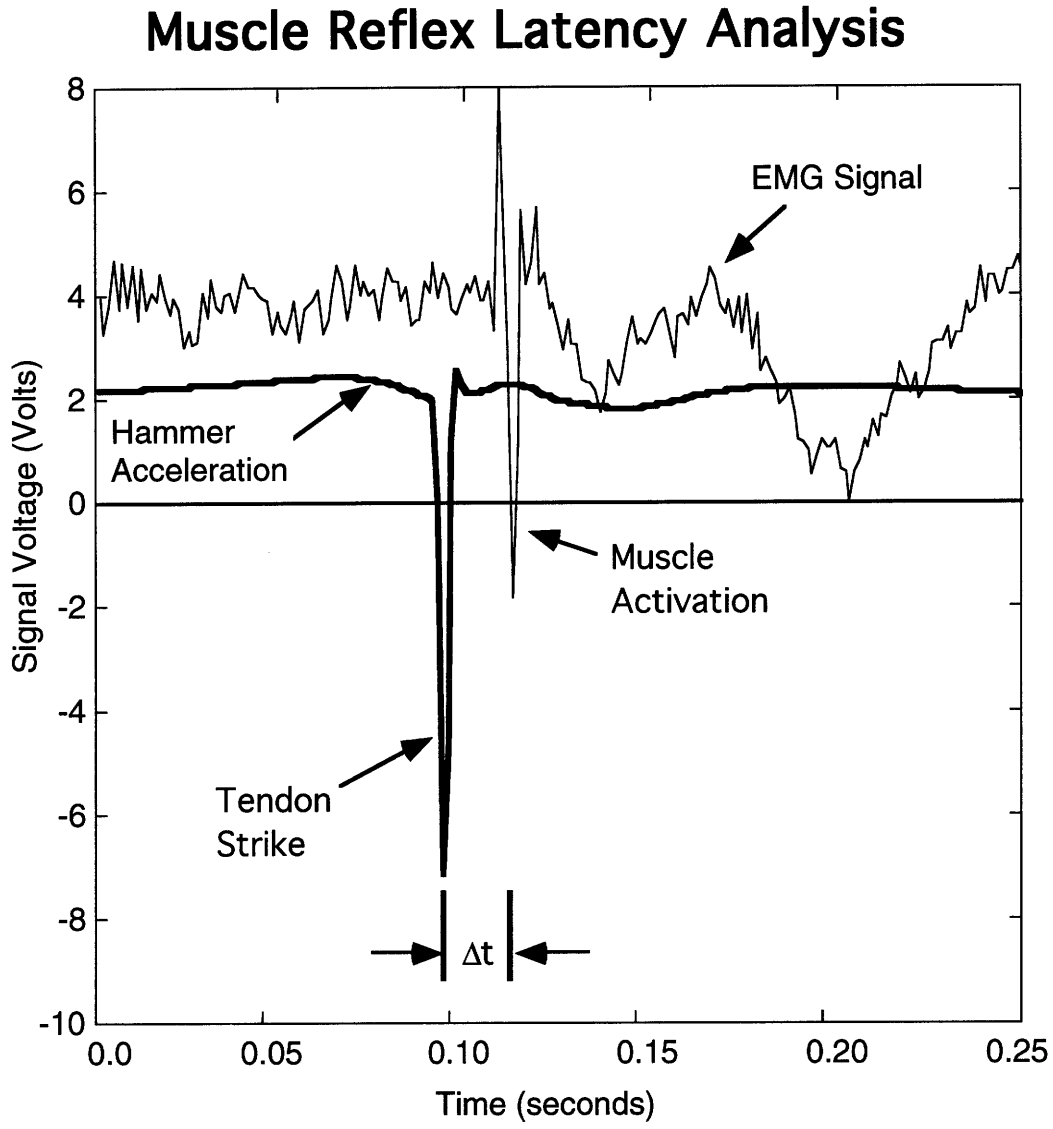

Figure 4.3 Reflex Latency Analysis. By measuring the acceleration of the strike hammer and the muscle activity (EMG), the stretch reflex latency time can be determined. A spike appears in the acceleration plot at the point of contact. This is followed by an increase in muscle activity which is marked by a large spike in the EMG signal. The delay between the two signals is the reflex latency.

4.4.3 Posturography Analysis

The analysis techniques for the posture measurements are split into two main parts, spatial analysis that is concerned with the location of the center of pressure of the subject, and temporal analysis that is concerned with the time domain characteristics of postural behavior. Spatial analysis methods are discussed first followed by a discussion of temporal analysis.

The first step in analysis of posture is to determine the center of pressure of the subject. The variables available from the forceplate are the forces and moments in the x, y, and z axes. The conventions for moment and force directions were discussed in Section 1.4, 1.5.2 Conventions. By dividing the moment by the force, the distance from the CoP to the center of the forceplate can be determined using the following equations:

$$x = \frac{-M_y - F_x z}{F_z} \qquad \text{Eq 4.1}$$

$$y = \frac{M_x - F_y z}{F_z} \qquad \text{Eq. 4.2}$$

where F_x, $_y$, and $_z$ are the forces in the x, y, and z axes
M_x, and $_y$ are moments about the x, and y axes, respectively and
x, y, and z are the distances from the origin of the forces.

Since the distance from the top of the plate to the center of the axis, z, is known, and the moments and forces are measured variables, the only unknowns in the two equations are the x and y positions, respectively. A typical plot of CoP position over time is shown in Figure 4.4.

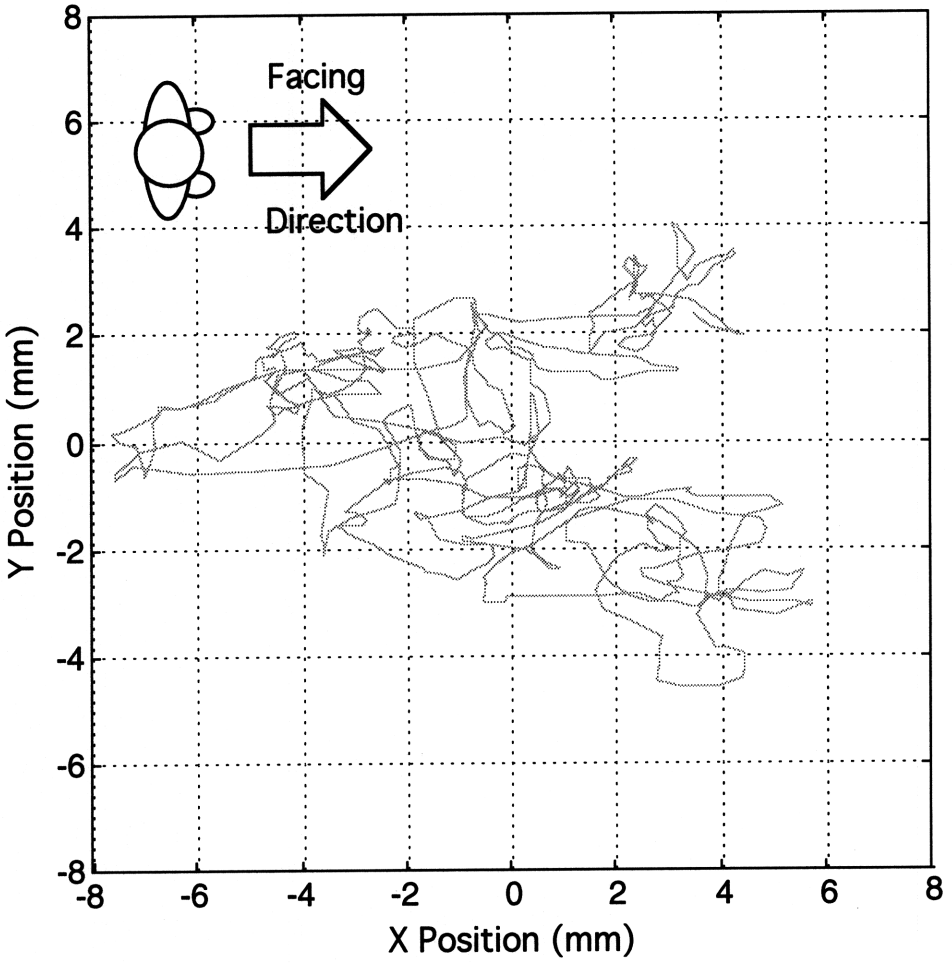

Figure 4.4 shows a typical time trace of the Center of Pressure (CoP) of a human subject during a 30 second trial. Typically, the subject sways significantly more in the sagittal plane (X axis) than in the coronal plane (Y axis). Each trial was conducted with feet shoulder width apart, hands at the sides, and eyes open and fixated directly in front of the subject.

Once the x and y coordinates have been determined, the first and last 5 seconds of each trial were discarded to eliminate the effects of sways which could have taken place early or late during the trial. The average position was subtracted from the x and y position to give the subject's position zero mean in each axis. The rms position of the CoP was determined in the x and y axes and also as a resultant rms.

Temporal analysis is somewhat more complex. The primary underlying assumption of temporal analysis is that quiet standing is a random process and that, although CoP position can not be predicted outright, it is possible to characterize its behavior stochastically. It was assumed that standing can be modeled as a two dimensional random walk, or as a pair of uncoupled one dimensional random walks. Over time, the mean square displacement $<\Delta x^2>$ of a one-dimensional random walk is related to the time interval Δt by the expression:

$$\left\langle \Delta x^2 \right\rangle = 2D\Delta t \qquad \text{Eq. 4.3}$$

where the parameter D is the diffusion coefficient, or the average measure of stochastic activity of the person standing. This relationship can be further generalized by the non-linear relationship:

$$\left\langle \Delta x^2 \right\rangle = \Delta t^{2H} \qquad \text{Eq. 4.4}$$

where H can be any real number between 0 and 1. This variable is somewhat more revealing than D in that H relates past trends in data to future behavior of the system. An H value of 0.5 corresponds to classical Brownian motion in which past behavior is in no way related to future behavior of the system. If $H>0.5$, the system is said to exhibit *persistence*, which means that the system is likely to keep behaving in the same manner as it previously was. The opposite situation occurs when $H<0.5$, or when the past and future increments of the system behavior are negatively correlated, meaning that the system is more likely to change behavioral patterns. This is referred to as *anti-persistence*.

The first step in analyzing the trial in the time domain involves comparing the position of the CoP at time t to the position of the CoP at time $t+\Delta t$. This was done as Δt went from zero to 10 seconds. This method of analysis is shown in Figure 4.5. Although the figure shows only total displacement analysis, the same analysis was repeated in one dimension for both the x and y axes. This step provided the basic building block for temporal analysis [Collins, 1993].

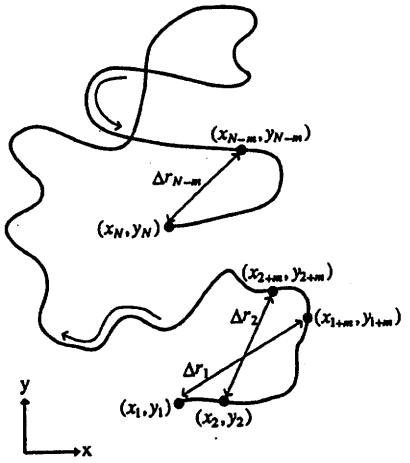

Figure 4.5 Temporal analysis of CoP stabilogram for a data set with N data points.

However, due to the natural variation in temporal signatures, it was necessary to average several 30 s trials at this point. Therefore either 8 (for pre-exposure trials) or 6 (for post exposure) trials were averaged together. The average was then plotted with the average squared distance between points ($\langle r^2 \rangle$) versus change in time (Δt). This plot is normally comprised of two lines with different slopes, the first with a somewhat higher slope than the second. The point at which these two lines meet is called the critical point. Figure 4.6 shows the general form of this plot [Collins, 1993].

From Figure 4.6, six variables are derived, the diffusion coefficients of the system, that are actually the slopes of the two lines for the x, y, and total distance cases. These variables are represented by D_S, D_{XS}, D_{YS}, D_l, D_{Xl}, and D_{Yl}, where the s subscript means one half of the short time constant slope, and the l subscript is one half of the slope of the long time constant line. These are found through simple regression of the two lines with the short time constant lines forced to cross through the origin and the long time constant line allowed two degrees of freedom (slope and intercept).

By plotting the mean square distance versus the time interval on a log-log scale, the H values of the system can be calculated through regression, this time allowing two degrees of freedom for both the short term, and long term behavior. All of these variables have been recorded and tabulated for comparison.

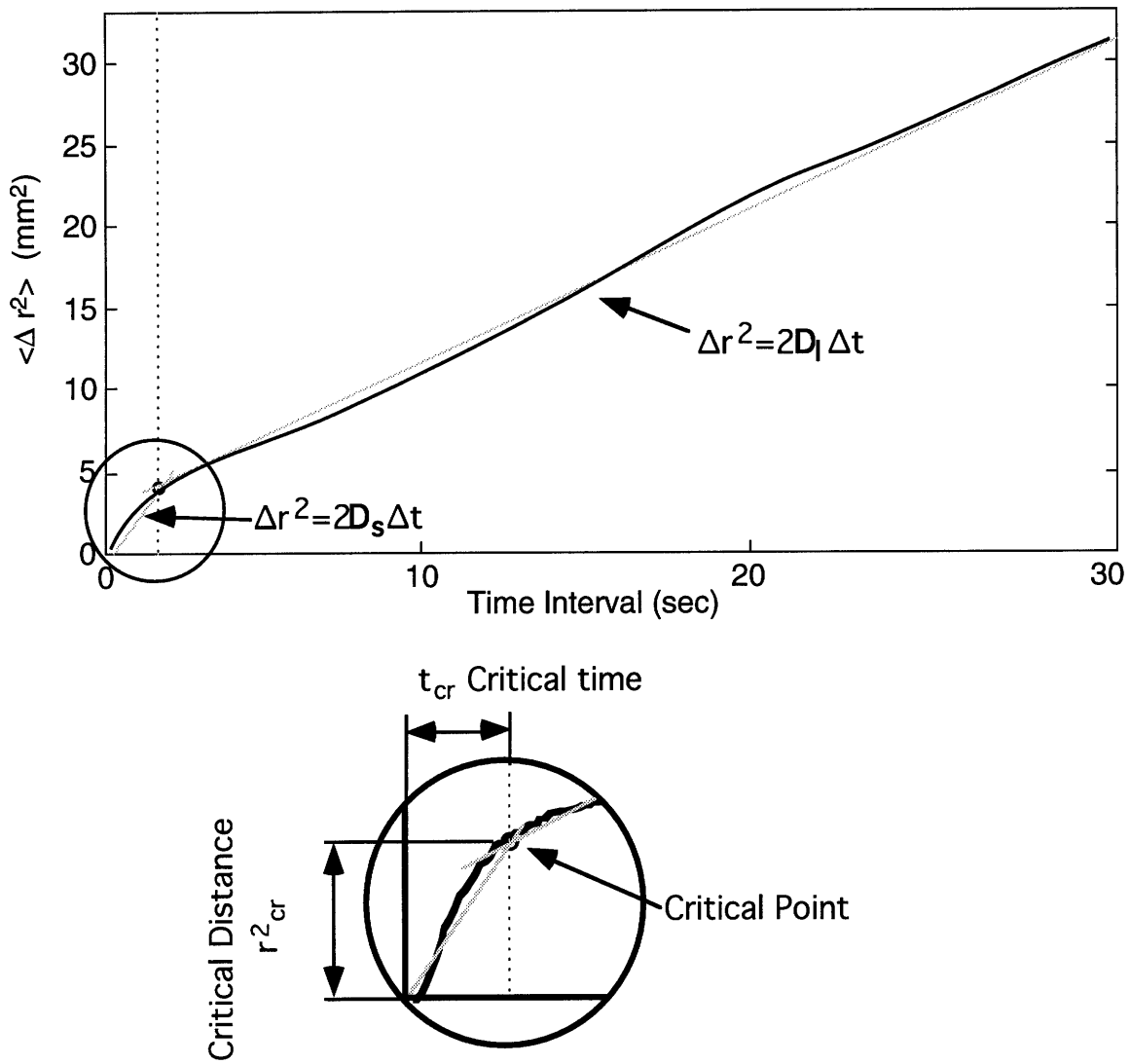

Figure 4.6 Stabilogram Diffusion Plot. This plot shows schematically how the temporal data is presented and analyzed. The data in the top plot (solid lines) is observed to have two different slopes (lighter lines), a steep slope close to zero, and a more shallow slope at higher time intervals. The slope of these lines is equal to 2*D where D is the Diffusion Coefficient. The intersection of these two lines is called the critical point. The critical time and critical distance can be derived easily from the critical point.

The posture data was acquired by the LabView™ script **posture.vi**. The wiring diagram summary is located in Appendix C. The first part of this analysis was conducted by the Matlab™ script **posture_analyze.m** which can be found in Appendix D. The averaging steps and computation of D and H values was carried out by the script **posture_analyze_step2.m**, also located in Appendix D.

4.4.4 Gait Analysis

The gait analysis was carried out in two steps, forceplate analysis, and video analysis. The forceplate analysis, was largely automated and is discussed first, followed by a description of the video data analysis procedure, most of which was manually conducted.

The LabView™ program **Forceplate.vi** was used for data acquisition and can be found in Appendix C. Forceplate data consisted of either 6 or 8 steps in sequence, with three forces and three moment variables recorded. Using the Matlab™ script **forceplate_analysis.m**, the forces were calibrated and the steps were parsed for individual analysis (See Appendix D). The first step in the analysis was tagging the beginning of each step. This was done by defining the beginning of the step as the first of 10 sequential $\mathbf{f_z}$ points which were all above 13 Newtons of force. This method allowed automated tagging, but was robust enough as to avoid false alarms due to signal noise. Next, contact time (the length of the step in time) was determined, as was the time to peak (time from the beginning of the step to the peak in vertical force). Peak forces were determined for maximum vertical force ($\mathbf{f_{zmax}}$), maximum shear force ($\mathbf{f_{shearmax}}$), and maximum total force ($\mathbf{f_{max}}$). The mean and standard deviation was determined for the pre exposure and all of the post exposure conditions. Comparisons were then made across subject, condition, and trial number.

As mentioned before, the video analysis was a manual and time consuming process. The lack of an intact end-to-end video analysis system necessitated the use of several different systems, none of which had automated interfaces available. To aid in the ease of identifying landmarks, reflective markers were placed on the subjects' shoulder, hip, knee, and ankle joint. Also, a calibration matrix in the camera visual field was used. The matrix consisted of three reflective points forming two perpendicular lines, allowing the video data to be properly scaled and the axes to be properly aligned.

The first step in the analysis procedure was to record the subject as she walked over the forceplate. Once the data was recorded, it was downloaded, at 10 frames per second, one step at a time, to a Power Mac 8100/80 through a high quality S-video cable using the software package, FusionRecorder™. This video data was then transferred to Adobe Photoshop™ using the cut and paste clipboard of the Mac operating system. Using the cursor tracker in Adobe, the x and y coordinates of each point (three calibration points and four segment points) were recorded for each frame of the step. Figure 4.7 shows a

typical analyzed step. For demonstrative purposes several steps have been superimposed. Also, the colors have been added to avoid confusion. This figure illustrates how the joint positions are tracked as the subject moves across the forceplate. These values were then typed into a Matlab script called **video_scale.m** (See Appendix D). This script scaled the data and aligned the axes properly. It also determined the angles of the ankle, knee and hip. The angles are defined as shown in Figure 4.8. This script also determined the lengths of the shin, thigh, and trunk segments in order to verify the validity of the video analysis procedures. The final function performed by this script was the determination of the landing and takeoff angles of the leg, and the maximum vertical excursion of the hip during the step.

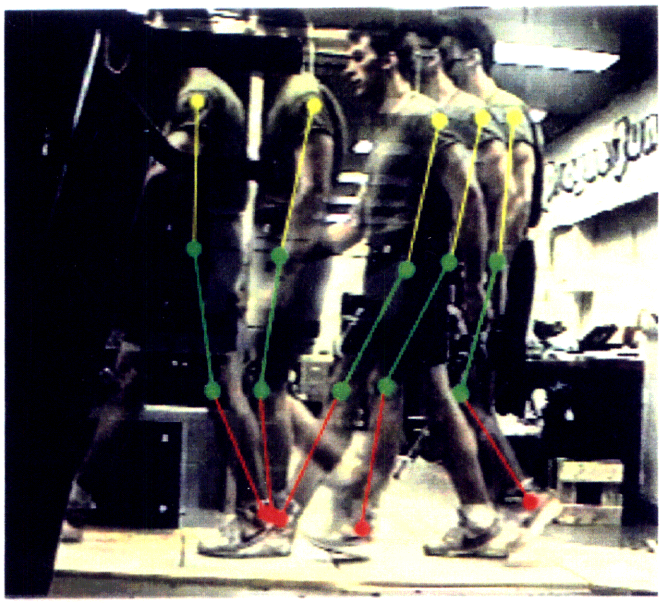

Figure 4.7 shows the position of the joint marker landmarks sequentially during a single step.

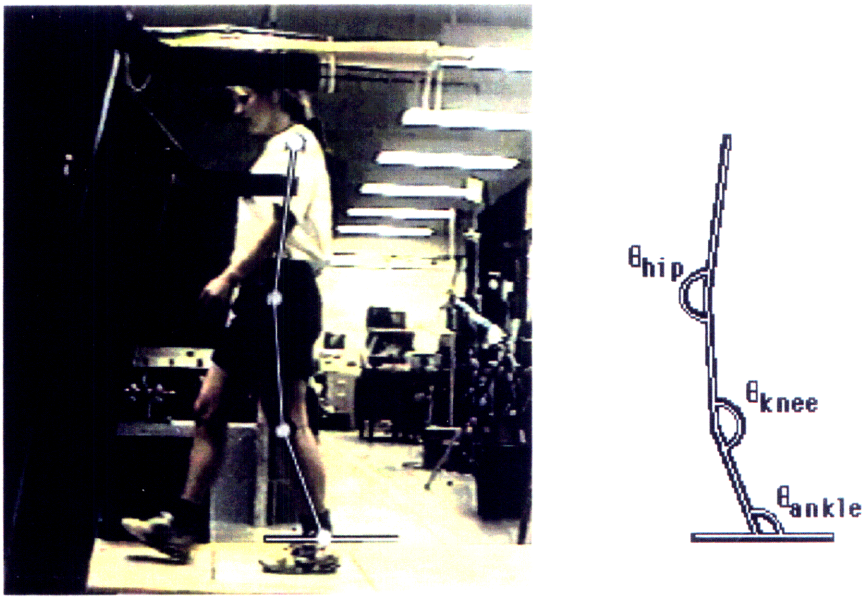

Figure 4.8a shows the joint marker locations for a single frame. Part b of this figure provides the convention by which angles are defined in the gait analysis scripts.

Chapter 5 Results and Discussion

This chapter presents the experimental results of this study and discusses them in the context of the background literature and control model. Section 5.1, Results, summarizes the results of the various protocols involved in this experiment. Specifically, Section 5.1.1, Metabolic Analysis, reveals the energy expenditures associated with partial gravity locomotion. Section 5.1.2, Gait Analysis, presents changes found in ground reaction forces and visual characteristics of gait such as joint angles following simulated low gravity exposure. Section 5.1.3, Posture, presents results of the posture protocol and also compares the estimator based, inverted pendulum model with the data recorded from subjects. Section 5.2, Discussion, recounts the important results of this thesis and describes their relevance to past and present research. Section 5.2.1, Limitations of Experimental Design, lists some of the problems with the protocol, and possible solutions. The significance of the metabolic experiment is described in Section 5.2.2, Workload. Musculoskeletal changes are discussed in Section 5.2.3, Gait and Stretch Reflex. Finally, Section 5.2.4, Posture Data reveals the significance of results in the posture protocol discussing experimental data as well as results from the estimator based control model.

5.1 Results

This section presents the significant results of the experiment. Section 5.1.1 reveals the results of the metabolic analysis protocols. Section 5.1.2 describes the findings of the gait analysis portion of the experiment. Finally, Section 5.1.3 details the posturography results of both the experimental and the estimator based control model. Comparisons are made between the two and the success of the model is evaluated.

5.1.1 Metabolic Analysis

This section presents data from the metabolic protocol of the experiment as described in Section 4.3.1, Metabolic Experiments. Recall that during locomotion, steady state oxygen consumption reveals the energy required for travel provided that sub-maximal exercise is maintained throughout. Under normal gravity conditions, energy requirement has been shown to increase linearly with speed [Newman, 1992]. The effect of gravity on workload is addressed in this section.

Workload was measured by oxygen uptake, or $\dot{V}_{O_2}$. The results of the energetics study are shown for nine subjects for lunar, Martian, and normal gravity conditions. Subject 006 yielded data which fell below 2 standard deviations of the mean data and was therefore not pooled with the remaining subjects.

The average resting metabolic rate across subjects was 1.2± 0.74 ml/(kg•min) and is known to be independent of gravity level. Baseline metabolic rate was subtracted from the data to allow the additional energy necessary for locomotion to be attained. Figure 5.1 shows the summary of workload data, plotting the oxygen consumption, $\dot{V}_{O_2}$, normalized over body mass, against gravity level. Note that running required significantly more oxygen per unit time than did walking. This was true for all gravity levels. Note also that, for both running and walking, a reduction in simulated gravity level is accompanied by a linear reduction in the amount of oxygen consumed. By regressing a line through the data points, a relationship between gravity level and oxygen uptake is attained. A linear regression of the data reveals the relationship to be:

$$\dot{V}_{O_2\,\text{Walking}} = 0.82g + 4.16 \qquad \text{Eq. 5.1}$$

$$\dot{V}_{O_2\,\text{Running}} = 21.21g + 7.06 \qquad \text{Eq. 5.2}$$

Figure 5.1 shows that, although less energy is needed for locomotion in reduced gravity at both speeds recorded, there is a larger decrease in the energy needed for running than there is for walking. A 63% reduction in g-level resulted in a 49% reduction in the energy necessary for running, but only a 5% reduction in walking energy. Similarly, a reduction in g-level of 83% caused a 61% reduction in oxygen uptake during running, but only a 16% reduction in walking oxygen uptake. This creates an interesting result, shown in Figure 5.2.

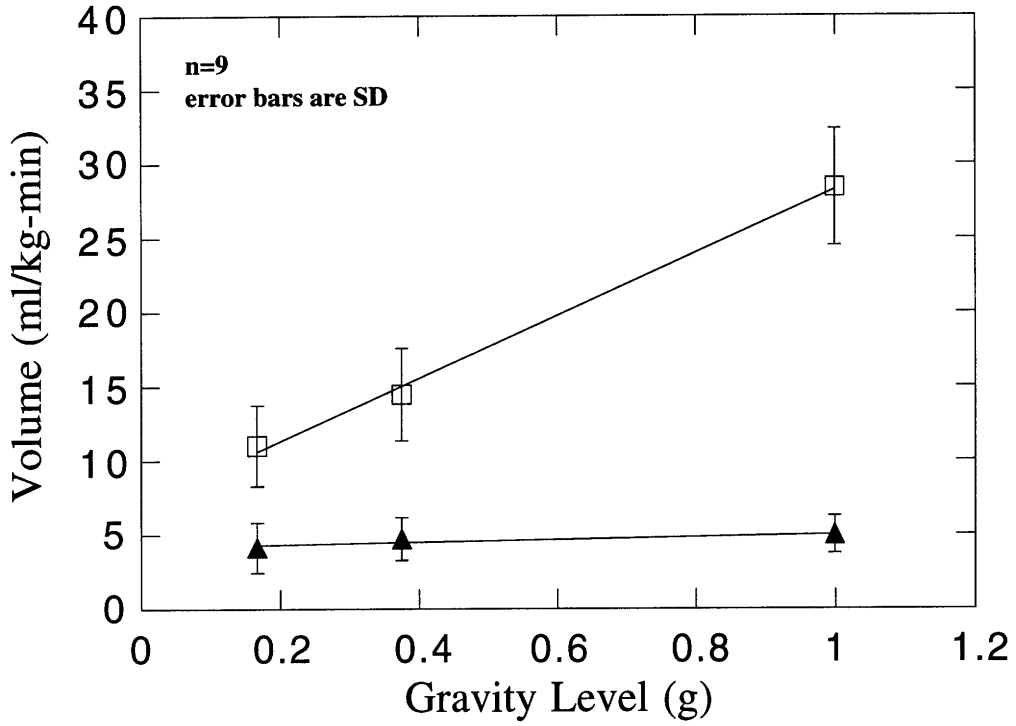

Figure 5.1 Workload versus gravity level for nine subjects. Workload decreases as a function of gravity level.

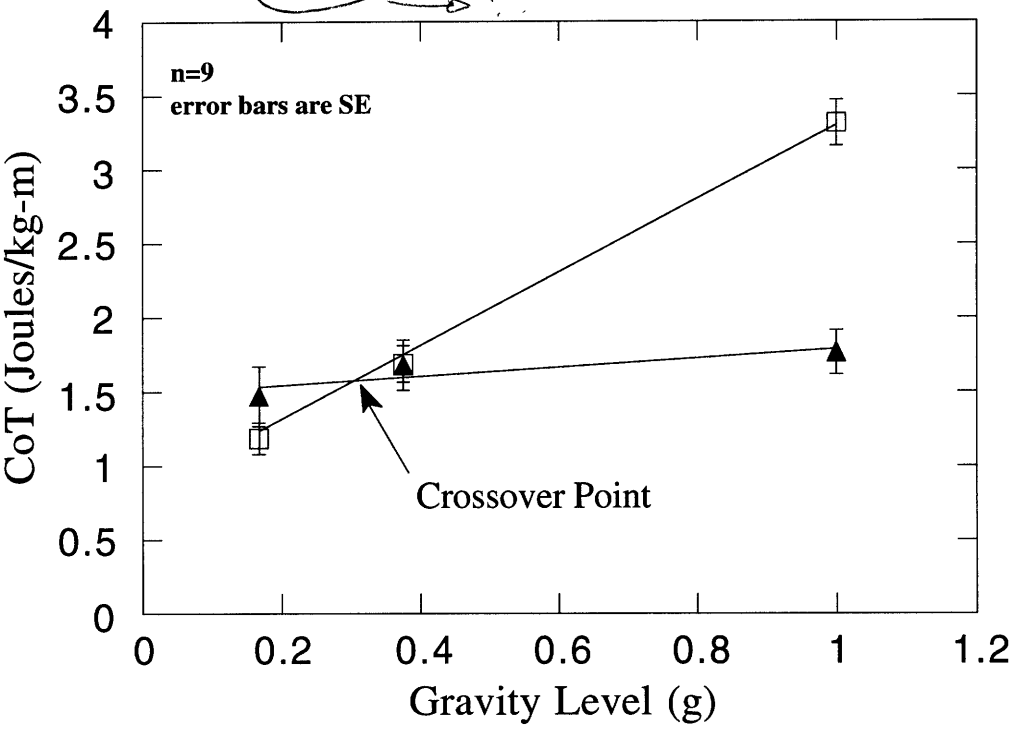

Figure 5.2 Cost of Transport decreases with respect to gravity. Below the crossover point, running is more efficient than walking.

For Figure 5.2, the energy consumed was again plotted against gravity level, but this time, the energy term has been normalized over mass and *distance* rather than over *time* as was previously the case. This new term is called Cost of Transport (CoT) and represents the amount of energy required to move a unit mass a unit distance. Figure 5.2 shows that there is a linear relationship between CoT and gravity level. By again regressing the data, the relationship is found to be:

$$\frac{\text{Joules}}{\text{kg} \bullet \text{m}_{\text{Walking}}} = 2.47g + 0.82 \qquad \text{Eq. 5.3}$$

$$\frac{\text{Joules}}{\text{kg} \bullet \text{m}_{\text{Running}}} = 0.30g + 1.48 \qquad \text{Eq. 5.4}$$

Notice that if these two relationships are equated, it is seen that at a g-level of 0.3, running and walking are equally efficient. At gravity levels above 0.3, walking is the more efficient means of locomotion. However, at g-levels below 0.3, running is actually more efficient than walking.

Figure 5.3 shows the workload measurements for all 10 subjects, including subject 006 who was eliminated for the summary data. Notice that although all subjects show the same general trend as the data presented in Figure 5.2, individual crossover g-levels varied appreciably between subjects and some subjects did not exhibit crossover in the realm tested.

Cost of Transport (CoT) versus Gravity Level

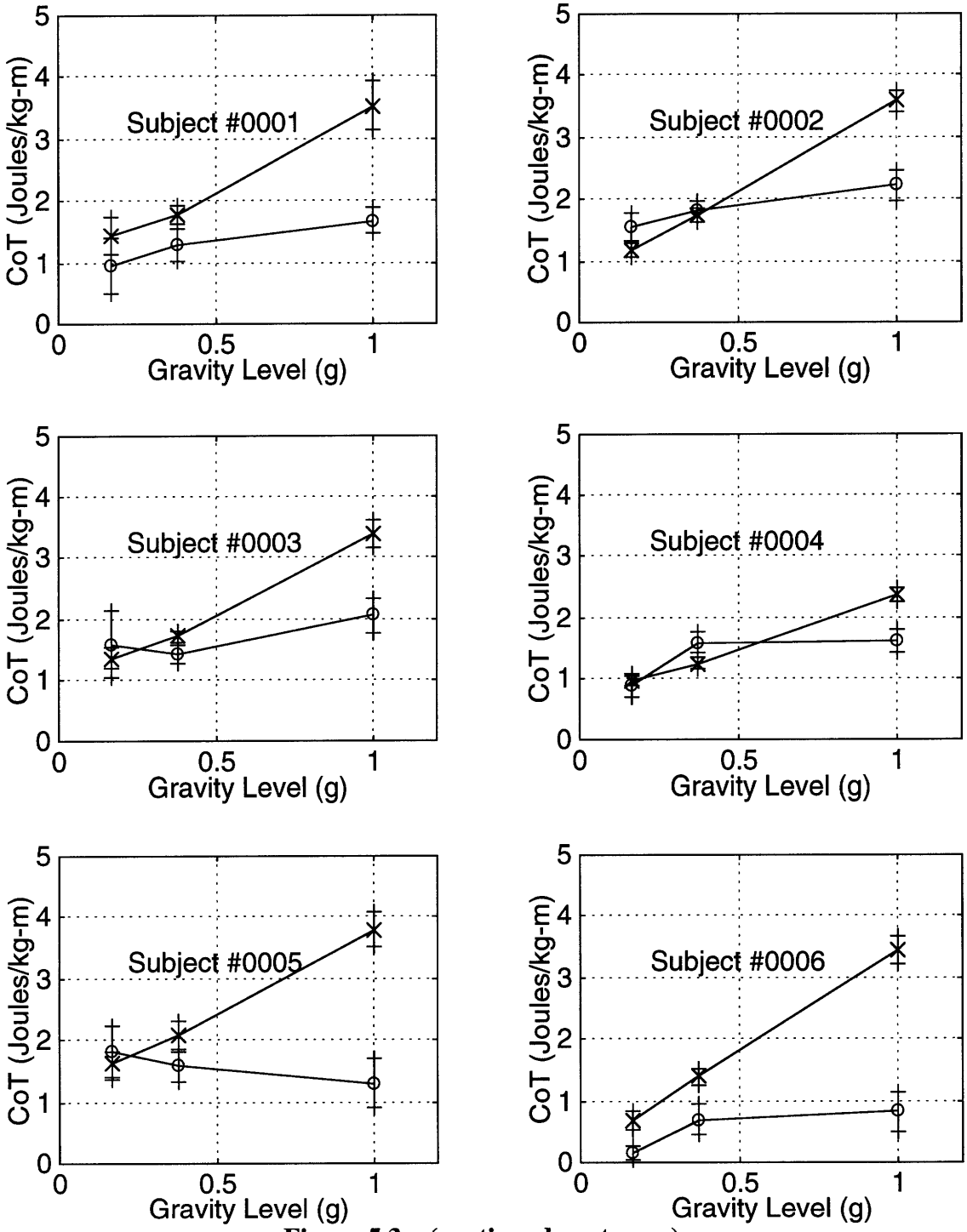

Figure 5.3 a (continued next page)

Cost of Transport (CoT) versus Gravity Level

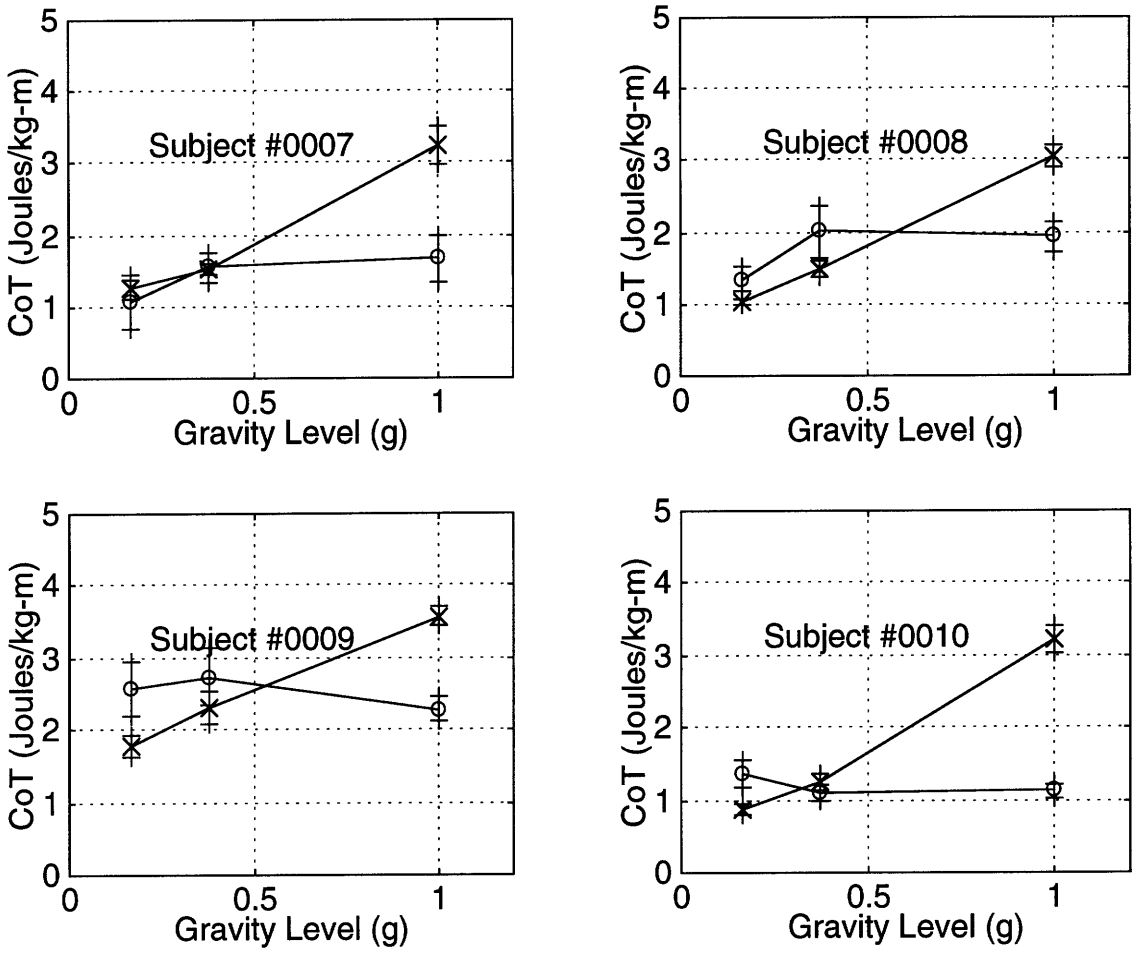

Figure 5.3 b (continued from previous page). Cost of Transport (CoT) versus gravity level for each of the ten subjects. Each point represents the steady state Cost of Transport, x denotes running and o denotes walking. The cost of running dropped dramatically at lower g's in all subjects. Walking showed a somewhat lower CoT at lower g levels, but the change was not as large as for running. As a result, at low g-levels, running is a more efficient way to travel than walking. This *crossover* was noted in 8 out of 10 subjects.

5.1.2 Gait Analysis

The results of the gait analysis protocol can be separated into three groups, the reflex latency analysis, the forceplate measurements, and the video measurements. The reflex results are presented first, followed by the forceplate data. The video data is then presented, and the trends noted between the video and forceplate data are discussed.

Reflex Analysis

The mechanisms governing the stretch reflex are completely located in sub-cortical (outside of the brain) pathways. The response is hard-wired between the spindles of the muscles, and the white matter of the spinal column. Therefore, no change in stretch reflex behavior is anticipated following brief exposure to low g locomotion.

The stretch reflex was evaluated by measuring the latency between spindle stimulation (hammer strike on patellar tendon) and muscular response (EMG signal increase). It is expected that this latency will vary slightly from subject to subject, but remain constant within each subject. This was, in fact, the case.

Four subjects were tested in each of the four conditions, one pre-exposure, and three post-exposure. As expected, there was no significant difference in stretch reflex latency in any of the conditions tested. Figure 5.4 presents the reflex latency data for all conditions. The latency was found to be approximately 25.4 ± 2.2 ms for the pre-exposure condition. No significant change was noted in any of the post-exposure conditions. This result confirms the hypothesis that stretch reflex latency would not be affected by acute exposure to reduced gravity.

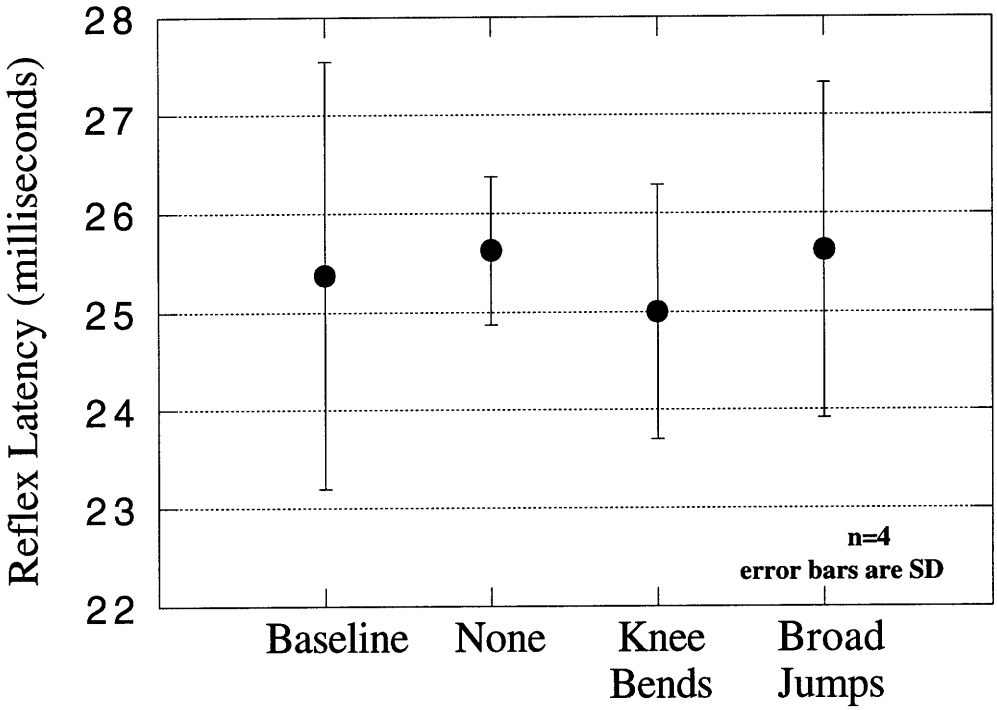

Figure 5.4 Stretch Reflex Latency was found to be unchanged by exposure to reduced gravity locomotion. None of the post-exposure trials were statistically different than the pre-exposure, baseline condition. A stretch reflex latency of approximately 25 milliseconds was found.

Ground Reaction Forces

The force measurements of this section are derived from ground reaction force profiles. Forces and moments were recorded in all three axes. Variables used for analysis include maximum normal force, f_Z; maximum shear force, f_S; maximum total force, f_{max}; contact time, t_C (defined as the total time from heel-strike to toe-off); and time to peak, t_P (defined as the time between heel strike and the maximum vertical force). Figure 5.5 introduces the force plot of a typical step with the important variables labeled. The first peak in f_Z is caused by heelstrike. As the person places their heel on the forceplate, a force slightly higher than body weight is exerted. As the subject swings through the step, the force decreases to a level equaling body weight. As plantar-flexion occurs, a reaction force is applied to the forceplate, creating a second peak just before toe off. The force curve returns to zero upon toe off.

Figure 5.6 shows the forceplate traces of subject E for the pre-exposure (solid lines) and post-exposure/no exercise trials (dashed lines). Notice that the peaks in all forces are slightly higher in the post-exposure case. This could be due to the fact that the subject is not walking as smoothly as in the baseline condition. As the heel is slammed down harder, higher peaks are seen in both the x and z axes. Also notice that the length of the force trace is slightly lower in the post-exposure case. This decrease in contact time means that the subject is swinging through the step more quickly than before the exposure to simulated low g. This indicates a period of readjustment immediately following exposure.

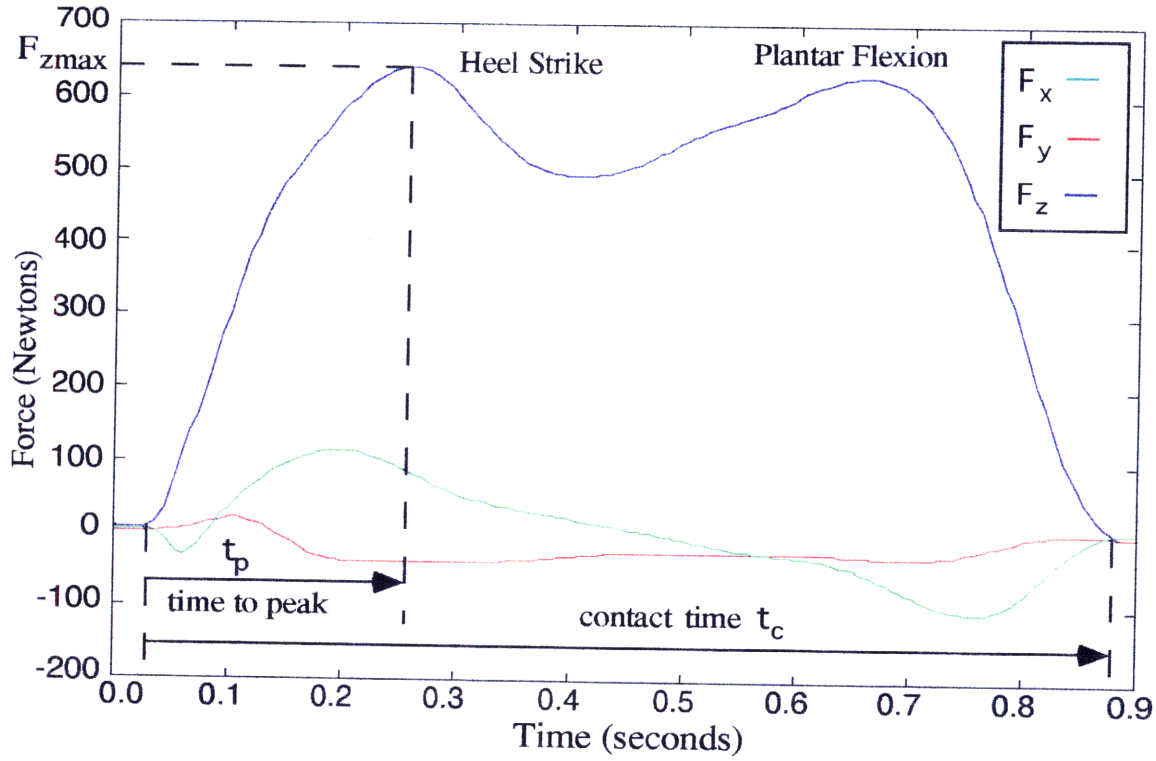

Figure 5.5 This plot shows the three ground reaction force traces of a typical step. F_{max}, t_p, and t_c are labeled on the plot.

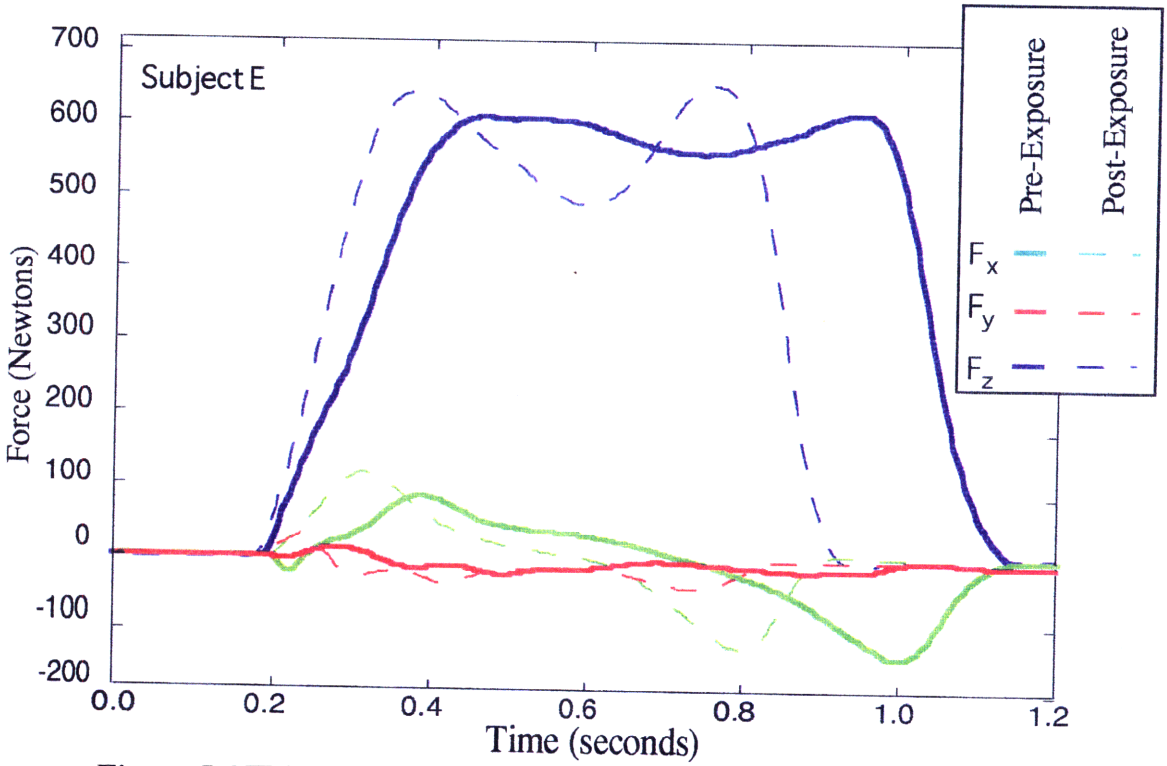

Figure 5.6 This plot compares the pre-exposure ground reaction forces to the post-exposure GRF's. Following exposure to low-g, the step is shorter and exhibits higher peak forces in all axes.

For summary data, all forces were divided by the individual subject's baseline mean force. This removed some of the inter-subject variation and allowed consistent trends in the data to be recognized. The first of the trends is an increase in maximum vertical ground reaction force following exposure to simulated reduced gravity. Figure 5.7 shows the relationship of f_{zmax} and test condition. Notice that the increase is greatest in the No Exercise condition. The No Exercise data was significantly higher than the pre-exposure condition ($p=0.016$). The knee bends trials showed a similar increase in f_{zmax} that yielded a p value of $p=0.037$. A very small increase in f_{zmax} was also noted for the Jumps case, but was not statistically significant.

Not surprisingly, f_{max} showed results similar to those of f_{zmax}. Since the vast majority of total force is the normal component, it makes sense that the two variables exhibit similar trends. Figure 5.8 shows maximum force versus condition. Again, the data was normalized against the pre-exposure baseline to allow subject pooling. As before, for the No Exercise case, the force was significantly higher than the pre-exposure condition ($p=0.002$). The knee bends condition exhibited a similar, but smaller increase in f_{zmax} that was significant at the 0.01 level. An increase in f_{zmax} was also noted for the Jumps case and had a significance of $p=0.014$.

Figure 5.9 shows both the maximum and minimum forces in the x direction, with the direction of motion of the subject defined as the positive x direction. These forces are normalized by the bodyweight of the subject. This is a measure of how much shear force the subject is exerting during a typical step. There was no statistical difference between pre-exposure trials and any of the post exposure trials for either the minimum or the maximum case. The variable $f_{shearmax}$ is calculated by adding the x and y force vectors. As was the case with f_{zmax} and f_{max}, f_{xmax} is the larger component of $f_{shearmax}$. One would therefore expect $f_{shearmax}$ to possess trends similar to f_{xmax}. This is the case. Figure 5.10 shows that there is a slight increasing trend in the shear forces exerted, but that this trend is by no means significant. The maximum shear force is virtually unchanged following reduced g exposure.

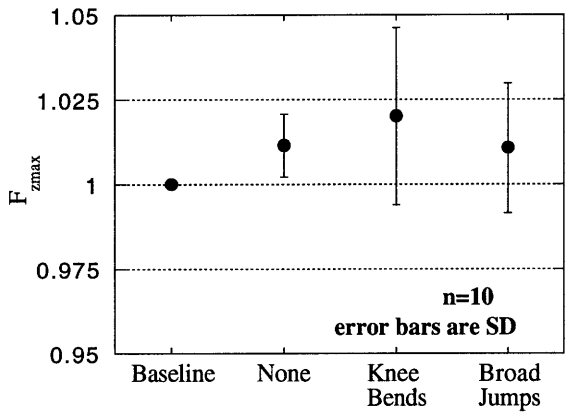

Figure 5.7 Maximum Normal Force versus Condition. Fz_{max} was significantly higher for the 'None' and 'Knee Bends' Conditions. 'Broad Jumps' condition showed no significant difference.

Figure 5.8 shows that F_{max} follows roughly the same trend as F_{zmax}. Significant differences were noted in all conditions.

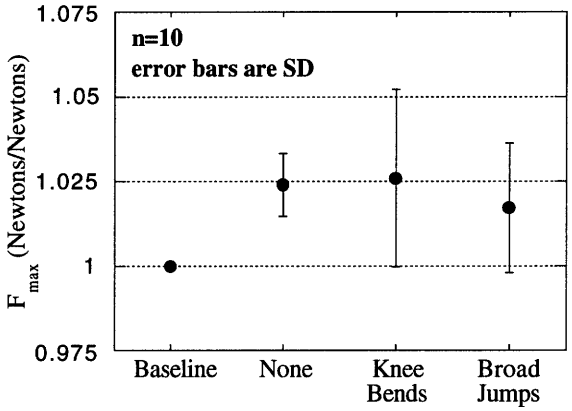

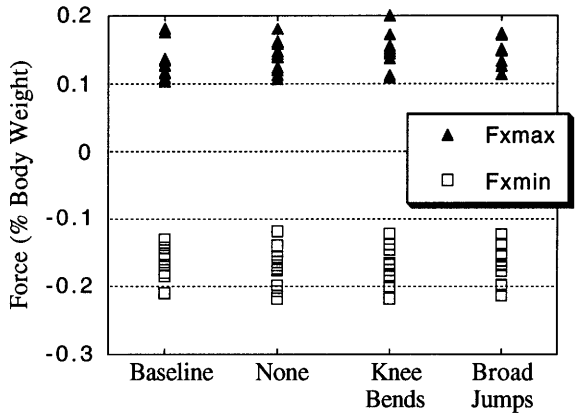

Figure 5.9 shows the forces in the x axis. Neither the forward nor the backward forces showed any significant difference between conditions.

Figure 5.10 Maximum Shear Forces. This plot shows that there was a slight increase in shear forces following exposure, but this change was not statistically significant.

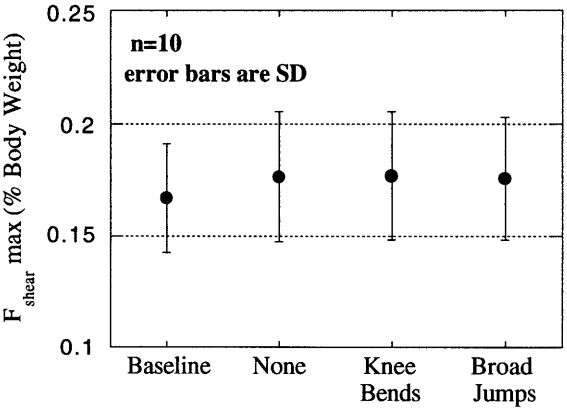

Contact time is an indication of how quickly the subject is getting through the support phase of walking. Figure 5.11 shows that the time spent in contact with the floor during support decreases slightly following exposure. This trend is most clearly apparent in the None case, slightly less apparent in the Knees case, and even less so for the Jump case. Although none of the trends in contact time were statistically significant, this trend seems to verify the changes noted in f_{max} and f_{zmax}. The jumps seem to allow the subject to return to baseline behavior better than the knee bends which, in turn, appear better then doing nothing at all.

Changes in time-to-peak, t_p, could indicate a change in walking strategy since the peak represents the time course of the heel strike and first part of the stance phase. By dividing t_p by the contact time, a ratio between heel strike and total stance phase can be attained. This method revealed no change in t_p following exposure. Figure 5.12 shows that time to peak was roughly 26% of total contact time. This value was not affected by the brief simulated gravity reduction nor was the post exposure exercise a factor.

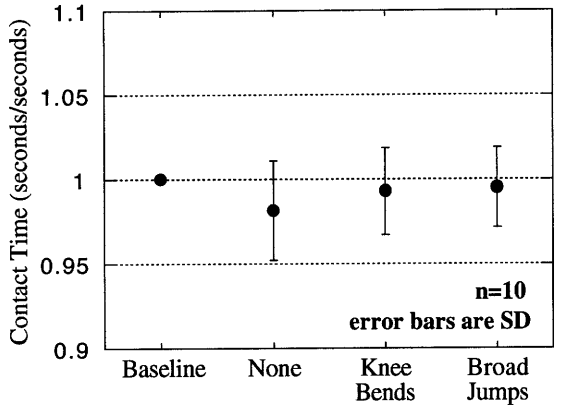

Figure 5.11 Contact Time versus Condition. There was a decreasing trend in contact time across conditions.. However, none of these trends were significant.

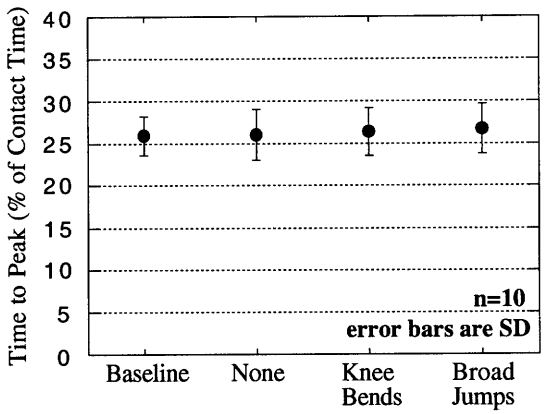

Figure 5.12 Time to Peak versus Condition. There was no significant change in time to peak in any condition.

Video Data

The video analysis system recorded gait analysis trials, downloaded the data to the computer, located key joint positions in two dimensional space, and finally, determined and recorded joint angles. This process has been detailed in Section 4.4.4, Gait Analysis.

The joint locations are recorded sequentially and plotted by Matlab™ which yields a plot like the one shown in Figure 5.13 as an example showing subject G walking through an entire step in the pre-exposure condition. Note the presence of stance knee flexion as the subject moves through stance phase, plantar flexion as the stance phase is completed, and swing leg knee flexion as the subject moves the left leg forward for another stance phase. From this plot is recorded the vertical excursion of the center of mass (E), the heel strike angle (θ_h), the take-off angle (θ_{to}), and finally, the maximum knee flexion angle (θ_k). No significant difference was realized in any of these variables in any of the condition cases. Figure 5.14 shows all of the variables compared versus condition.

One advantage of the video data is that it could be synched with the forceplate data to reveal more about the subjects' gait. Figure 5.15 shows Subject A with both video and forceplate data displayed. The location of the back leg of the subject was interpolated from other data, and the head was added for visual effect. The position of the video data corresponds to the time at which it occurred. This figure demonstrates the effect of heel strike (first peak), plantar flexion (second peak), and toe off (end of signal).

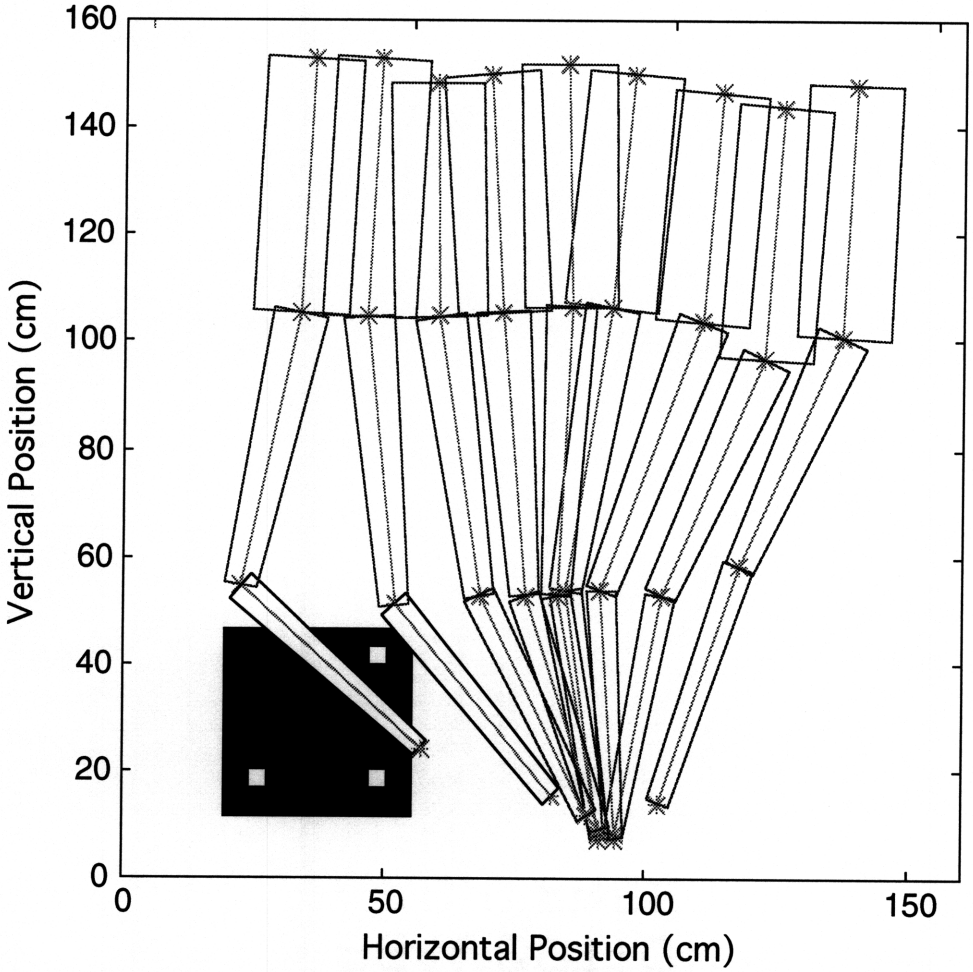

Figure 5.13 shows the progression of subject G through a single step. Note the stance knee flexion during midstep and the plantar flexion near the end of the step. Also, notice the knee flexion after the step as the leg swings forward for the next step. The black square represents the calibration markers which were placed in the camera's visual field to aid in video analysis.

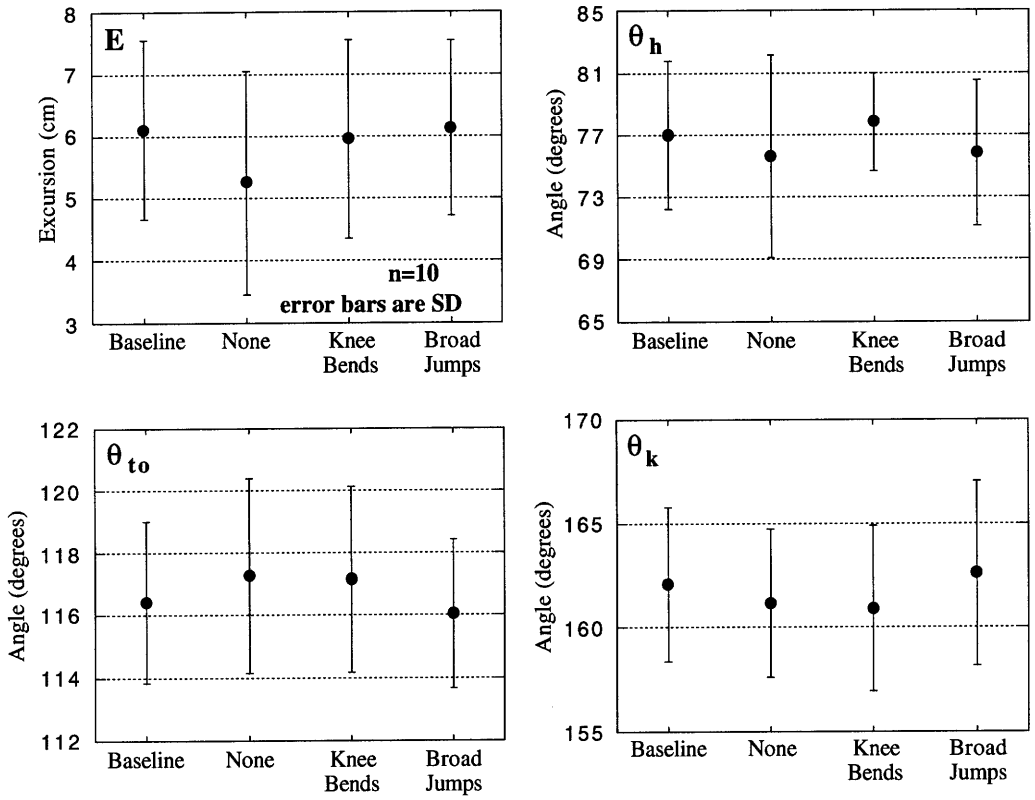

Figure 5.14 Video Analysis Variables. None of the video analysis variables showed any significant change in any of the conditions tested. There was a decreasing trend in the vertical excursion of the center of mass (E), but this change was not significant. Heel strike angle (θ_h) showed no consistent trends in any condition. Take off angle (θ_{to}) showed a slight increasing trend, but this was not significant. The knee flexion angle decreased slightly following reduced gravity exposure, but again, this change was not significant.

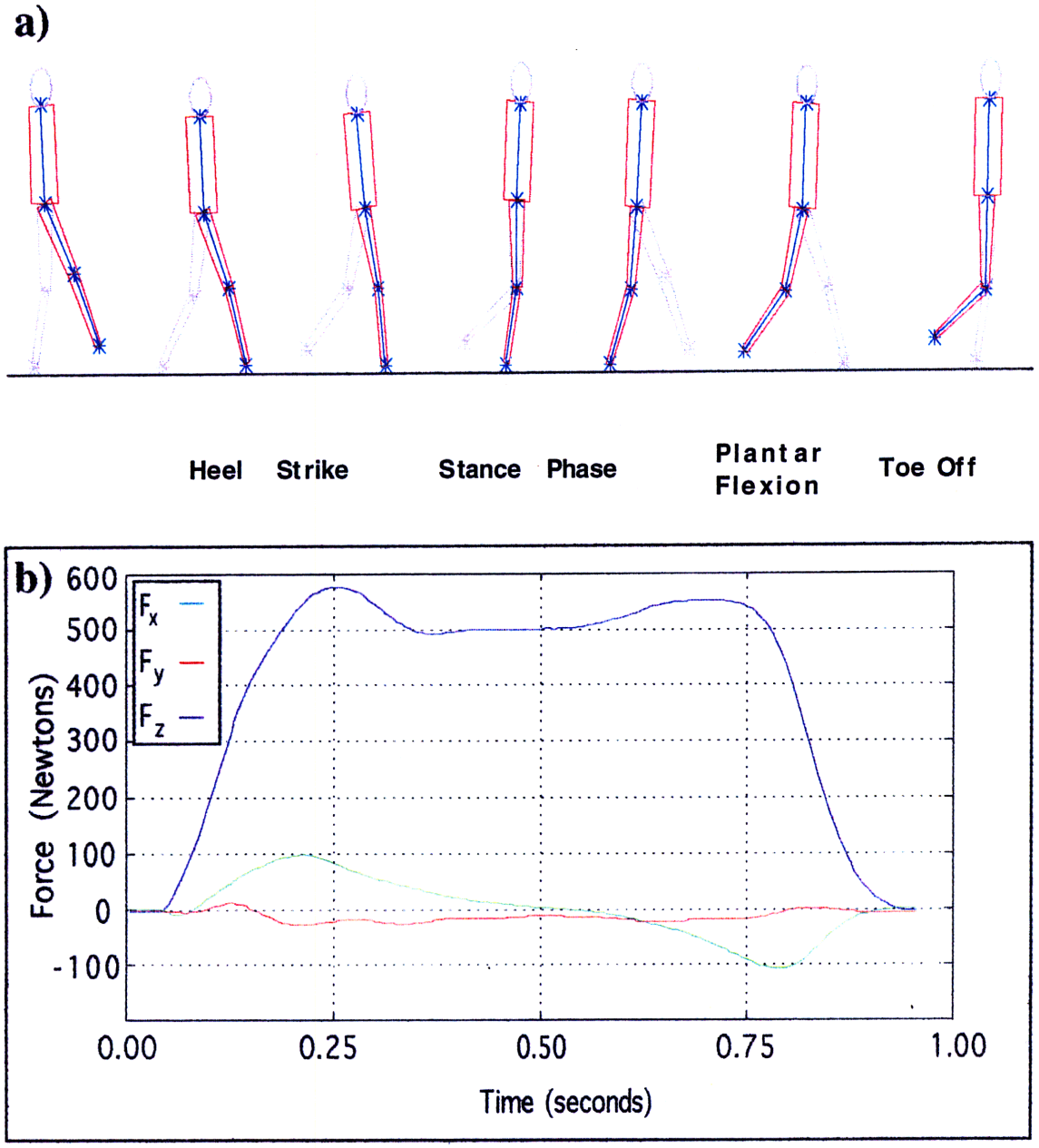

Figure 5.15 Synchronized Video and Forceplate Data. Part a) of this plot shows the time course of joint position through a single step. The light blue lines and red trapezoids represent actual position data recorded and the associated body segment locations. The light purple lines represent body segments whos positions were not recorded, but calculated or inferred based on the data recorded. Part b) of this plot shows the ground reaction forces of the same step. The pictures from part a) correspond to the forces directly below them on the force plot. Note the appearance of heel strike, plantar flexion, and toe off in part a), and their corresponding effects in the force plot in part b).

5.1.3 Posture

This section presents the data from the posture protocol of this experiment. Section 5.1.3a, Subject Posture Data, summarizes the data collected from the ten subjects who participated in this experiment. The results of the model developed for this experiment are presented and compared in Section 5.1.3b, Model Posture Data. All of the data is presented in two categories, spatial and temporal variables. Important spatial variables presented include root mean square (rms) of CoP location in the x and y axes as well as the straight line rms (rms_x, rms_y, and rms_r). The temporal variables presented in this section are the temporal diffusion coefficients (D_S and D_l), the correlation factors (H_S and H_l), the critical time (t_{cr}), and the critical distance (d_{cr}).

5.1.3a Subject Posture Data

The easiest way to appreciate the changes in the spatial characteristics of the CoP time course plots is to view them in their raw form. Figure 5.16 shows the CoP plots for subject J for all four test conditions as an example. Rms values have been given for both the x and y axes. Understandably, there was less sway in the y axis than in the x axis. By providing a stable base of support, our feet keep us from swaying too far to the side. This is not true in the x axis and, as a result, the magnitude of body sway is much larger front-to-back. Note that, compared to baseline, the rms for the None condition has increased in both axes. The same trend is found to a lesser extent in the Knee case. The Jump condition exhibits no apparent changes in rms in either axis.

Pooling the data from all subjects yielded similar trends. Before pooling the data, each subject's data was normalized by their own pre-exposure baseline value. This was necessary due to large inter-subject differences in rms values. Nine out of ten subjects showed increases in rms following exposure. Subject A showed a decrease in rms for all conditions following partial gravity exposure. The possible explanations for this subject's counter-intuitive behavior are discussed in the following Discussion section. Figures 5.17, 5.18, and 5.19 show the rms for the combined axes, x axis, and y axis, respectively. Figure 5.17 shows an increase in rms_r in the No exercise case of nearly 20%. This increase was statistically significant ($p=0.001$). There was an increasing trend in rms for the Knee condition, but this change was not significant. There was almost no change in the rms for the Jump case. This fact, in addition to the large variance of the data, yielded no significant difference between the Jump case and the pre-exposure condition.

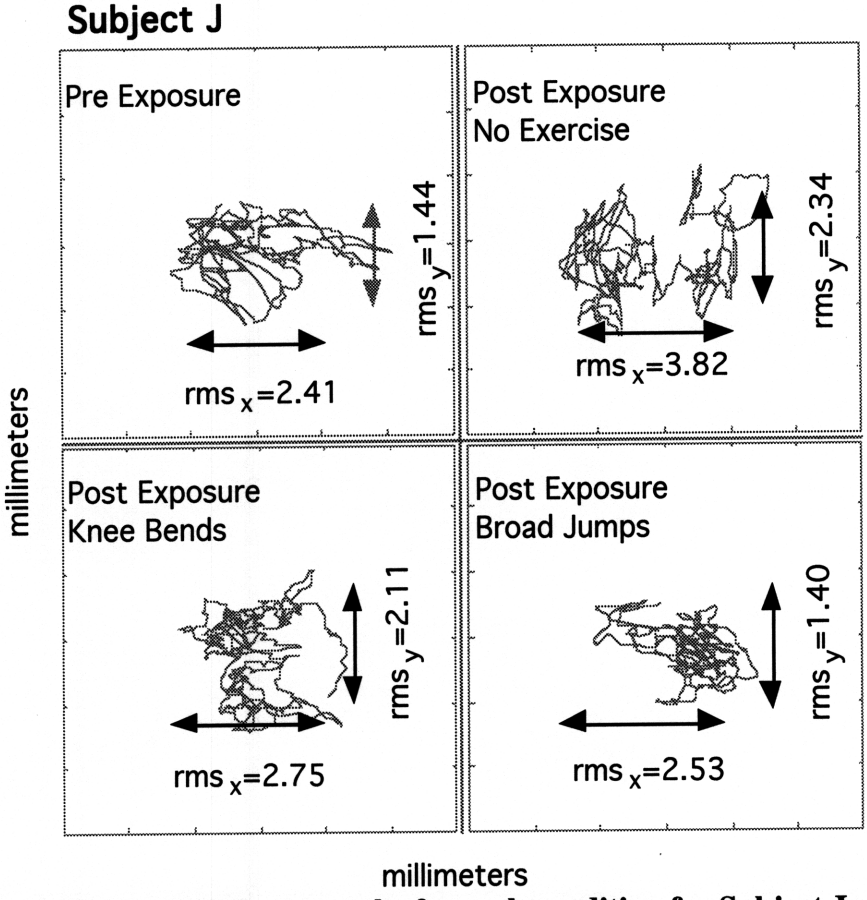

Figure 5.16 shows the CoP Trace results for each condition for Subject J. Each trial is representative of all trials for the corresponding condition. Note that rms underwent a dramatic increase following exposure if no exercise was performed. The knee bends were somewhat successful in lowering the rms, and broad jumps returned the rms values to nearly baseline values.

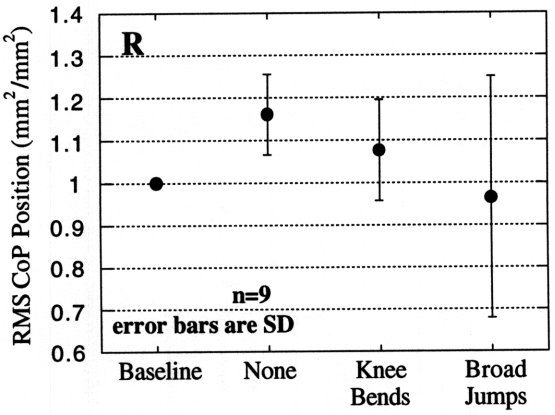

Figure 5.17 RMS versus Condition. Root mean square increased post-exposure. None condition showed a significant increase (p<.001). Knee bends and broad jumps produced no significant changes.

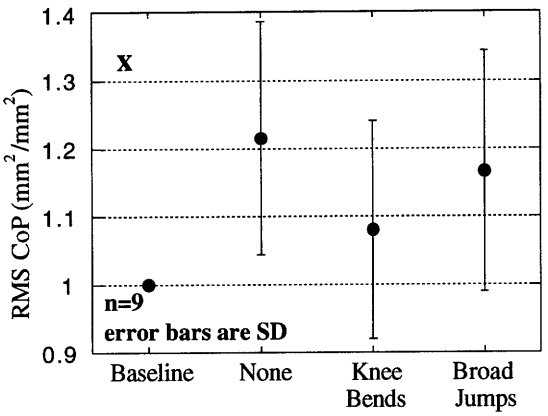

Figure 5.18 reveals a significant change in rms in the None condition and an increasing trend in the other conditions.

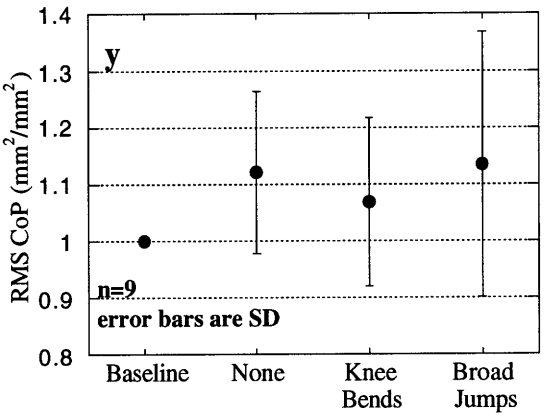

Figure 5.19 shows an increasing trend in all post exposure cases. However, None of these trends were significant.

Rms_X also showed an increase for the None condition. As was the case for rms_r, this increase was statistically significant (p=0.009). The increase in rms was not as high in either the knee bend or broad jump cases and was not significant for either case. As is shown in Figure 5.19, there was no significant change in rms in any case in the y axis. This despite the fact that there was an increasing trend in all cases. Any changes that occur in the y axis are apparently within the noise level of this experiment.

The increases found in rms values, as well as the increases found in ground reaction forces were most pronounced in the case when no post-exposure exercise was performed, and least evident when broad jumps were performed. From these results, it is concluded that the changes that occur during brief exposure to reduced gravity can be countered through exercise. The performance of activity delivering high peak forces was successful to some degree in alleviating the changes brought on by low g locomotion. Activities that provided both high peak forces *and* fast rates of change in forces were even more successful in combating the debilitating effects of partial g simulation. Apparently these exercises cause the body to readapt to the 1 g environment more quickly than would normally occur without exercise.

The temporal data were found using the methods described in Section 4.4.3, Posturography Analysis. Trials were averaged across condition in order to remove the natural sway present in individual trials. Eight trials were averaged pre-exposure, and six trials for each of the post exposure conditions. A typical temporal plot is shown in Figure 5.20. The square of the distance is plotted on the y axis, with the time interval along the

x axis. The three lines represent the x, y, and total distance cases, with the smallest being the y axis, the second line being the x axis, and the linear sum of x and y representing the total distance. Notice that each line possesses a steep portion at low time intervals and a longer, more shallow portion at higher time intervals. The slope of these lines is called the diffusion coefficient and is a measure of the random activity of the system within that interval.

The diffusion coefficients are shown in Figure 5.21. Although there is no change in either variable post-exposure, it is obvious that the short term diffusion coefficient (D_S) is significantly higher than the long term coefficient (D_l) ($p<0.001$). This indicates a higher level of stochastic activity in the short term than in the long term. The possible causes of this condition are discussed later. A summary of diffusion coefficient values are listed in Tables 1 and 2 in Appendix E.

Figure 5.22 shows the relationship between correlation factor of the CoP position time course and the condition. As with diffusion coefficient, no significant change is noted in H for any of the post-exposure conditions. However, H_S is significantly greater than 0.5 ($p<0.0005$) while H_l is significantly lower than 0.5 ($p<0.0005$). Recall that an H value greater than 0.5 represents persistent behavior which means that the CoP tends to keep moving in the direction which it is currently moving. An H value below 0.5 indicates anti-persistent behavior, or the CoP is more likely to switch directions than not. The short term persistence is caused by the inertial properties of the system. A physical system tends to move in one direction until an outside force changes that direction. The anti-persistence seen in the long term due to the closed-loop nature of the plant. Since failure to reverse direction would result in falling over, anti-persistence must be practiced. The significance of this result is more thoroughly explained in Chapter 6, Discussion and Conclusions. H values are summarized in Tables 3 and 4 in Appendix E.

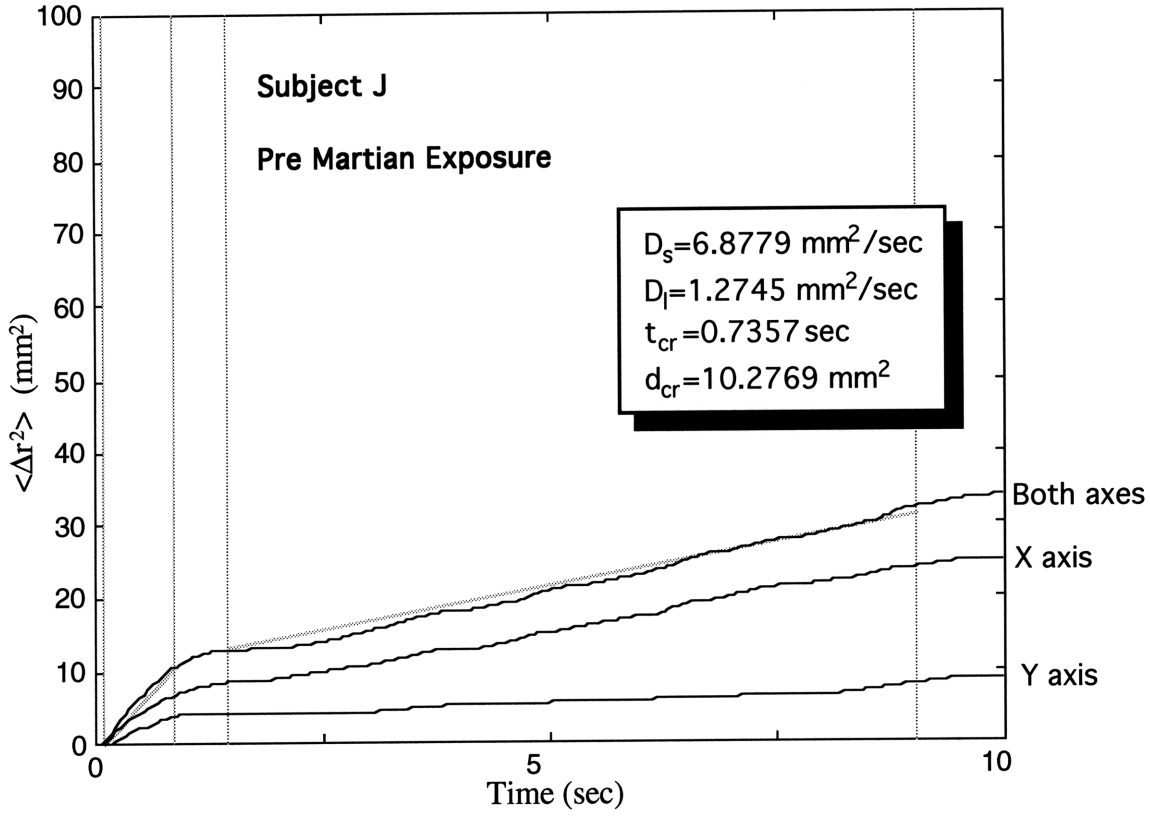

Figure 5.20 shows the diffusion stabilogram plot for subject J. Subject J, like all subjects, showed more sway in the X axis than the Y. This subject also exhibited a much higher short term Diffusion coefficient than long term.

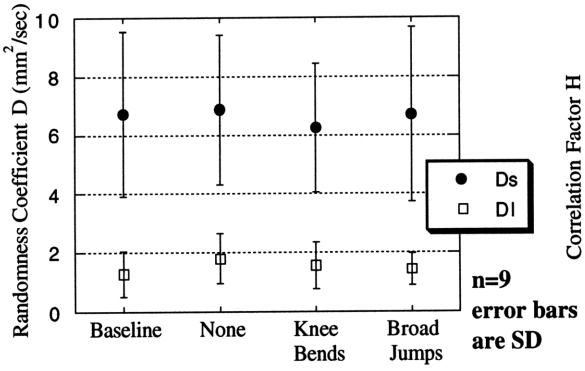

Figure 5.21 Diffusion Coefficient versus Condition. D_S was significantly greater than D_l for all conditions (p<.001) .

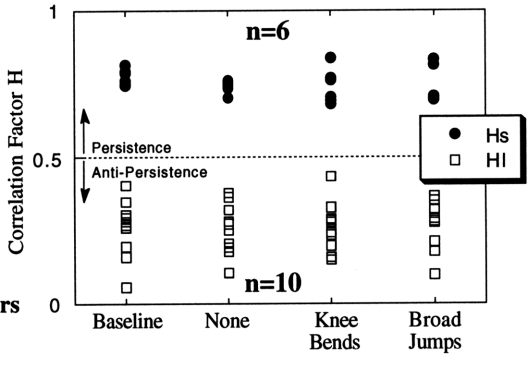

Figure 5.22 Correlation Coefficient versus Condition. H_S was significantly greater than H_l for all conditions (p<.0005).

The location of the critical point (the point at which the long term and short term strategies intersect) showed no consistent trend with respect to condition. Figure 5.23 show that there was no relationship between exposure to simulated reduced g and critical point location. There was a small increase in critical time, but this change was not significant. There was no change in the critical distance. This result is discussed following the presentation of the model data.

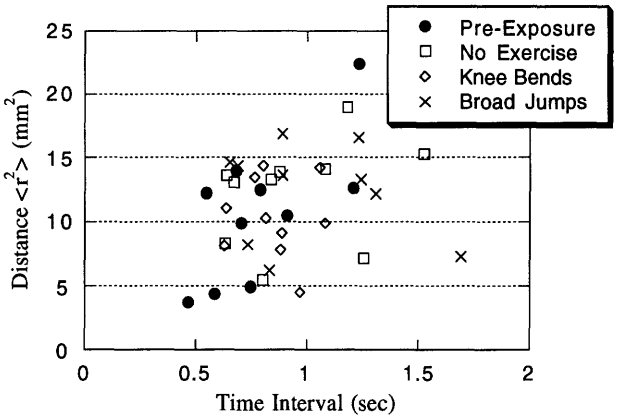

Figure 5.23 shows that there was no significant change in either critical distance or critical time across conditions.

5.1.3b Model Posture Data

In order to ease direct comparison, this section presents the data in the same format as Section 5.1.3a, Subject Posture Data. By matching the spatial characteristics of subject data, the model also replicates the temporal aspects of posture data and, through manipulation of the variable muscle gain, the post exposure changes in postural performance can be duplicated. It should be noted that this model uses stochastic inputs yielding results that change slightly with every trial, much like the human subjects' trials. Therefore, parameters were not matched exactly, rather, a range was determined for each variable. A model variable was considered to match the human subject's variable if the values determined from the model data fell within the range of the subject data.

The estimator model produces plots strikingly similar to the experimental measurements. Figure 5.24 shows the results of 4 trials performed by the model with different muscle gains ranging from 0.7 to 1.0. The specific value of the muscle gain is not as important as the trend produced by muscular gain manipulation. By lowering the gain, the rms value significantly increases in both the x and y axes. If the gain were lowered enough the estimator-plant model would become unstable and the subject would fall. Instability occurs at gains below 0.6. By raising the gain above 1.0, the system improves performance slightly, but eventually, this too causes instability. In fact, the total range of stable gains is only about 0.5 at the extremes and performance begins to suffer greatly even before instability ensues.

The temporal plot of eight averaged posture trials is shown in Figure 5.25. Averaging was necessary since the model, like the human subjects, possessed natural sway in each trial. Averaging several trials removed specific sway characteristics. The diffusion coefficients and correlation factors fall within the range of those found from subject data. Figure 5.26 shows the temporal variables of Subject J compared to the variables produced by the model. In each case, the model produced variables that fall within the population of the subject's data, verifying success in capturing the important temporal characteristics of quiet standing.

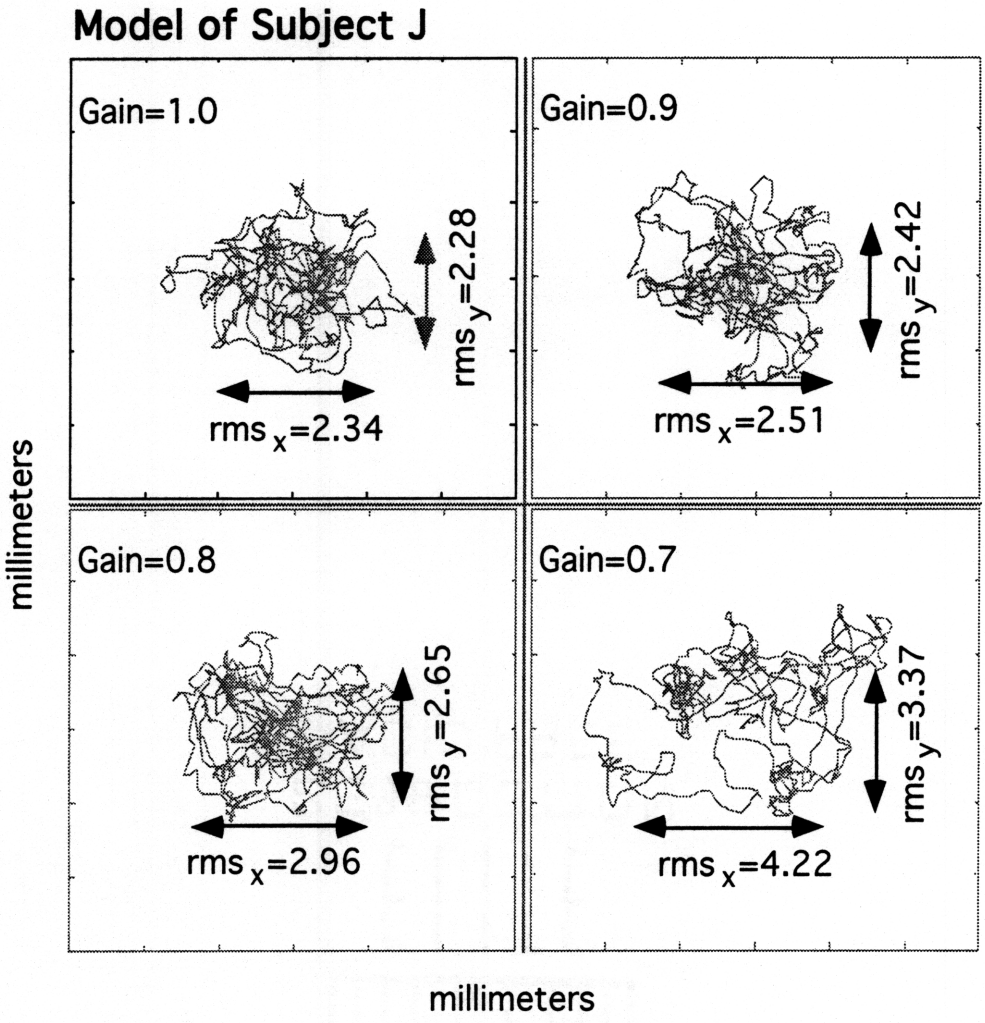

Figure 5.24 reveals that the model was successful in mimicking the performance exhibited by 9 of the 10 subjects. By lowering the variable muscle gain in the model, the rms increases in each axis, just as occurred in post-exposure trials of the subjects.

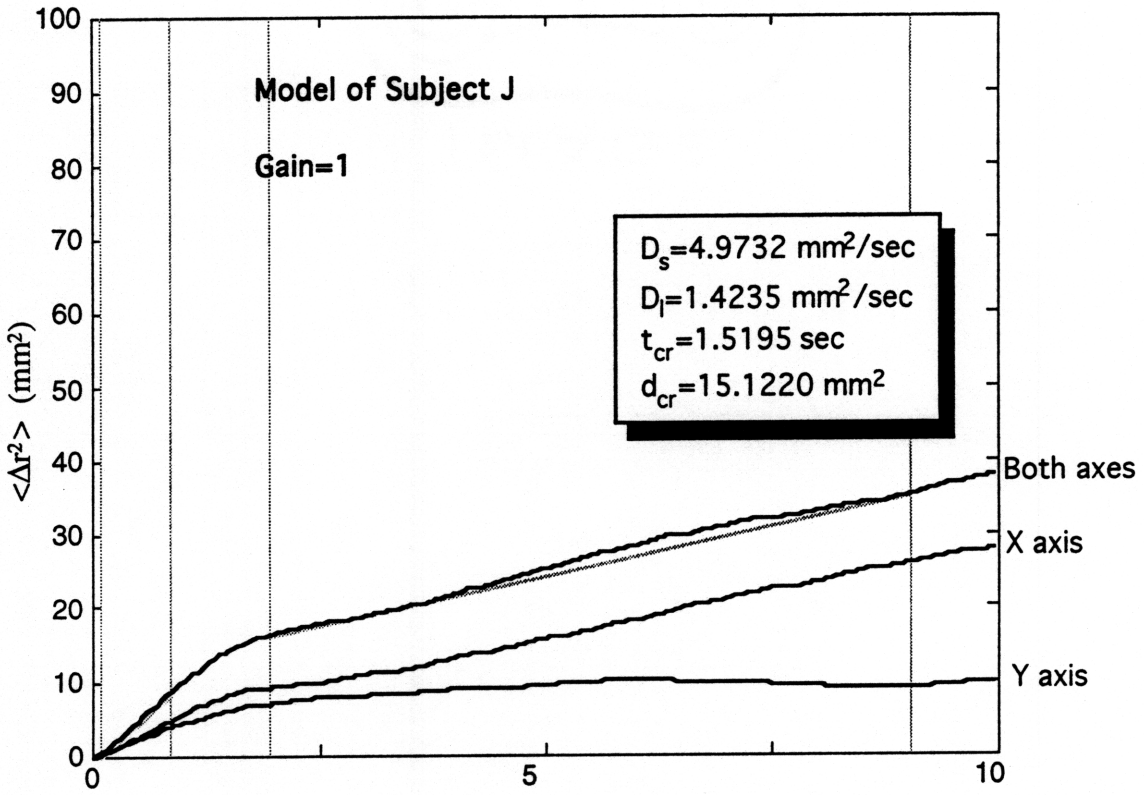

Figure 2.25 shows that the model was successful in replicating the performance of subject J in the pre-exposure condition. Using a 10 trial average, all of the parameters listed are close to those demonstrated by the human subject.

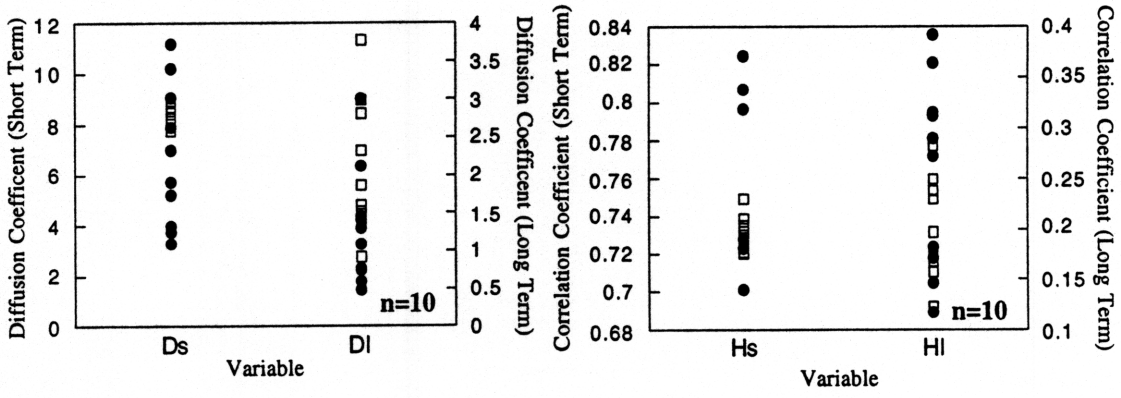

Figure 5.26 Temporal Variable Comparison. The temporal variables derived from human data are plotted as dark circles. The model data are plotted as empty squares. The model succeeded in matching all of the temporal variables.

5.2 Discussion

This section begins by noting the limitations of the experiment, due to both the hardware used and the protocols selected. Section 6.2, Workload, discusses the results found regarding changes in metabolic needs as a factor of gravity reduction. Section 6.3 evaluates the ability of the estimator based model to successfully capture the important characteristics of posture, and introduces a new, slightly modified model that could explain the post-exposure behavior of Subject A.

5.2.1 Limitation of Experimental Design

The primary limits to this experiment involved successful simulation of the reduced g environment. Although the harness apparatus used proved an effective method of partial gravity simulation, there were unavoidable, yet undeniable shortcomings of the design. The most basic of these problems is the fact that, although the harness can unload a subject's body weight, the pull of gravity on individual body segments cannot be eliminated. The arms and legs of the subject still have the same inertial and weight characteristics as they normally do. Therefore, the forces necessary for overcoming the force of gravity are unchanged and the subject may use more energy for locomotion than would be necessary in an actual reduced g environment.

Another problem with this simulator is that the bicycle seat which is used for unloading the subject can cause discomfort while walking or running. Although subjects claim to be locomoting normally, and appear to be doing so, it is difficult to say what effect the discomfort of the seat may cause.

The biggest problem with the protocols used was that there were too many experiments to run. The change being investigated has a rapid recovery rate. Therefore the test must be run quickly in order to measure any changes. Determination of the test order was difficult and somewhat arbitrary. Readaptation could have caused earlier test to yield better results than later tests,

5.2.2 Workload

The results found for the metabolic portion of this experiment showed that, within the gravity range tested, energy expenditure is linearly related to g-level, and that, below a certain 'crossover point', running becomes a more efficient means of travel than walking.

These results validate past findings by Farley, and Newman. Also, the percentage of change in energy expenditure was similar to results of Newman who found a 41% reduction in O_2 uptake in Martian g and a 67% reduction in Lunar g conditions, compared to the results of the current study that yielded a 49 and 61% reduction in energy expenditure in Martial and Lunar gravity conditions, respectively.

5.2.3 Gait and Stretch Reflex

As hypothesized, the stretch reflex did not change following acute exposure to reduced gravity locomotion. Since this reflex is hard-wired between the muscles and spinal column, it is not surprising that no change occurred. Also, the data verified the results of van den Kroonenberg who found that stretch reflex latency was approximately 24 ms for young as well as elderly subjects [Kroonenberg, 1995].

The results of the gait analysis protocol validated the use of the inverted pendulum model for limited walking cases. The video data revealed that the hip followed an arc-like trajectory between heel strike and toe-off. This trajectory is predicted by the inverted pendulum model. As an anecdotal result, the earlier predictions of Shavelson and Margaria that reduced gravity locomotion would be difficult were verified by this experiment. Many subjects complained that while walking in simulated lunar gravity it was very difficult to maintain contact with the ground. This difficulty is undoubtedly due to the fact that the change in potential energy at 1/6 g is not large enough to support forward motion at that speed without an aerial phase.

5.2.4 Posture Data

The protocol followed for the posture section of this experiment is based largely upon experiments conducted by Collins [Collins, 1993]. Therefore, it could be expected that the results are similar Fortunately, that is the case. However, a difference was noticed between the long and short term temporal characteristics of human gait. The short term behavior of the CoP trajectory time trace exhibited much more random behavior than the long term. Also, the short term behavior showed a persistent trend while the long term showed anti-persistent trends. This data matches findings by Collins.

However, a discrepancy arises over the interpretation of results. Collins refers to the short term behavior as Open loop, and the long term behavior as Closed loop. As the

model has shown, the system loop is continuously closed. Thus, the observed behavior must be explained through other means. The short term persistence exhibited could be explained by the inertial characteristics of the system. As the pendulum swings in any direction, its motion tends to stay in that direction until an outside force (ankle torque) changes the direction. Due to the mass of the system and therefore moment of inertia of the system, this change cannot be instantaneous. The combination of mass and inertial characteristics leads to persistent behavior. The long term behavior is more a product of the loop closure than the plant itself. Without closed loop control, any perturbation in the states causes the system to go unstable, i.e., the subject would fall. By closing the loop, stability is attained by reversing the direction of motion when the subject starts to fall. The reversal of motion direction is necessary in order to maintain stability. This situation causes the plant to exhibit anti-persistent behavior. So it is apparent that it is the characteristics of the system, rather than an intermittent loop closure that causes the observed behavior.

As discussed in Section 5.1.3b, Model Data, the estimator based model proved to be an excellent model of quiet standing performance. It captured both the spatial and temporal qualities of CoP trajectory time trace. The reflex loop by itself produces a quick, jerky response, yet succeeds in stabilizing the inverted pendulum plant. The addition of vestibular cues provides a smoother response which more closely resembles the trajectory followed by the CoP. Additionally, the use of a variable muscle gain within the plant produced the same result as low gravity locomotion, the end result being in a larger postural sway and a higher root mean square CoP position.

However, the current model fails to explain why one subject actually underwent a decrease in rms position rather than an increase. According to the hypothesis of reduced gains in lower leg musculature, and also according to the model developed, an increase in postural sway is expected. The altered response of one subject can be explained by an additional model element. The model in its current state ignores the effects of voluntary hyperactivation of the leg muscles. In fact, the model assumes no voluntary corrective action. This may, in fact, be an invalid assumption. By adding a cognitive variable in the feedback path, the model can replicate the response elicited by subject A, while simultaneously predicting performance for the other nine subjects.

The subjects were instructed not to change their postural strategies during the post exposure trials. Nine out of ten subjects appear to have followed these direction. These

subjects did not change their postural strategy and hence their performance was adversely affected by the decrease in muscle gain. However, it is proposed that subject A was aware of the decreased muscular gain and, in an effort to compensate for this decrease, the subject cognitively increased his muscular activity level to enhance performance. This hypothesis seems plausible since subject A was a fully informed subject and was totally aware of the hypothetical changes that would take place following reduced g exposure.

This phenomenon was tested by inserting a variable activation level gain in the vestibular feedback path, as shown in Figure 5.27. Like the variable muscle gain in the plant, this gain had a very narrow band of stability. Despite this fact, through careful choice of gain magnitude, the inclusion of a variable cognitive activation gain in the model produced results similar to the results exhibited by subject A. The rms values of the CoP actually decreased in the post exposure case, despite the fact that the muscular gains were decreased. The original hypothesis regarding the lowering of muscular gains following brief exposure to reduced gravity is validated by the expansion of the subjects' CoP trajectories and by the ability of the model to duplicate this result.

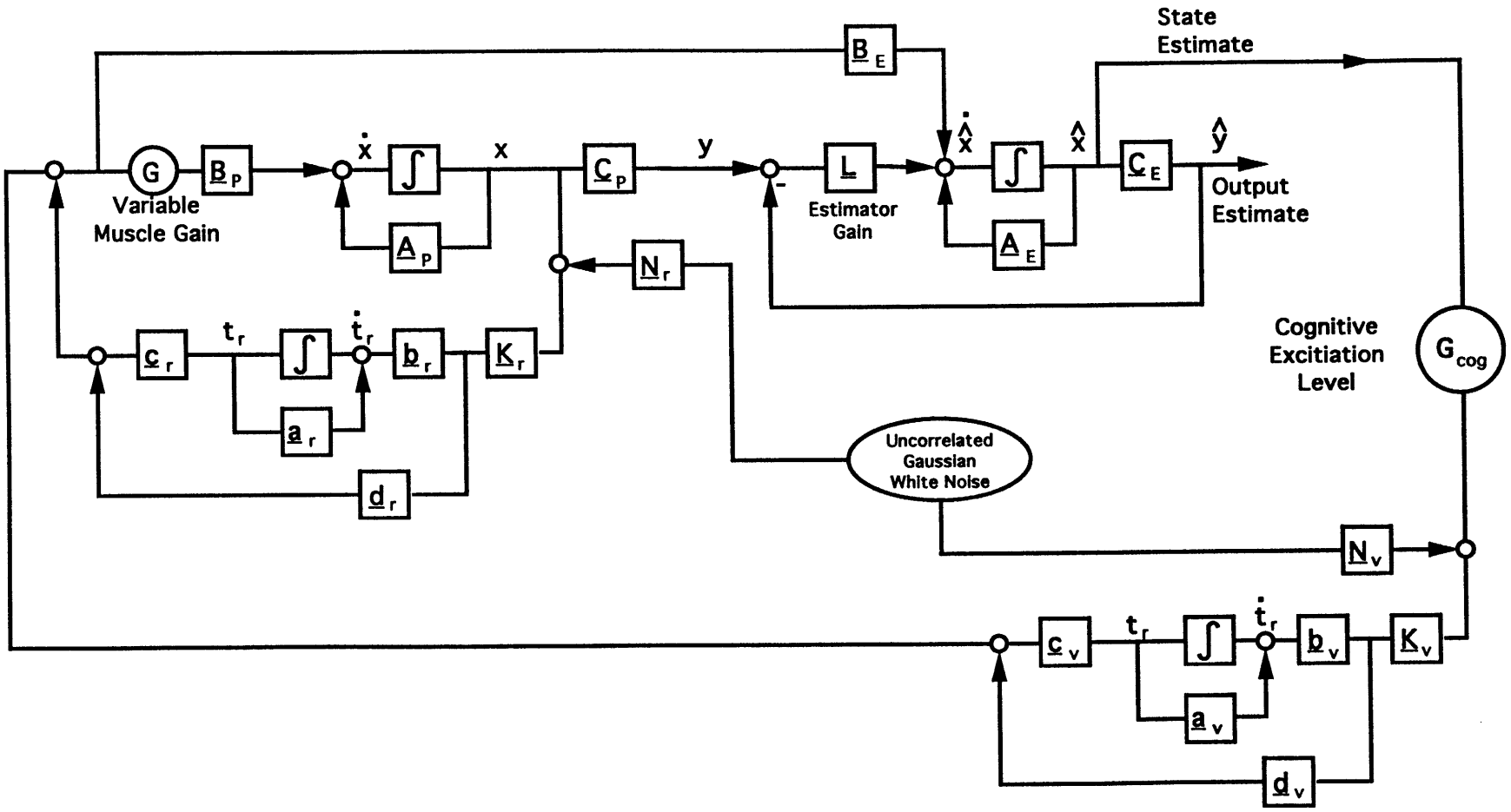

Figure 5.27 Complete Estimator-Based State-Space Model of Posture with Variable Cognitive Excitation Level. Normally, as the varibable muscle gain G is lowered, the performance of the system degrades. By raising G_{cog}, performance can be maintained and even improved over original levels despite the lower muscular gains.

Chapter 6 Summary and Conclusions

This thesis investigates the effect of gravity on the mechanics and energetics of human locomotion. Having evolved in a 1 g environment, humans are optimally adapted to that environment. Their presence in a new arena requires adaptation before normal activity can be resumed, and upon return to Earth, a readaptation must occur.

Recommendations for future experiments include the addition of a visual protocol in the postural task, allowing the influence of vision on postural stability to be investigated. Such an addition will add more realistic elements to the estimator based control theory model. Also, enhancements to the current video analysis system could possibly lead to a better understanding of post exposure gait changes. The current system is limited to two dimensional analysis and has limited resolution. Additionally, experimental protocols need to be developed that better reveal changes following partial g exposure. By conducting the posture protocols immediately following exposure, more dramatic results may be obtained.

The thesis introduction provides the motivation for this research, identifying the research questions and contributions of the thesis. These experiments are designed to: 1) determine the metabolic costs associated with partial gravity locomotion; 2) investigate the presence of the 'heavy legs' syndrome following brief low g exposure; and 3) develop a model that encompasses the important characteristics of postural stability. The contributions of this experiment include 1) the design of an effective reduced gravity simulator; 2) providing an experimental database; and 3) the use of modern control techniques to effectively model human posture.

Chapter two provides sufficient background on muscular behavior, locomotion, energetics and workload, and the estimator based control model. Running and walking are fundamentally different. During walking, the constant exchange of potential and kinetic energy results in a very efficient means of locomotion. Running, on the other hand, delivers increases in KE and PE at the same time, resulting in a very inefficient gait. Only through the recovery of energy through elastic means, does running become remotely efficient. This lack of energy recovery is the reason running is more than twice as energy consuming as walking on Earth. The disparity in energy consumption becomes less pronounced in reduced gravity. Postural stability is shown to decrease following prolonged exposure to microgravity, and may be caused by vestibular dysfunction,

muscular atrophy, or by changes in postural strategy adopted in space. This decrease in stability causes a more postural sway and therefore a larger deviation in the location of the subject's center of mass. This increased deviation may be a function of decreased muscular gains.

Partial gravity simulation techniques are outlined in Chapter three, with a heavy concentration on suspension techniques since that is the simulation technique used for this study. The advantages and disadvantages of all simulation techniques are noted and discussed in this chapter.

Chapter four details the experimental methods and hardware used to conduct this experiment. Ten subjects participated in each segment of the experiment. Those participating in the metabolic study ranged in age from 21 to 40 years, in height from 1.62 to 1.83 m, and weight from 512 to 770 N. The subject population for the musculoskeletal experiments ranged in age from 20 to 30 years, height from 1.57 to 1.95 m, and weight from 512 to 936 N. All experiments were run at the MIT's Man-Vehicle Laboratory with the approval of MIT's Committee On the Use of Humans as Experiment Subjects (COUHES).

Chapter four also outlines the estimator based model of human posture. The model uses modern state space control techniques, with optimal control properties to model the characteristics of quiet standing. The model contains two feedback loops, an inner reflexive loop, and an outer vestibular loop. Each loop adds realistic time delays (30 and 80 milliseconds for each respective loop) to add validity to the model. The vestibular loop also includes an estimator that reconstructs the states of the system from its own internal representation of the model.

Chapter 5 presents the experimental results and provides a detailed discussion of these results. The metabolic protocol showed that the metabolic cost of both running and walking decreased linearly as simulated gravity level was reduced. This test also revealed that below a 0.3 g's, the Cost of Transport of running was less than that of walking, largely due to the fact that, when walking in partial g environments, a great deal of energy is required to maintain upright posture, and that all of that energy is basically lost. The forward momentum associated with running, and the increased aerial phase in low g, makes running a more efficient means of travel.

The musculoskeletal protocol showed that changes were present in all three post exposure cases (None, Knee, and Jump) in both gait and postural analysis. Increased vertical ground reaction forces were noted following low g locomotion. These changes were most pronounced in the case when no post-exposure exercise was performed (None), and least evident when broad jumps were performed (Jump).

Similar trends were observed in the postural analysis. Postural instability increased in all cases following partial g exposure. As in the gait analysis, this change was largest when no post-exposure exercise was performed, and smallest when the broad jumps were executed. From this result, it is concluded that the performance of exercise following brief exposure to reduced gravity succeeds in countering the deleterious effects of reduced g locomotion. It was also concluded that the high peak forces exerted during the knee bends leads to readaptation by the subject and that by the addition of rapid change in forces through the performance of broad jumps, the readaptation is accelerated. A similar result was found by Cavanagh who noted that exercises that delivered high rates of change of forces (such as rowing) were more effective in combating deconditioning than exercises which did not (such as cycling) [Cavanagh, 1992].

The temporal analysis, which compares the change in position of the Center of Pressure (CoP) to the change in time interval, showed no change from pre to post-exposure, but revealed some interesting qualities about standing. The diffusion coefficients revealed the presence of higher stochastic activity in the short term than in the long term. The correlation coefficients showed that the trajectory of the CoP exhibits persistent behavior in the short term and anti-persistent behavior in the long term. Persistence means that any recent trend in performance is likely to be maintained. Conversely, anti-persistence indicates that the plant will most likely exhibit performance different than recently demonstrated.

The estimator model used was successful in replicating both the spatial and temporal characteristics of human standing. By lowering a **variable muscle gain** in the plant, results were attained that matched the results of the human subjects. A lowered gain results in increased root mean square position of CoP in both the x and y axes, and produces no change in the temporal characteristics of the trials.

The post exposure trials of Subject A showed a decrease rather than an increase in rms position. It was hypothesized that this decrease was the result of an increase in activity at

the cognitive level. This subject, sensing the change in muscle gain, hyperactivated his muscles in an effort to compensate for a recognized decrease in muscle gain. This was modeled by including a **activation level gain** in the cortical feedback path, and by increasing the model gain. Increasing the gain yielded the same results exhibited by subject A. The rms position decreased despite lower muscular gains.

It can be concluded that the 'heavy-legs' phenomenon does, in fact, exist, and that it is caused by a change in muscular gains by the central nervous system in an effort to adapt to partial gravity locomotion. This adaptation leaves the muscles ill-suited to perform their tasks once return to 1 g takes place, resulting in heavy legs. This sensation can be relieved through the performance of exercises requiring high maximum forces (knee bends) and high rates of change of forces (broad jumps). The knee bend and broad jump exercises succeed in restoring the muscular gains toward pre-exposure levels, allowing normal locomotion to occur after acute partial gravity exposure.

The final chapter restated the highlights of the first five chapters. Chapter six outlined the motivation for the experiment, provided sufficient background for the thesis, described the hardware used and subjects who participated in the experiment, presented the results of all experiments conducted, and discussed the importance of the results.

This thesis investigated changes in human leg muscles following acute exposure to simulated Martian and lunar gravity, specifically, the hypothesis that muscular gains are lowered during reduced gravity exposure and a period of readaptation occurs upon return to a 1 g environment. The gait analysis protocols revealed increased ground reaction forces following low g exposure. The reflex protocol verified the hypothesis that reduced g exposure would not change reflex latency. The posturography experiment showed a significant increase in postural sway. The estimator based control model of posture successfully replicated the experimental data by lowering a variable muscle gain in the model, adding validity to the hypothesis that muscular gains are lowered during acute low g exposure. Subject A showed a decrease in postural sway following partial g exposure. The model was able to duplicate this data by inserting an additional, cognitive activation gain which was increased post exposure. Raising this gain caused less postural sway than before low g exposure, as exhibited by Subject A. The success of this model lends more credibility to the variable muscle gain hypothesis.

References

Alexander, R. McN. "Three Uses for Springs in Legged Locomotion." International Journal of Robotics 9.2 (1990).

Amundsen, L.R. "Isometric Muscle Strength Testing with Fixed-Load Cells." Muscle Strength Testing. Ed. L.R. Amundsen. 1987. 89-111.

Astrand, P.O., and K. Rodahl. Textbook of Work Physiology. 3rd ed. New York: McGraw-Hill Book Company, 1986. 756.

Blickhan, R., and R.J. Full. "Locomotion Energetics of the Ghost Crab." Journal of Experimental Biology 130 (1987): 155-174.

Boyd, I.A. "The isolated mammalian muscle spindle." The Motor System in Neurobiology. Ed. Evarts, Wise and Bousfield. 1985. 154-167.

Cavagna, G. A. "Force platforms as ergometers." Journal of Applied Physiology 39. No 1 (1985): 174-179.

Cavagna, G.A., N.C. Heglund, and C.R. Taylor. "Mechanical work in terrestrial locomotion: two basic mechanisms for minimizing energy expenditure." American Journal of Physiology 233.5 (1977): R243-R261.

Cavagna, G.A., H. Thys, and A. Zamboni. "The Sources of External Work in Level Walking and Running." Journal of Physiology 262 (1976): 639-657.

Cavagna, G.A., A. Zamboni, and T. Faraggiana. "Jumping on the Moon: Power Output at Different Gravity Values." Aerospace Medicine April (1972): 408-415.

Cavanagh, P.R., B.L. Davis, and T.A. Miller. "A Biomechanical Perspective on Exercise Countermeasures for Long Term Space Flight." Aviation Space and Environmental Medicine .63 (1992): 482-485.

Collins, J.J., and C.J. DeLuca. "Random Walking during Quiet Standing." Physical Review Letters 73.5 (1994): 764-767.

Collins, J.J., and C.J. DeLuca. "Open-loop and Closed-loop control of posture: A random-walk analysis of center-of-pressure trajectories." Experimental Brain Research 95 (1993): 308-318.

Davis, B.L., and P.R. Cavanagh. "Simulating Reduced Gravity: A Review of Biomechanical Issues Pertaining to Human Locomotion." Aviation, Space, and Environmental Medicine June (1993): 557-566.

DeLuca, C. J. Physiology and Mathematics of Myoelectric Signals. IEEE Transactions on Biomedical Engineering. IEEE, 1979. BME-26: 313-325.

Dietz, V., and G.A. Horstmann. "Afferent Control of Posture." Tutorials in Motor Neuroscience. Ed. J. Requin and G.E. Stelmach. Netherlands: Kluwer Academic Publishers, 1991. 209-222.

Farley, C.T, and T.A. McMahon. "Energetics of walking and running: insights from simulated reduced gravity experiments." American Physiological Society (1992): 2709-2712.

Fedak, M. A., L. Rome, and H. J Seeherman. "One-step N2-dilution technique for calibrating open-circuit VO2 measuring systems." American Physiological Society (1981): 772-776.

Fox, S.C. "Posture Control in a Partial Gravity Environment." M.S. University of Houston, 1993.

Full, R.J. "Locomotion Energetics of the Ghost Crab." Journal of Experimental Biology 130 (1987): 137-153.

Getting, P.A. Understanding Central Pattern Generators: Insights Gained From the Study of Invertebrate Systems. Neurobiology of Vertebrate Locomotion. Ed. S. Grillner, et al. Stockholm: MacMillan Publishers, 1985. 213-244.

He, J., R. Kram, and T.A. McMahon. "Mechanics of running under simulated low gravity." American Physiological Society (1991): 863-870.

Heglund, N.C., G.A. Cavagna, and C.R. Taylor. "Energetics and Mechanics of Terrestrial Locomotion." Journal of Experimental Biology 97 (1982): 41-56.

Heglund, N.C., et al. "Energetics and Mechanics of Terrestrial Locomotion." Journal of Experimental Biology 97 (1982): 57-66.

Hewes, D.E. "Reduced Gravity Simulators for Studies of Man's Mobility in Space and on the Moon." Human Factors 11(5) (1969): 419-432.

Horrigan, D.J., et al. Overview of Crew Member Energy Expenditure During Shuttle Flight 61-B Ease/Access Task Performance. Space Construction Conference. Langley Research Center: 1986. 228-235.

Houk, J. C. "Cooperative Control of Limb Movements by the Motor Cortex, Brainstem and Cerebellum." Models of Brain Function. Ed. Cotterill. Cambridge, England: Cambridge University Press, 1989. 309-325.

Kearney, R.E., and I.W. Hunter. "System identification of human stretch reflex dynamics: Tibialis anterior." Experimental Brain Research 56 (1984): 40-49.

Kearney, R.E., and I.W. Hunter. "System Identification of Human Triceps Surae Stretch Reflex Dynamics." Experimental Brain Research 51 (1983): 117-127.

Keller, T.S., A.M. Strauss, and M Szpalski. Prevention of Bone Loss and Muscle Atrophy During Manned Space Flight. 42nd Congress of the International Astronautical Federation. Montreal, Canada: American Institute of Aeronautics and Astronautics, Inc., 1991. 1-13.

Kroonenberg, A. van den. "Dynamic Models of Human Falls for Prediction of Hip Fracture Risk." Ph.D. Massachusetts Institute of Technology, 1995.

Layne, C.S., and B.S. Spooner. "Microgravity Effects on "Postural" Muscle Activity Patterns." Advanced Space Research 14.8 (1994): (8)381-(8)384.

Margaria, R. Biomechanics and Energetics of Muscular Exercise. Oxford, England: Oxford University Press, 1976.

Margaria, R., and G. Cavagna. "Biomechanics of Exercise at Reduced Gravity." (1971):

Margaria, R., and G.A. Cavagna. "Human Locomotion in Subgravity." Aerospace Medicine December (1964): 1140-1146.

McMahon, T.A. "The Role of Compliance in Mammalian Running Gaits." Journal of Experimental Biology 115 (1985): 263-282.

McMahon, T.A. Muscles, Reflexes, and Locomotion. Princeton, New Jersey: Princeton University Press, 1984.

McMahon, T.A., and G.C. Cheng. "The Mechanics of Running: How Does Stiffness Couple with Speed?" Journal of Biomechanics 23 Suppl. 1 (1990): 65-78.

Newman, D.J. Class Notes-Aerospace Physiology and Life Support Engineering. M.I.T., 1993.

Newman, D.J. "Human Locomotion and Energetics in Simulated Partial Gravity." Ph.D. Massachusetts Institute of Technology, 1992.

Newman, D.J. "Human Locomotion and Energetics in Simulated Partial Gravity." Ph.D. Massachusetts Institute of Technology, 1992.

Newman, D.J., and H.L. Alexander. Human Locomotion and Workload for Simulated Lunar and Martian Environments. 42nd Congress of the International Astronautical Federation. Montreal, Canada: International Astronautical Federation, 1991. 1-7.

Newman, D.J., and H.L Alexander. "Human Locomotion and Workload for Simulated Lunar and Martian Environments." Acta Astronautica 29.8 (1993): 613-620.

Paloski, W.H., et al. "Vestibular Ataxia Following Shuttle Flights: Effects of Microgravity on Otolith-Mediated Sensorimotor Control of Posture." American Journal of Otology 14.1 (1993): 9-17.

Paloski, W.H., et al. Spaceflight-Induced Changes in Posture and Locomotion. International Society of Biomechanics XIVth Congress. Paris, FR: 1993. 40-41.

Paloski, W.H., et al. "Recovery of Postural Equilibrium Control following Spaceflight." Annals of the New York Academy of Sciences 656 (1992): 747-754.

Paloski, W.H., et al. Neurosensory Adaptation Associated with Postural Ataxia Following Spaceflight. XIth International Symposium of the Society for Postural and Gait Research. Ed. M. Woollacott and F. Horak. Portland, OR: University of Oregon Books, 1992. 1: 311-314.

Pandy, M.G., and F.E. Zajac. "Optimal Muscular Coordination Strategies for Jumping." Journal of Biomechanics (1990):

Pearson, K. "The Control of Walking." Scientific American (1978): 72-86.

Prescott, E.J., and E.C. Wortz. "Metabolic Costs of Upper Torso Exercises vs Torque Maneuvers Under Reduced gravity Conditions." Aerospace Medicine .October (1966): 1046-1049.

Robertson, W.G., and E.C. Wortz. "Effect of Lunar Gravity on Metabolic Rates." Aerospace Medicine August (1968): 799-805.

Runge, C.F., et al. Estimating Joint Torques From Kinematic and Reaction Force Data: A New Approach. XVth Annual International Conference of IEEE. Ed. Y.J. Andrews. 1993.

Sanborn, W.G., and E.C. Wortz. "Metabolic Rates During Lunar Gravity Simulation." Aerospace Medicine .April (1967): 380-382.

Shavelson, R.J. "Lunar Gravity Simulation and its Effect on Human Performance." Human Factors 10(4) (1968): 393-402.

Stein, R.B. "What Muscle Variables(s) Does the Nervous System Control in Limb Movement." Behavioral and Brain Sciences 5 (1982): 535-577.

Taylor, C.R., et al. "Energetic Cost of Generating Muscular Force During Running." Journal of Experimental Biology 86 (1980): 9-18.

Wortz, E.C. "Work in Reduced Gravity Environments." Human Factors 11(5) (1969): 433-440.

APPENDIX A

OPTIMAL CONTROL BACKGROUND

The purpose of this section is to provide a *brief* background on optimal control. This is by no means a comprehensive explanation of control theory, but it should provide enough background to allow the reader to understand the principles involved in cost minimization and follow the control steps used in this thesis.

The feedback gains used in the development of the posture model are Linear Quadratic Regulators (LQR). A regulator is a control device which attempts to minimize the states of the system, in this case, the sway angle of the inverted pendulum. A Linear Quadratic Regulator calculates the optimal feedback gain matrix $\underline{K}$ such that the feedback law $u=-\underline{K}x$ minimizes the cost function:

$$J = \int \left\{ x' \underline{Q} x + u' \underline{R} u \right\} dt \qquad \text{Eq.B1}$$

where $\underline{Q}$ is the cost matrix of the states
and $\underline{R}$ is the cost matrix of the controls.

In many systems, the cost matrices $\underline{Q}$, and $\underline{R}$ have physical meaning in either time, or real dollars. In many other systems, the control engineer must assign values to $\underline{Q}$, and $\underline{R}$. In such cases, the actual value of the matrices is not as important as the relative value of one matrix compared to the other. In such cases, the engineer must make a best guess as to the relative costs involved with each state and control. Such was the case in this thesis.

The LQR solution is subject to the constraint equation

$$\dot{x} = \underline{A}x + \underline{B}u \qquad \text{Eq.B2}$$

where x is the state vector
u is the control vector
and $\underline{A}$ and $\underline{B}$ are state equation matrices

This cost function is optimized by solving the Algebraic Riccati Equation (ARE):

$$0 = \underline{S}^{-1}\,\underline{A} + \underline{A}^{T}\,\underline{S} - \underline{S}\,\underline{B}\,\underline{R}\,\underline{B}^{T}\,\underline{S} + \underline{Q} \qquad \text{Eq.B3}$$

where $\underline{S}$ is the solution to the ARE.

The optimal feedback gain $\underline{K}$ can then be found through the equation:

$$\underline{K} = \underline{B}^{T}\,\underline{S} \qquad \text{Eq.B4}$$

By using the control feedback u=-$\underline{K}$x, this gain minimizes the cost function J.

This thesis also uses an estimator to reconstruct the states of the system. In a case where all of the states are not available for feedback, a system must use known quantities of the system such as the input and output of the system, to try and reconstruct the internal states of the system. The estimator-plant systems assumes that the plant adheres to the equations:

$$\dot{x} = \underline{A}x + \underline{B}u + \underline{G}w \qquad \text{Eq.B5}$$

$$y = \underline{C}x + \underline{D}u + v \qquad \text{Eq.B6}$$

where w and v are uncorrelated white noise disturbances
and $\underline{G}$ is the shaping matrix which acts upon the estimated state noise

The estimator gain matrix $\underline{L}$ is found, again using the Algebraic Ricatti Equation. The optimal gain is placed into the loop as shown in Figure 2.15. This now allows the state to be reconstructed by the estimator.

$$\dot{\hat{x}} = \underline{A}\hat{x} + \underline{B}u + \underline{L}\left(\underline{C}x - \underline{C}\hat{x} - \underline{D}u\right) \qquad \text{Eq.B7}$$

By subtracting the estimated output ($\underline{C}\hat{x}$) from the real output ($\underline{C}x$), the estimator stabilizes itself and will eventually provide a good estimate of the state vector x.

APPENDIX B

EXPERIMENTAL SUBJECT CONSENT FORM

This Appendix shows the informed consent form that all subjects read and signed before participating in either the metabolic or musculoskeletal portion of this study. The informed consent form was part of the documentation presented to MIT Committed on the Use of Humans as Experimental Subjects (COUHES) in order to obtain permission to run these experiments.

EXPERIMENTAL SUBJECT CONSENT FORM
"Etiology of perceived strength changes in the muscles of the legs following locomotion under simulated low gravity"

Principal Investigator:
Prof. Dava J. Newman[1]

Student Investigator:
Karl U. Schultz[2]

I. VOLUNTARY PARTICIPATION, RIGHT TO WITHDRAW

Participation in this experiment is voluntary and the subject may withdraw consent and discontinue participation in this experiment at any time without prejudice.

II. PURPOSE AND OBJECTIVE OF EXPERIMENT

Upon returning to Earth's gravity, astronauts have complained of weakness in their legs and a feeling of "heavy legs", making locomotion difficult for a significant period of time. It is important to study this phenomenon for many reasons. First, when returning to 1G from space flight, pilots must have an adequate perception and motor control to assure mission success. Secondly, it is important to understand how deconditioning occurs under conditions of low gravity, and the time course of muscular recovery. Lastly, understanding the how and why of this "heavy legs" feeling will aid in developing countermeasures for this condition.

The goal of this experiment is to study and quantify the performance of muscles involved in extending the knee under conditions of simulated low gravity (between 0G and 1G). In order to do this, the subject will be seated upon a suspended bicycle seat (so that the ensuing locomotion will be performed at a fraction of their body weight), and will run on a stationary treadmill for a short period of time. Data will be collected on muscle strength, stretch-reflex latency, and mechanical impedance of the leg muscles before and after the treadmill exercise. The final aim of the experiments will test the hypothesis: The perceived *heavy legs* feeling following exercise of short duration under simulated low gravity is not due to changes in muscle strength or the stretch-reflex latency.

III. EXPERIMENTAL PROTOCOL

Human Participants:

It is intended to collect data from up to 12 human subjects over the next twelve months. However, the plan for the Fall '94 semester is to run pilot studies with at least 2 subjects. The subject is free to ask any questions concerning the procedures followed. The specific measurements are detailed below.

---

[1]C.S. Draper Assistant Professor of Aeronautics and Astronautics, MIT, 33-119.
[2]Master's Candidate, Class of 1995, M.I.T. Department of Aerospace/Astrospace Engineering.

Research Plan:

Developing the tests and instrumentation. In order to test the hypothesis that no changes in muscle strength or stretch-reflex properties can be measured during the recovery from the *heavy legs* feeling, it will be necessary to construct and validate instruments and procedures for measuring the relevant neuromuscular parameters.

a). Muscle strength. Subjects will sit on an elevated chair that does not allow the foot to touch the floor. Conventional ankle weights of the type used for weight training will be attached to their ankles using Velcro straps. Subjects will be asked to lift the ankle, extending the knee as high as they can, and hold that position for 10 seconds. The weight will be adjusted until the angle of the shank is 30 degrees with respect to the horizontal when the subject is raising the weight, and the value of the weight will be recorded.

b). Stretch-reflex latency. A set of electromyographic (EMG) electrodes mounted in a plastic capsule containing an EMG preamplifier will furnish an EMG signal from the extensors of the knee (quadriceps) upon voluntary knee extension. Then, with the subject relaxed, the patellar tendon stretch reflex will be evoked by giving a single light tap to the tendon distal to the patella. The time between the mechanical stretch, as detected by an accelerometer on the hammer, and the first action potential of the EMG response will be recorded and called the "reflex latency".

c). Mechanical impedance of the knee extensors. An apparatus has been constructed for measuring the mechanical response to a step change in the torque applied to the human knee. A mathematical model is used to extract a number of parameters from this step response, including the stiffness and damping contributed by the muscle, a time constant characteristic of the spindle organs, and a gain characteristic of the reflex.

Data reduction and analysis. Histograms showing the results of strength, latency, mechanical impedance, and tracking ability before and after the treadmill locomotion will be prepared. Results of the subjective measures of strength and *heavy legs* will be compared as a function of time during the recovery.

IV. FORESEEABLE INCONVENIENCE, DISCOMFORT, AND RISKS TO THE SUBJECT

A. Delayed-onset muscle soreness may occur due to physical exercise performed as part of the experiment.

B. Hoisting the subject on a suspended harness may cause minor discomfort during the period of locomotion.

C. Standard risks involved with running or walking.

V. RISK MINIMIZATION

A. Treatment for sore muscles and other injuries incurred from participation in this experiment will be available through the M.I.T. Medical Department, at the expense of the subject's insurance carrier where applicable.

B. It will be possible for the experimenter to release the suspension or stop the mill during any point in the experiment without danger to the subject. All subjects will be familiarized with the equipment and trained in how to properly run on the treadmill.

VI. REMEDY IN THE EVENT OF INJURY

In the unlikely event of physical injury resulting from participation in this research, the subject understands that medical treatment will be available from the MIT Medical Department, including first aid emergency treatment and follow-up care as needed, and that his/her insurance carrier may be billed for the cost of such treatment. However, no compensation can be provided for medical care apart from the foregoing. The subject further understands that making such medical treatment available, or providing it, does not imply that such injury is the investigator's fault. The subject also understands that by his/her participation in this study he/she is not waiving any of his/her legal rights.* .

VII. VIDEOTAPED AND PHOTOGRAPHED IMAGES OF SUBJECTS

The subject may be videotaped or photographed during the experimental process, and such images may be used in the analysis of data and the presentation of experiment results.

VIII. COMPENSATION

The subject will receive no compensation for participating in this experiment.

IX. ANSWERS TO QUESTIONS

The subject may receive answers to any questions related to this experiment by contacting the Principal Investigator at (617) 258-8799.

X. IN THE EVENT OF UNFAIR TREATMENT

The subject understands that he/she may also contact the Chairman of the Committee on the use of Humans as Experimental Subjects, M.I.T. (617) 253-6787, if the subject feels that he/she has been treated unfairly as a subject.

XI. SIGNATURE

I, _____, have read and understand the information contained
(Subject's Printed Name)

in this consent form and agree to participate as a subject in this experiment.

_____ _____
(Subject's Signature) (Date)

* Further information may be obtained by calling the Institute's Insurance and Legal Affairs Office at (617) 253-2822.

APPENDIX C

LABVIEW™ SCRIPTS USED FOR DATA ACQUISITION

This appendix contains the transcripts of all Virtual Instruments (VI's) written for this thesis in the LabView™ data acquisition program from National Instruments™. Version 3.1 was used. Each of these VI's use canned VI's which are included with the basic LabView™ package. These sub-VI's were used for initialization of the acquisition board, acquisition of the data, data processing, and data streaming to a Matlab™ compatible format. The acquisition scripts written by the author included in this appendix are:

HAMMER_ACCEL
POSTURE
and FORCEPLATE

One additional sub-VI was included in this appendix due to its utility during this experiment. This sub-VI allowed the data to be streamed and stored in a format readable by the Matlab™ analysis software with no additional effort on the part of the author. This VI is called:

WRITE_TO_SPREADSHEET_FILE.vi

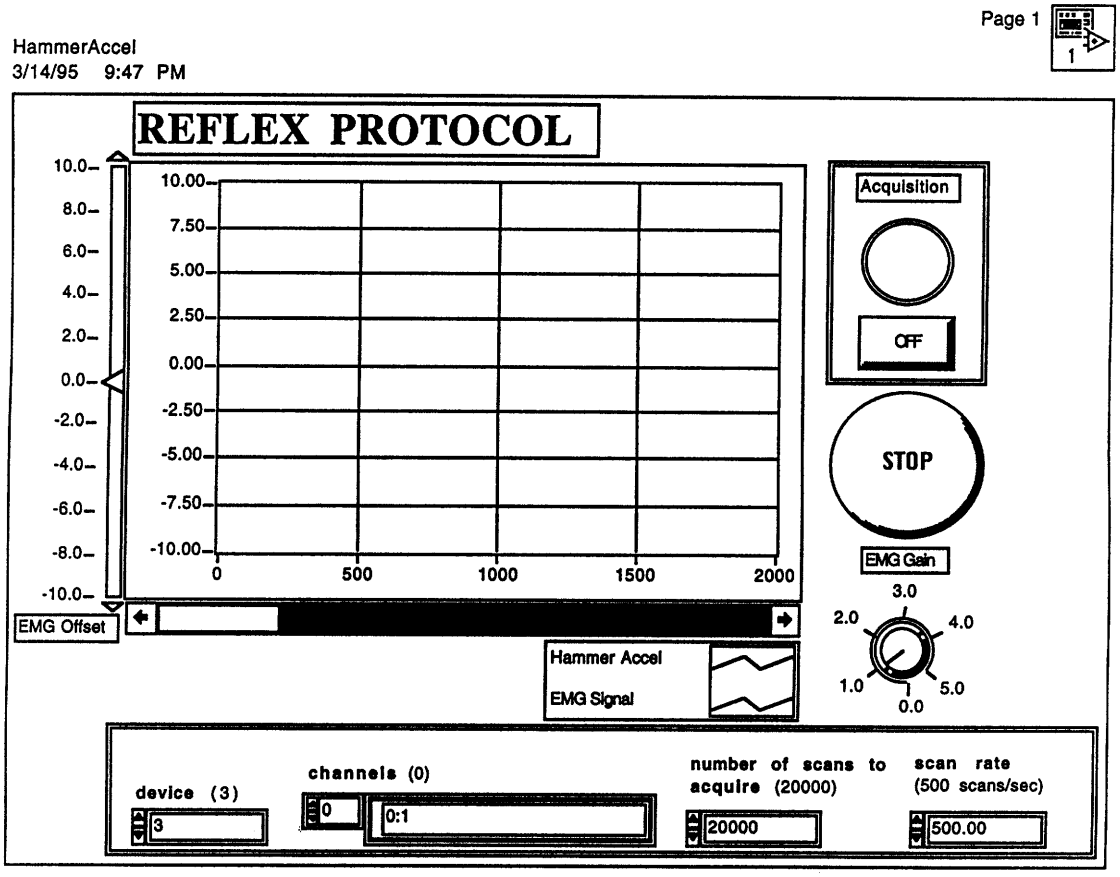
HammerAccel
3/14/95 9:47 PM
Page 1
1
REFLEX PROTOCOL
10.0
8.0
6.0
4.0
2.0
0.0
-2.0
-4.0
-6.0
-8.0
-10.0
EMG Offset
10.00
7.50
5.00
2.50
0.00
-2.50
-5.00
-7.50
-10.00
0
500
1000
1500
2000
Acquisition
OFF
STOP
EMG Gain
3.0
2.0
4.0
1.0
5.0
0.0
Hammer Accel
EMG Signal
device (3)
3
channels (0)
0
0:1
number of scans to acquire (20000)
20000
scan rate (500 scans/sec)
500.00

Block Diagram

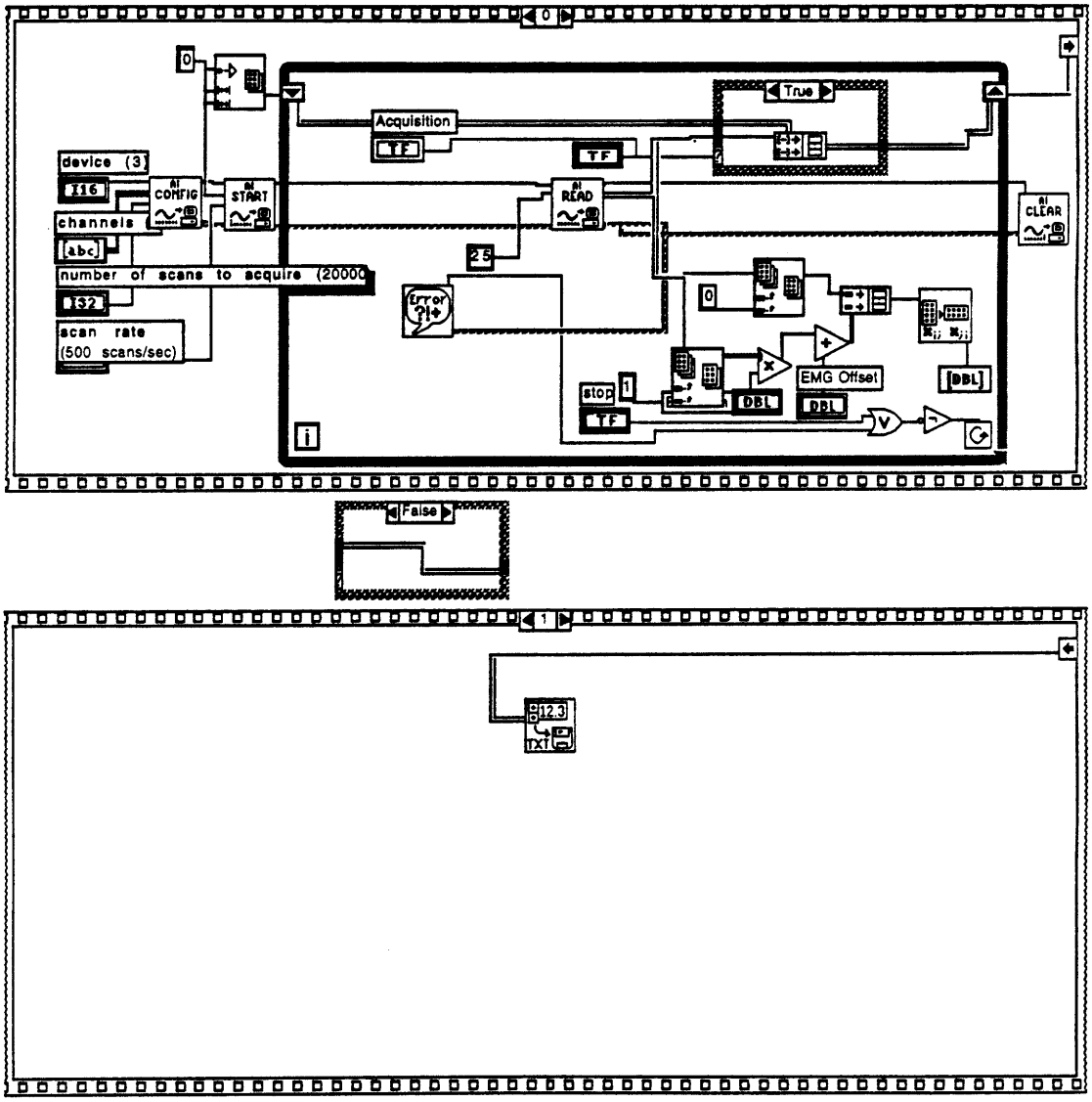

Forceplate
4/22/95 6:44 PM

Page 1

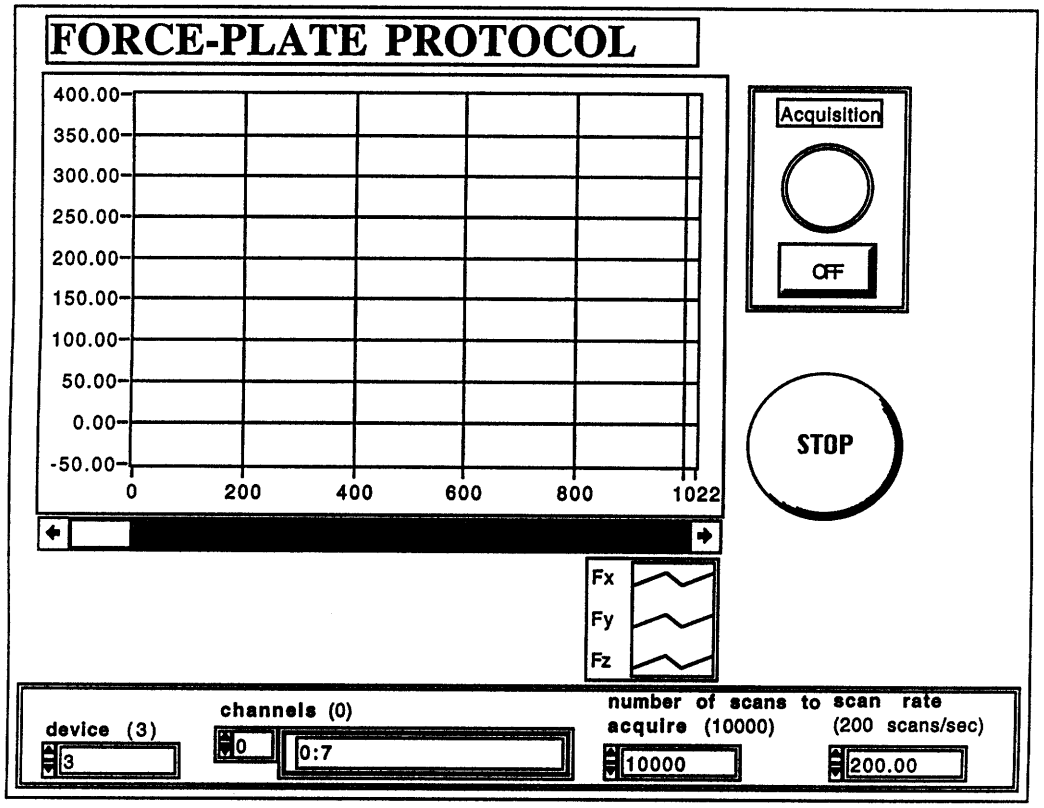

Forceplate
4/22/95 6:44 PM

Block Diagram

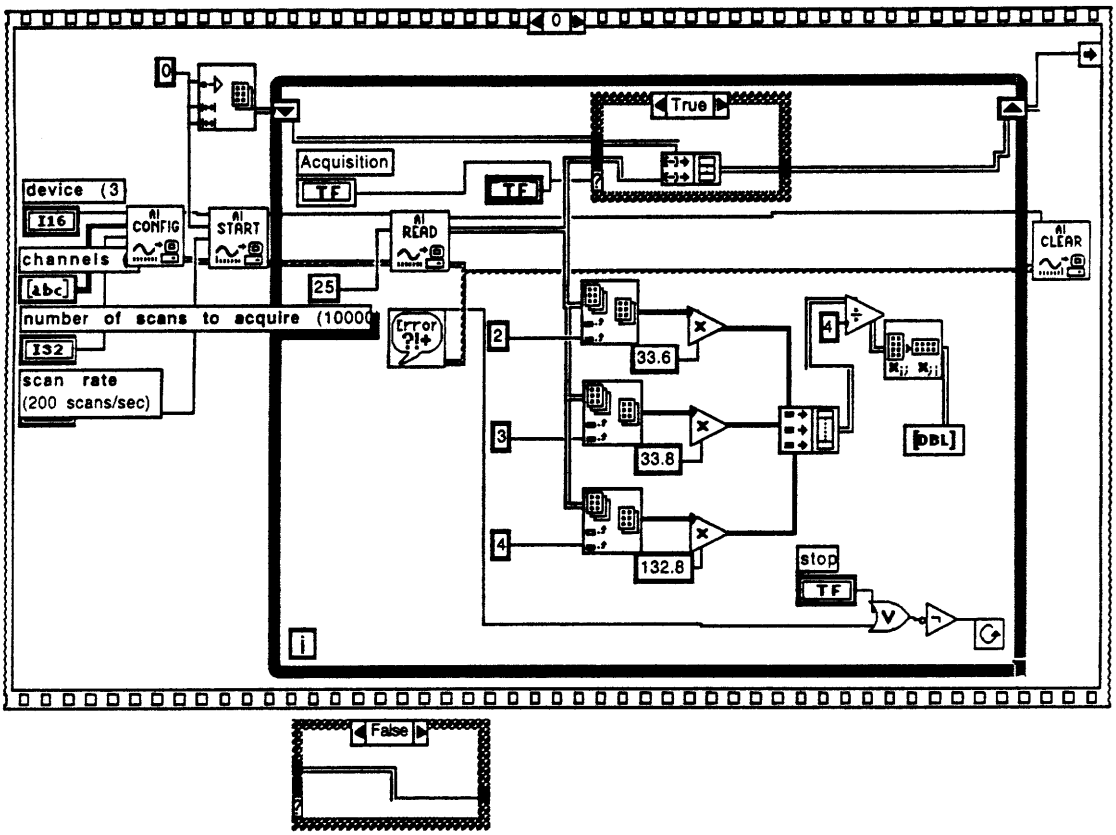

Page 3

Forceplate
4/22/95 6:44 PM

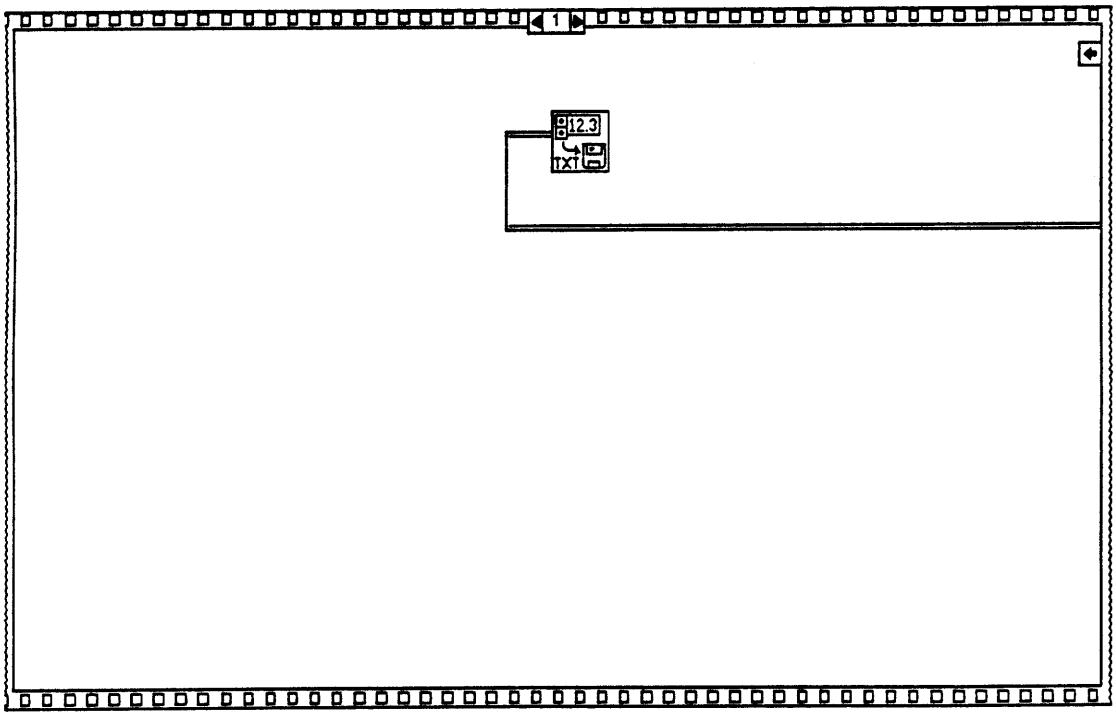

Page 1

Posture
3/14/95 6:34 PM

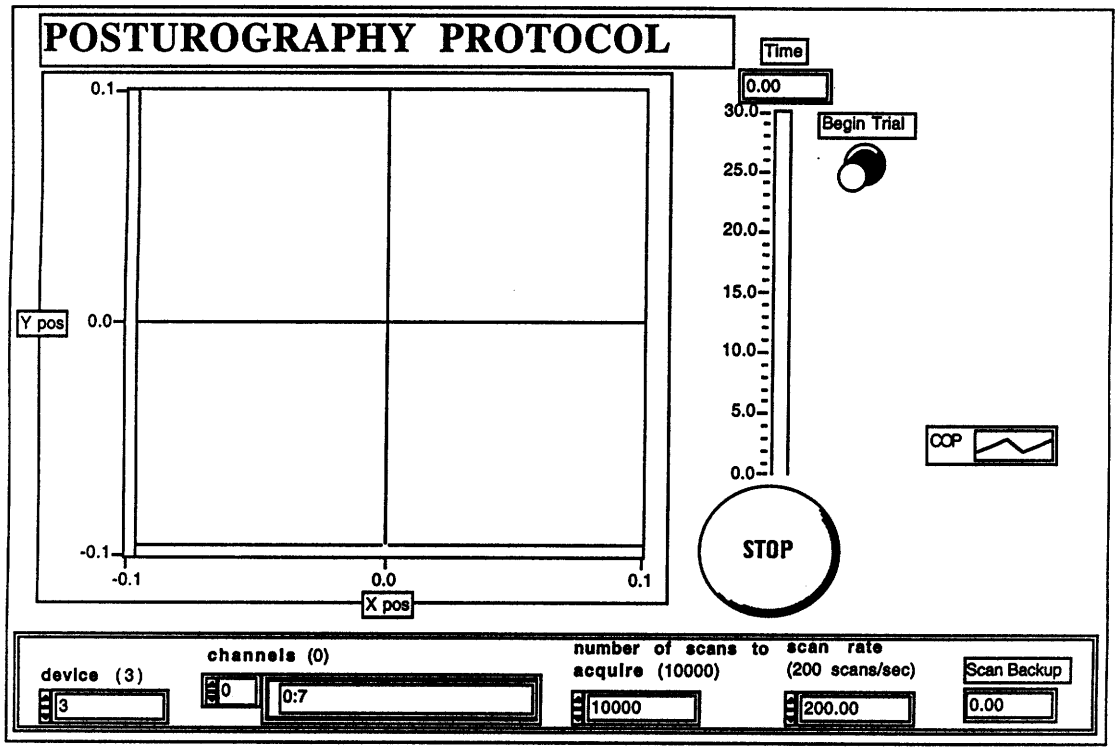

Posture
3/14/95 6:34 PM

Block Diagram

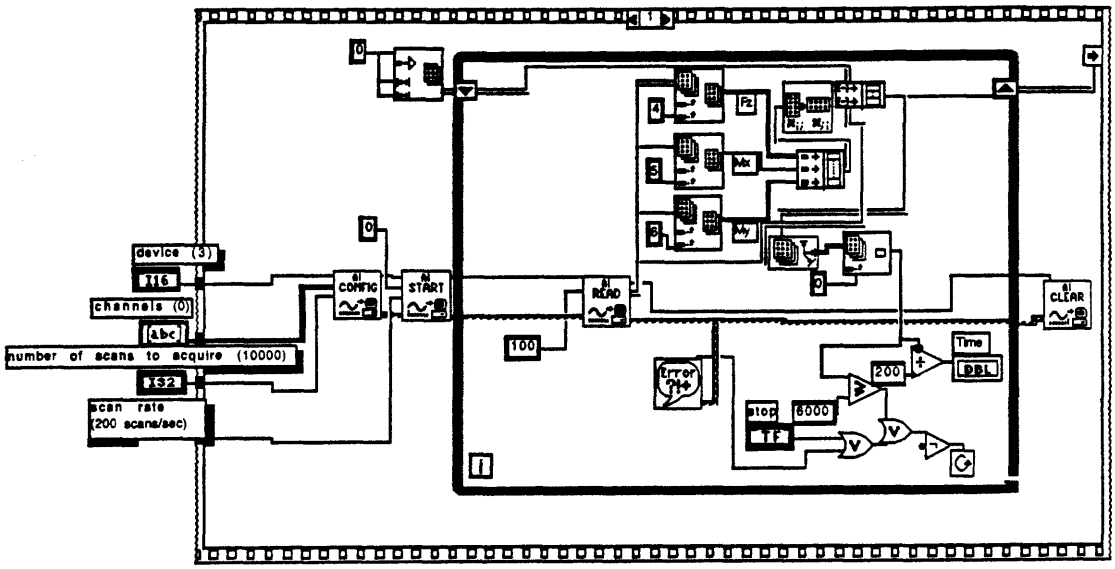

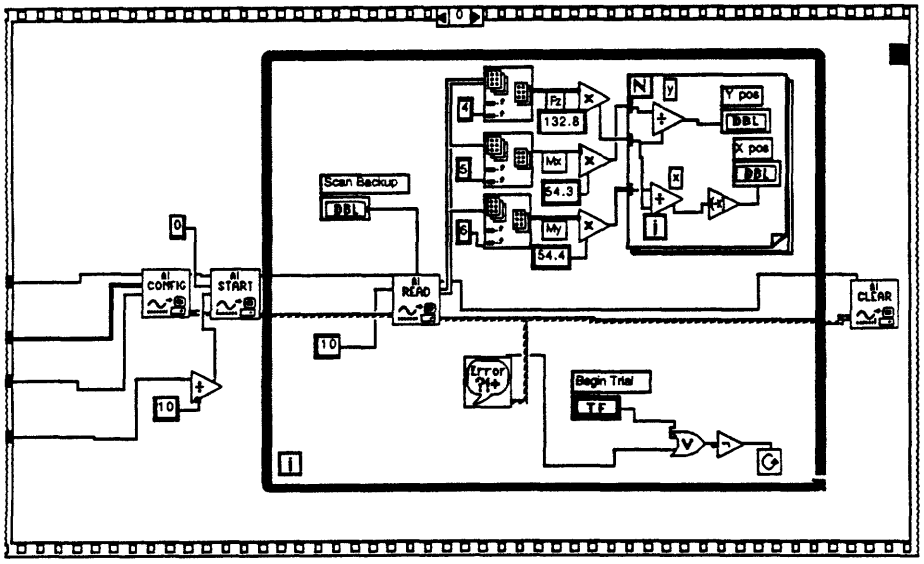

Posture
3/14/95 6:34 PM

Page 3

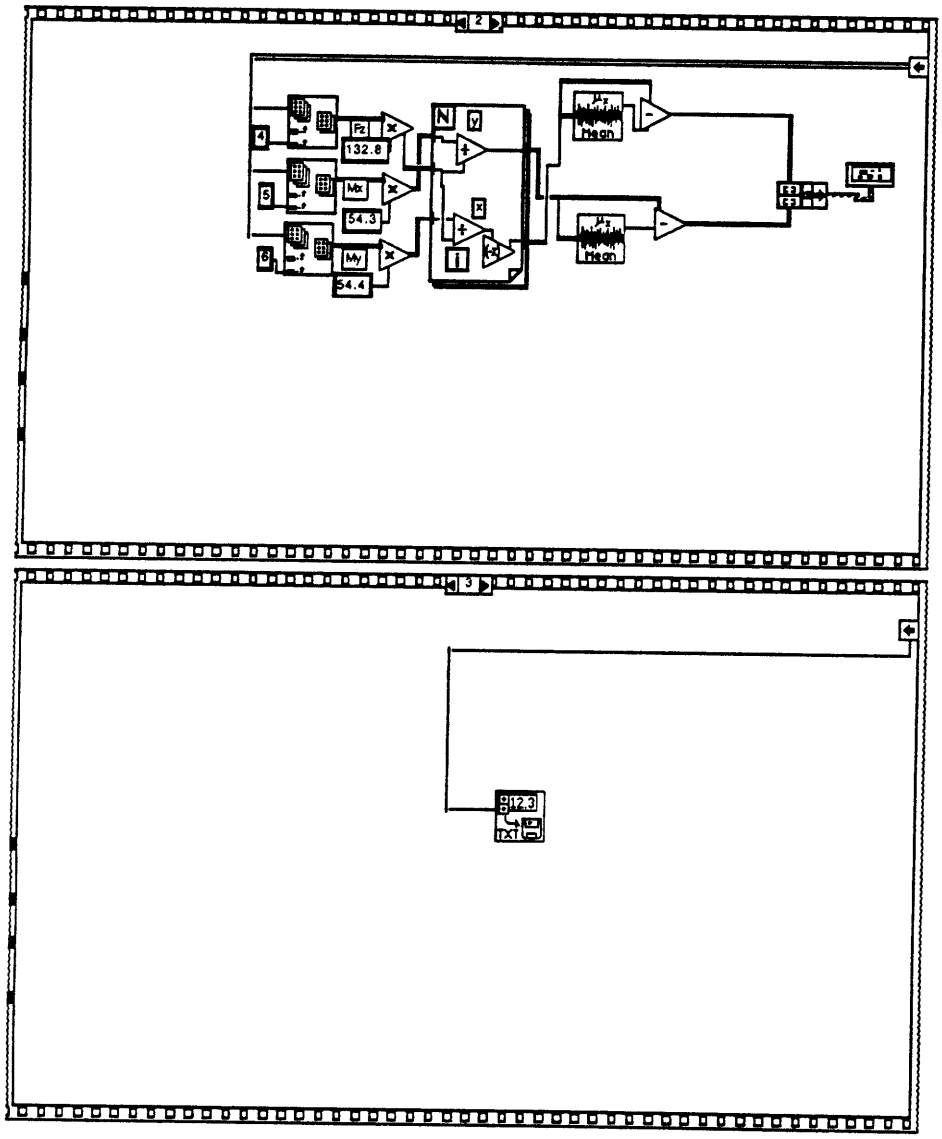

Write To Spreadsheet File.vi
5/22/95 4:47 PM

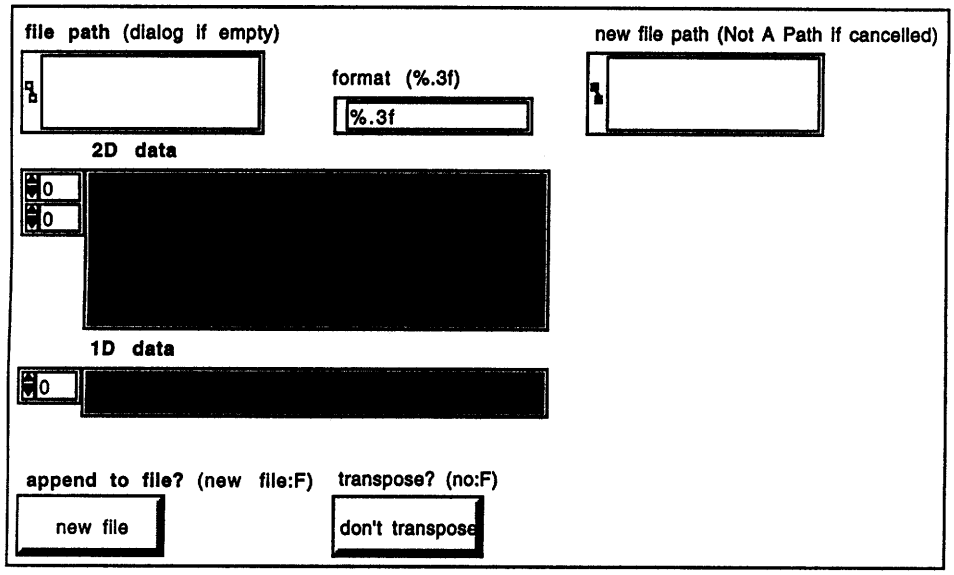

Write To Spreadsheet File.vi
5/22/95 4:05 PM

Block Diagram

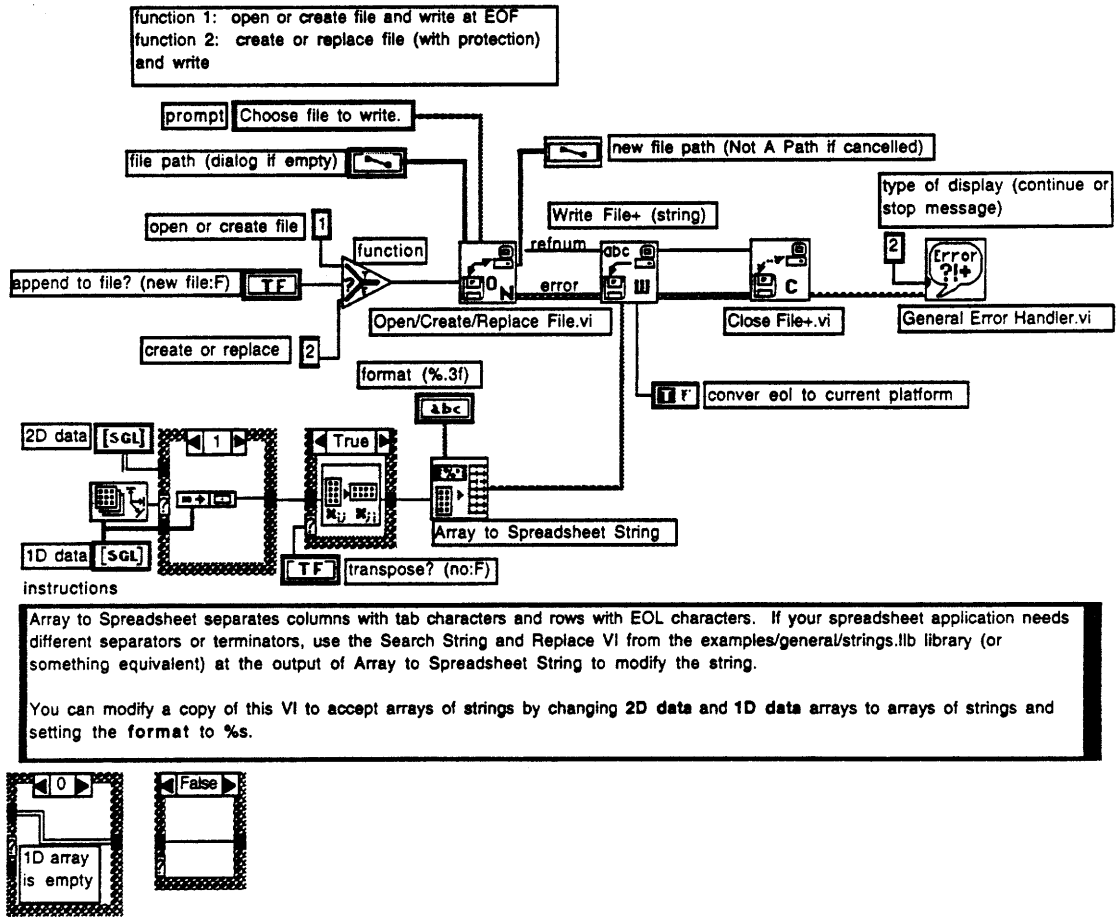

APPENDIX D

MATLAB™ SCRIPTS USED FOR ANALYSIS

This appendix contains the transcripts of all scripts written for this thesis in the Matlab™ analysis program. Version 4.2 was used. Subroutines from the Matlab™ Control Toolbox in used in some of the scripts.

The analysis scripts included in this appendix are:

REFLEX_ANALYZE.M
POSTURE_ANALYZE.M
POSTURE_ANALYZE_STEP2.M
FORCEPLATE_ANALYSIS.M
VIDEO_SCALE.M
CARTTOPOLAR.M
and POLARTOCART.M

This appendix also includes the transcript of the estimator based model used to model the human during quiet standing. This script is entitled

MUSCLE_PENDULUM_MODEL.M

```
%%% REFLEX_ANALYZE.M
%%%
%%% KARL U. SCHULTZ
%%%
%%% THIS PROGRAM DETERMINES REFLEX LATENCY
%%%

clear
clg

%%% SET UP DATA PATHS AND FILENAME
datapath='macintosh_hd:karl:thesis:analysis:data:';
datapath_out='macintosh_hd:karl:thesis:analysis:Summarydata:';
filename='ARPN1';

%%% DEFINE CONSTANTS
count=1;

%%% LOAD THE FILE
eval(['load ',datapath,filename])
eval(['x=',filename,';'])              %SET THE DATA VARIABLE NAME x

%%% PLOT THE ACCELEROMETER DATA
plot(x(:,1))
grid
text(1,-1,'Click on the threshold for capture')
point=ginput(1);
y=point(2);

%%% DETERMINE HOW MANY KNEE TAPS THERE WERE
i=1;
while (i<length(x))
        if (x(i,1)<y)
                point(count)=i;
                i=i+10;
                count=count+1;
        end
i=i+1;
end

clear i

%%% DEFINE THE DATA FOR EACH KNEE TAP
for i=1:(count-1)
hammerhit(:,i)=x(point(i)-5:point(i)+15,1);
emghit(:,i)=x(point(i)-5:point(i)+15,2);
end

%%% DETERMINE THE TIME DELAY BETWEEN THE MAX EMG SIGNAL AND
%%% MINIMUM ACCELERATION

for i=1:(count-1)
 [m,index1]=min(hammerhit(:,i));
 [m,index2]=max(emghit(:,i));
 time(i)=index2-index1;
end
```

```
%%% SAVE THE DATA
eval(['save ',datapath_out,filename,'sum.mat time'])
```

```
%%%POSTURE_ANALYZE.M
%%% KARL SCHULTZ
%%% MARCH 1995
%%%
%%% THIS PROGRAM WILL ANALYZE POSTUROGRAPHY DATA TAKEN FROM THE AMTI
OR6-5
%%% FORCEPLATE.
%%%
clear
clg

%%% SET UP PATH NAMES AND FILE NAMES
datapath='Macintosh_hd:users:karl:thesis:data:';
datapath_out='Macintosh_hd:users:karl:thesis:summarydata:';
filename='DPPN4';

%%% DEFINE CONSTANTS
parse=10; %TAKES EVERY X POINTS (DEFAULT==10)
time=10;  %THE AMOUNT OF TIME THROUGH WHICH TO ANALYZE (DEFAULT==10 sec)
skip=time*200/parse;  %INTERNAL VARIABLE
t=linspace(0,time,200*time/parse);  %DEFINES TIME VECTOR

%%% DEFINE SENSITIVITY MATRIX
sens=[2.974 .001 -.003 .008 -.016 .005;-.002 2.956 -.011 -.023 .019 .026;.001 -.006 .753 .004 .008
-.018;.001 -.005 0 1.84 .003 .026;-.005 .001 0 0 1.838 -.019;-.008 -.018 .002 .004 -.001 3.52];
cal=inv(sens);

%%% LOAD FILE AND CLEAR ORIGINAL DATA
eval(['load ',datapath,filename,';']);
eval(['xx=',filename,';']);
eval(['clear ',filename]);

%%% SCALE DATA USING THE CALIBRATION MATRIX
temp=(cal*xx(1:length(xx),3:8)'*100)';
fx=temp(1:parse:length(temp),1);
fy=temp(1:parse:length(temp),2);
fz=temp(1:parse:length(temp),3);
mx=temp(1:parse:length(temp),4);
my=temp(1:parse:length(temp),5);
mz=temp(1:parse:length(temp),6);

%%% COMPUTE POSITION OF FORCE
x=(my+fx*1.5/12)./(-fz)*12*25.4;  %%%FINDS THE X POSITION IN mm
y=(mx-fy*1.5/12)./fz*12*25.4;              %%%FINDS THE Y POSITION IN mm

%%% COMPARE x(t) to x(t+Δt) vs. Δt
%%% THIS COMPUTES THE TEMPORAL PROPERTIES OF THE TRIAL
for i=1:skip
dx2(:,i)=mean((x(1:length(x)-skip+1)-x(i:length(x)-skip+i)).^2);
dy2(:,i)=mean((y(1:length(y)-skip+1)-y(i:length(y)-skip+i)).^2);
dr2(:,i)=mean((y(1:length(y)-skip+1)-y(i:length(y)-skip+i)).^2+(x(1:length(x)-skip+1)-x(i:length(x)-
skip+i)).^2);
end

%%% COMPUTE MEAN AND RMS VALUES FOR x AND y
avgx=mean(x);
avgy=mean(y);
rmsx=mean(sqrt((x-avgx).^2))
```

```
rmsy=mean(sqrt((y-avgy).^2))
rmsr=rmsx+rmsy

%%% SAVE THE DATA
eval(['save ',datapath_out,filename,'sum.mat rmsx rmsy rmsr dx2 dy2 dr2'])
```

```
%%% POSTURE_ANALYZE_STEP2.M
%%% KARL SCHULTZ
%%% MARCH 1995
%%%
%%% THIS PROGRAM WILL ANALYZE POSTUROGRAPHY DATA TAKEN FROM THE AMTI
OR6-5
%%% FORCEPLATE.
%%%
clear
clg

%%% SET UP PATH NAMES AND FILE NAMES
datapath='Macintosh_hd:users:karl:thesis:data:';
datapath_out='Macintosh_hd:users:karl:thesis:summarydata:';
filename='APPN'; %FILE NAME
number=8; %HOW MANY FILES ARE THERE?

%%% DEFINE CONSTANTS
parse=10; %TAKES EVERY X POINTS (DEFAULT==10)
time=10; %THE AMOUNT OF TIME THROUGH WHICH TO ANALYZE (DEFAULT==10 sec)
skip=time*200/parse; %INTERNAL VARIABLE (HOW MANY POINTS ARE SKIPPED)
t=linspace(0,time,200*time/parse); %DEFINES TIME VECTOR

%%START ANALYSIS PROGRAM


%%% LOAD EACH DATA FILE IN SEQUENCE
for count=1:number
eval(['load ',datapath_out,filename,num2str(count),'sum.mat'])
Rmsx(count)=rmsx;
Rmsy(count)=rmsy;
Rmsr(count)=rmsr;
Fdr2(count,:)=dr2;
Fdx2(count,:)=dx2;
Fdy2(count,:)=dy2;
end

%%% TAKE DATA AVERAGES
dr2=mean(Fdr2);
dx2=mean(Fdx2);
dy2=mean(Fdy2);
rmsx=mean(Rmsx);
devx=std(Rmsx);
rmsy=mean(Rmsy);
devy=std(Rmsy);
rmsr=mean(Rmsr);
devr=std(Rmsr);


%%% PLOT DATA AND DETERMINE OPEN AND CLOSED LOOPS
%%% THIS DETERMINES THE SHORT AND LONG TERM PERIODS OF TEMPORAL DATA
clg
plot(dr2)
hold on
plot(dx2);
plot(dy2);
%axis([0 length(dr2) 0 100])
title('Subject XXX Trial # 1')
```

```
xlabel('Time (sec)')
ylabel('<Δ r ^2>  (mm ^2)')
text(1,90,'Click on one point on the first line (steep slope)')
s1=2;
plot([s1 s1],[0 100],':g');
s2=ginput(1);
s2=ceil(s2(1));
plot([s2 s2],[0 100],':g');

clg
plot(dr2)
hold on
plot(dx2);
plot(dy2);
%axis([0 length(dr2) 0 100])
title('Subject XXX Trial # 1')
xlabel('Time (sec)')
ylabel('<Δ r ^2>  (mm ^2)')
plot([s1 s1],[0 100],':g');
plot([s2 s2],[0 100],':g');
text(1,90,'Click on two points on the second line (shallow slope)')
l1=ginput(1);
l1=ceil(l1(1));
plot([l1 l1],[0 100],':g');
l2=ginput(1);
l2=ceil(l2(1));
plot([l2 l2],[0 100],':g');


%%% DEFINE t, dr, dx, AND dy FOR THE RANGES INPUTTED ABOVE
%%% THESE VARIABLES ARE USED FOR DETERMINING Ds AND Dl
sdr=dr2(s1:s2);
sdx=dx2(s1:s2);
sdy=dy2(s1:s2);
st=t(s1:s2);
ldr=dr2(l1:l2);
ldx=dx2(l1:l2);
ldy=dy2(l1:l2);
lt=t(l1:l2);

%%% DEFINE VARIABLES FOR LOG/LOG PLOTS
%%% THESE VARIABLES ARE USED FOR DETERMINING Hs AND Hl
logsdr=log10(sdr);
logsdx=log10(sdx);
logsdy=log10(sdy);
logst=log10(st);
logldr=log10(ldr);
logldx=log10(ldx);
logldy=log10(ldy);
loglt=log10(lt);

%%% REGRESS LINES
%%% THIS DETERMINES THE SLOPE OF EACH LINE
Ds=(sdr/[st])/2
Dxs=(sdx/[st])/2
Dys=(sdy/[st])/2
Dl=(ldr/[lt;ones(size(ldr))])/2
Dxl=(ldx/[lt;ones(size(ldr))])/2
```

```
Dyl=(ldy/[lt;ones(size(ldr))])/2

%%% REGRESS LOG/LOG LINES
%%%   THIS DETERMINES THE CORRELATION COEFFICIENT OF EACH LINE
Hs=(logsdr/[logst;ones(size(logsdr))])/2
Hxs=(logsdx/[logst;ones(size(logsdr))])/2
Hys=(logsdy/[logst;ones(size(logsdr))])/2
Hl=(logldr/[loglt;ones(size(logldr))])/2
Hxl=(logldx/[loglt;ones(size(logldr))])/2
Hyl=(logldy/[loglt;ones(size(logldr))])/2


%%%   PLOT THE RESULTS
clg
plot(t,dr2);
hold on
st=[0 2];
lt=[0 10];
plot(st,st*2*Ds(1),':r')
plot(lt,lt*2*Dl(1)+2*Dl(2),':r')
axis([0 time 0 100])
title('Subject XXX Trial # 1')
xlabel('Time (sec)')
ylabel('<Δ r ^2>  (mm ^2)')

%%%%FIGURE OUT WHERE THE CRITICAL POINT IS
lowtime=linspace(0,3,1000);
shortline=lowtime*2*Ds;
longline=lowtime*2*Dl(1)+2*Dl(2);
diff=longline-shortline;
[dummy,index]=min(abs(diff));
criticaltime=lowtime(index);
criticaldistance=(shortline(index)+longline(index))/2;
```

```
%%% FORCEPLATE_ANALYSIS.M
%%% KARL U. SCHULTZ
%%% MARCH 1995
%%%
%%% THIS PROGRAM ANALYZES THE FORCEPLATE DATA FROM THE AMTI %%% OR6-5
FORCEPLATE
%%%

clear
clg

%%% SET UP DATA PATHS AND FILENAME

datapath='macintosh_hd:karl:thesis:analysis:data:';    %%%THIS SETS THE PATH
                                                       %%%OF THE DATA FILES
filename='AFPN1';          %%%THIS IS THE NAME OF THE FILE BEING ANALYZED

%%% DEFINE CONSTANTS

%%% DEFINE SENSITIVITY AND CAL MATRICES (THESE ARE GIVEN IN THE AMTI MANUAL)
%%%    THIS SCALES THE DATA AND ACCOUNTS FOR CHANNELS CROSSTALK
sens=[2.974 .001 -.003 .008 -.016 .005;-.002 2.956 -.011 -.023 .019 .026;.001 -.006 .753 .004 .008
-.018;.001 -.005 0 1.84 .003 .026;-.005 .001 0 0 1.838 -.019;-.008 -.018 .002 .004 -.001 3.52];
cal=inv(sens);


%%% LOAD THE FILE
eval(['load ',datapath,filename,';'])  %%%LOAD THE PROPER FILE
eval(['xx=',filename,';']);            %%%SET THE VARIABLE NAME xx
eval(['clear ',filename]);             %%%CLEAR THE FILENAME VARIABLE

%%% PLOT THE DATA FILE
%%% THIS PLOTS THE fz VARIABLE SO THE OPERATOR CAN INPUT THE NUMBER OF STEPS
figure(1)
clg
plot(xx(1:15:length(xx),5));
x=axis;
hold on
ans=input('How many steps are there?')


%%% ZERO THE PLOT
%%% THIS ACCOUNTS FOR ANY OFFSET IN THE DATA
text(100,(x(3)+x(4)*3)/3.5,'Click on any zero plateau');
zero1=ginput(1);
zero1=zero1(1);
plot([zero1 zero1],[x(3) x(4)],'r--');
zero2=ginput(1);
zero2=zero2(1);
plot([zero2 zero2],[x(3) x(4)],'r--');
z1=min([zero1 zero2])*15;
z2=max([zero1 zero2])*15;
zero=mean((cal*xx(z1:z2,3:8)'*100)');

%%% SPLIT THE PLOT INTO ans NUMBER OF STEPS
%%% THIS PARSES THE DATA FILE INTO THE CORRECT NUMBER OF STEPS

text(100,(x(3)+x(4)*3)/4,'Click AFTER each step');
```

```
for click=1:ans
temp1=ginput(1);
tempo(click)=temp1(1);
plot([tempo(click) tempo(click)],[x(3) x(4)],'g:');
end
tempo=tempo*15;

%%%   REPEAT ANALYSIS ans NUMBER OF TIMES
%%%   THIS IS AN ITERATIVE PROCESS WHICH IS CARRIED OUT ON EACH STEP

in2=1;
for stepnumber=1:ans
in1=in2;
in2=round(tempo(stepnumber));


%%% DETERMINE WHETHER THE PERSON IS STEPPING FORWARD OR BACKWARD

if (stepnumber/2==floor(stepnumber/2))
        %%% THE NUMBER IS EVEN
                direction=-1;
else
                direction=1;
end

%%%% SCALE THE DATA USING THE CAL MATRIX

temp=(cal*xx(in1:in2,3:8)'*100)';
fx=temp(1:length(temp),1)*direction-zero(1);
fy=temp(1:length(temp),2)*direction-zero(2);
fz=temp(1:length(temp),3)-zero(3);
mx=temp(1:length(temp),4)*direction-zero(4);
my=temp(1:length(temp),5)*direction-zero(5);
mz=temp(1:length(temp),6)-zero(6);

t=linspace(0,length(fx)/200,length(fx));  %t IS THE TIME ARRAY

F=sqrt(fx.^2+fy.^2+fz.^2);                              %F IS THE TOTAL FORCE
Fshear=sqrt(fx.^2+fy.^2);                       %Fshear IS THE SHEAR FORCE

count=1;
stepbegin=0;

%%% DETERMINE WHERE THE STEP BEGINS,
%%% THE TIME TO PEAK, AND THE CONTACT TIME

for i=6:length(fx)-5
 if fz(i-5:i+5)>1
        y(count)=(mx(i)-fy(i)*1.5/12)/fz(i);
        x(count)=(my(i)+fx(i)*1.5/12)/(-fz(i));
        count=count+1;
        if (stepbegin==0)
                timestart(stepnumber)=i-7+in1;
                stepbegin=1;
        end

 end
end
```

```
rmax=0;
for i=1:length(x);
        for j=i:length(x)
         r=sqrt((x(i)-x(j))^2+(y(i)-y(j))^2);
         if r>rmax
                rmax=r;
         end
        end
end

for i=6:length(fx)-5
 if fz(i-5:i+5)>1
        break
 end
end
to=i-5;

%%%PLACE THE VARIABLES IN LARGER, GLOBAL VARIABLES

Fmax(stepnumber)=max(F);
Fshearmax(stepnumber)=max(Fshear);
[Fzmax(stepnumber),index]=max(fz);
Fxmax(stepnumber)=max(fx);
Fxmin(stepnumber)=min(fx);
Fymax(stepnumber)=max(fy);
Fymin(stepnumber)=min(fy);
deltx(stepnumber)=max(x)-min(x);
delty(stepnumber)=max(y)-min(y);
Rmax(stepnumber)=rmax;
contacttime(stepnumber)=(length(x)+10)/200;
timetopeak(stepnumber)=(index-to)/200;

end

Subject=filename(1);
if (filename(3)=='P')
        Condition='Pre-exposure';
elseif (filename(3)=='L')
        Condition='Post Lunar Exposure';
else
        Condition='Post Martian Exposure';
end
['Subject ' Subject '     Condition = ' Condition]
%%%OUTPUT THE DATA
Fmax
Fshearmax
Fzmax
Fxmax
Fxmin
Fymax
Fymin
deltx
delty
Rmax
contacttime
timetopeak
timestart
```

```
%%%SAVE THE DATA

eval(['save ',datapath_out,filename,'.mat Fmax Fshearmax Fzmax Fxmax Fxmin Fymax Fymin deltx delty
Rmax contacttime timetopeak timestart']);
```

```
%%% VIDEO_SCALE.M
%%%KARL U. SCHULTZ
%%% THIS PROGRAM TAKES THE VIDEO DATA
%%% UNSKEWES IT, AND SCALES IT PROPERLY.
%%% IT THEN DETERMINES ALL OF THE JOINT ANGLES AND THE VERTICAL
%%% EXCURSION

clear
clg


%%% SET VARIABLES
%%% THE DATA IS CUT AND PASTED FROM OTHER 'DATA' FILES
data_path='dummy';

%%% INPUT THE X AND Y COORDINATES OF THE CALIBRATION POINTS
onex=mean([1.16;1.16;1.16]);
oney=mean(-[1.826;1.826;1.826]);
twox=mean([1.146;1.146;1.153]);
twoy=mean(-[2.125;2.125;2.125]);
threex=mean([.847;.847;.847]);
threey=mean(-[2.104;2.111;2.111]);

%%% INPUT THE X AND Y COORDIANTES OF THE JOINTS
sx=[2.507;2.424;2.153;1.875;1.681;1.5;1.174;1.021];
sy=-[0.514;.514;.493;.438;.417;.417;.41;.382];
hx=[2.382;2.271;1.993;1.75;1.675;1.477;1.139;1.007];
hy=-[1.125;1.118;1.076;1.021;1.021;1.028;1.035;.979];
kx=[2.09;1.986;1.764;1.632;1.59;1.521;1.215;.861];
ky=-[1.625;1.632;1.625;1.625;1.625;1.625;1.632;1.597];
ax=[1.826;1.764;1.688;1.674;1.667;1.653;1.576;1.319];
ay=-[2.139;2.167;2.174;2.174;2.174;2.167;2.083;1.965];


%%% DETERMINE THE ACTUAL SPATIAL POSITION OF EACH POINT
for i=1:length(sx);
%%%SET ALL VARIABLES;
shoulderx=sx(i);
shouldery=sy(i);
hipx=hx(i);
hipy=hy(i);
kneex=kx(i);
kneey=ky(i);
anklex=ax(i);
ankley=ay(i);

%%% DETERMINE THE GAINS
ytilt1=threey-twoy;
xtilt1=twox-threex;
ytilt2=oney-twoy;
xtilt2=onex-twox;

%%% FIND THE ANGLE WHICH THE THING IS TILTED
ytilt1=threey-twoy;
xtilt1=twox-threex;
ytilt2=oney-twoy;
xtilt2=onex-twox;
angle1=atan(ytilt1/xtilt1);
```

```
angle2=atan(xtilt2/ytilt2);
angle=(angle1+angle2)/2;

%%% CONVERT THE DATA TO POLAR COORDINATES
[oner,onethet]=cart2polar(onex,oney);
[twor,twothet]=cart2polar(twox,twoy);
[threer,threethet]=cart2polar(threex,threey);
[shoulderr,shoulderthet]=cart2polar(shoulderx,shouldery);
[hipr,hipthet]=cart2polar(hipx,hipy);
[kneer,kneethet]=cart2polar(kneex,kneey);
[ankler,anklethet]=cart2polar(anklex,ankley);

%%% ADD THE PROPER SKEWING ANGLE
onethet=onethet+angle;
twothet=twothet+angle;
threethet=threethet+angle;
anklethet=anklethet+angle;
hipthet=hipthet+angle;
kneethet=kneethet+angle;
shoulderthet=shoulderthet+angle;

%%% CONVERT BACK TO CARTESIAN COORDINATES
[shoulderx,shouldery]=polar2cart(shoulderr,shoulderthet);
[hipx,hipy]=polar2cart(hipr,hipthet);
[kneex,kneey]=polar2cart(kneer,kneethet);
[anklex,ankley]=polar2cart(ankler,anklethet);
[onex,oney]=polar2cart(oner,onethet);
[twox,twoy]=polar2cart(twor,twothet);
[threex,threey]=polar2cart(threer,threethet);

%%% SCALE THE DATA PROPERLY
R=[25;25];        %%THIS IS THE ACTUAL DISTANCE BETEEN CAL POINTS
Xg=R(1)/(twox-threex);
Yg=R(2)/(oney-twoy);

%%%  SCALE THE DATA SO THE DISTANCES ARE CORRECT
%% X AXIS
shoulderx=shoulderx*Xg;
hipx=hipx*Xg;
kneex=kneex*Xg;
anklex=anklex*Xg;

%% Y AXIS
shouldery=shouldery*Yg;
hipy=hipy*Yg;
kneey=kneey*Yg;
ankley=ankley*Yg;



%%%%FIND THE DISTANCES OF THE SEGMENTS
shinl=sqrt((anklex-kneex)^2+(ankley-kneey)^2);
thighl=sqrt((kneex-hipx)^2+(kneey-hipy)^2);
trunkl=sqrt((hipx-shoulderx)^2+(hipy-shouldery)^2);

%%PLOT THE STUFF
plot(anklex,ankley,'*c')
hold on
```

```
plot(hipx,hipy,'*c')
plot(kneex,kneey,'*c')
plot(shoulderx,shouldery,'*c')
plot([anklex kneex hipx shoulderx],[ankley kneey hipy shouldery],'c')
grid
axis([60 220 -200 20])
axis('square')
%%%FIGURE OUT THE ANGLES
shiny=kneey-ankley;
shinx=kneex-anklex;
thighy=hipy-kneey;
thighx=hipx-kneex;
trunky=hipy-shouldery;
trunkx=hipx-shoulderx;

thet1=atan(shiny/shinx);
if (thet1<0)
        thet1=pi+thet1;
end
tempang=atan(thighy/thighx);
if (tempang<0)
        tempang=tempang+pi;
end
thet2=(pi-thet1)+tempang;
tempanghip=(pi-atan(trunky/trunkx));
if (tempanghip<0)
        tempanghip=tempanghip+pi;
end
thet3=tempang+tempanghip;

%%%SET PLOT TRAPEZOIDS
%%% THIS ADDS SOME KIND OF BODY DIMENSION TO THE POINTS
trunkplotx=[-6 -12 12 6 -6];
trunkploty=[0 trunkl trunkl 0 0];
thighplotx=[-3 -5 5 3 -3];
thighploty=[0 thighl thighl 0 0];
shinplotx=[-2 -3 3 2 -2];
shinploty=[0 shinl shinl 0 0];

[trunkplotr,trunkplotthet]=cart2polar(trunkplotx,trunkploty);
[thighplotr,thighplotthet]=cart2polar(thighplotx,thighploty);
[shinplotr,shinplotthet]=cart2polar(shinplotx,shinploty);

trunkplotthet=pi-(trunkplotthet+tempanghip-pi/2);
thighplotthet=(thighplotthet+tempang-pi/2);
shinplotthet=(shinplotthet+thet1-pi/2);

[trunkplotx,trunkploty]=polar2cart(trunkplotr,trunkplotthet);
[thighplotx,thighploty]=polar2cart(thighplotr,thighplotthet);
[shinplotx,shinploty]=polar2cart(shinplotr,shinplotthet);

thet1=thet1*180/pi;
thet2=thet2*180/pi;
thet3=thet3*180/pi;

%%%PLOT TRAPEZOIDS
plot(trunkplotx+hipx,trunkploty+hipy,'r')
plot(thighplotx+kneex,thighploty+kneey,'r')
```

```
plot(shinplotx+anklex,shinploty+ankley,'r')

%%%FILE THESE NUMBERS SEQUENTIALLY
Trunk(i)=trunkl;
Shin(i)=shinl;
Thigh(i)=thighl;
Shouldery(i)=shouldery;
Shoulderx(i)=shoulderx;
Hipx(i)=hipx;
Hipy(i)=hipy;
Kneex(i)=kneex;
Kneey(i)=kneey;
Anklex(i)=anklex;
Ankley(i)=ankley;
Shinang(i)=thet1;
Kneeang(i)=thet2;
Hipang(i)=thet3;
end

%%% DETERMINE THE VERTICAL EXCURSION OF THE STEP
Excursion=max(Hipy(2:length(Hipy)-1))-min(Hipy(2:length(Hipy)-1));
depangle=(max(Shinang(2:length(Shinang)-1))-min(Shinang(2:length(Shinang)-1)))/2;
```

```
%%% CARTTOPOLAR.M
%%%KARL U. SCHULTZ
%%% THIS CONVERTS CARTESIAN COORDINATES TO POLAR
function [r,theta]=cart2polar(x,y);

r=sqrt(x.^2+y.^2);
thet=atan(y./x);
for i=1:length(x)
 if (thet(i)==0) & (x(i)<0)
        theta(i)=pi;
 elseif (y(i)>0) & (x(i)<0) %%2ND quadrant
        theta(i)=pi+thet(i);
 else
 theta(i)=thet(i);
 end
end
```

```
%%% POLARTOCART.M
%%%KARL U. SCHULTZ
%%% THIS CONVERTS POLAR COORDINATES TO CARTESIAN
function [x,y]=polar2cart(r,theta);
x=r.*cos(theta);
y=r.*sin(theta);
```

```
%%% MUSCLE_PENDULUM_MODEL.M
%%%
%%% KARL U. SCHULTZ
%%%
%%% THIS SCRIPT PRESENT AN ESTIMATOR MODEL OF HUMAN
%%% POSTURE
%%%
%%% IT USES STATE SPACE CONSTRUCTION AND OPTIMAL FEEDBACK

clear

%%% SET CONSTANTS
g=9.81;          %%%GRAVITY
m=170/2.2;       %%%MASS OF SUBJECT (kg)
L=1;             %%%LEG LENGTH OF SUBJECT
Len=L;           %%%INTERNAL VARIABLE
I=m*L*L;         %%%MOMENT OF INERTIA OF POINT MASS m AT LENGTH l

K1=200;                  %%%HILL MODEL PARALLEL ELASTIC ELEMENT
K2=97190;        %%%HILL MODEL SERIES ELASTIC ELEMENT
B1=41710;        %%%HILL MODEL DAMPING ELEMENT

Ggain=1;         %%%MUSCLE GAIN
coggain=1;       %%%COGNITIVE ACTIVATIONLEVEL

%%%SET UP MUSCLE MODEL
numm=K2;
denm=[B1 K1+K2];
[Am,Bm,Cm,Dm]=tf2ss(numm,denm);
% MAKE IT 2-D
Am=eye(2)*Am;
Bm=eye(2)*Bm;
Cm=eye(2)*Cm;
Dm=eye(2)*Dm;

%%%SET UP INVERTED PENDULUM MODEL
A=[0 m*g*L/I 0 0;1 0 0 0;0 0 0 m*g*L/I;0 0 1 0];
B=[-1/I 0;0 0;0 -1/I;0 0];
C=[0 1 0 0;0 0 0 1];
D=[0 0;0 0];

%COMBINE 2 PLANTS INTO 1 6-STATE PLANT
[Ap,Bp,Cp,Dp]=series(Am,Bm,Cm,Dm,A,B,C,D);

%%%REFLEXIVE GAIN PARAMETERS
Qr=eye(6)*12;
Qr(5:6,5:6)=Qr(5:6,5:6)*4;  %MOTION IN Y-AXIS IS MORE COSTLY
                                                    %THIS KEEPS RMSy LOWER THAN
RMSx
Rr=eye(2)*.01;
Kr=lqr(Ap,Bp,Qr,Rr);              %OPTIMAL FEEDBACK

%%%VESTIBULAR GAIN PARAMETERS
Qv=eye(6)*16;
Qv(5:6,5:6)=Qv(5:6,5:6)*4;        %MOTION IN Y-AXIS IS MORE COSTLY
                                                    %THIS KEEPS RMSy LOWER THAN
RMSx
Rv=eye(2)*.3;
```

```
Kv=lqr(Ap,Bp,Qv,Rv);              %OPTIMAL FEEDBACK
Kv=Kv*coggain;                                %ADD COG FACTOR INTO FEEDBACK PATH

%%%PADE APPROXIMATION OF A PURE TIME DELAY OF 0.08 SECONDS
%%%FOR REFLEX PATH
[a,b,c,d]=pade(.03,1);
ar=eye(2)*a;
br=eye(2)*b;
cr=eye(2)*c;
dr=eye(2)*d;

%%%PADE APPROXIMATION OF A PURE TIME DELAY OF 0.08 SECONDS
%%%FOR VESTIBULAR PATH
[a,b,c,d]=pade(.08,1);
av=eye(2)*a;
bv=eye(2)*b;
cv=eye(2)*c;
dv=eye(2)*d;

%%%COST FUNCTION PARAMETERS FOR ESTIMATOR GAIN
Q1=eye(6);
R1=eye(2);
G1=eye(6);
[L,P,E]=lqe(Ap,G1,Cp,Q1,R1); %%L IS ESTIMATOR GAIN

Nr=eye(6)*.0085;
Nv=eye(6)*.0075;
NN=[0 0;0 0;0 0;1 0;0 0;0 1]*.000;  %AN OLD, UNUSED NOISE FACTOR

Ae=Ap;  %THIS SETS THE ESTIMATOR MATRICES EQUAL
Be=Bp;  %TO THE PLANT MATRICES
Ce=Cp;
De=Dp;
Bp=Bp*Ggain;    %THIS ADDS THE VARIABLE MUSCLE GAIN

Atemp=[Ap-Bp*dr*Kr -Bp*dv*Kv -Bp*cr -Bp*cv;L*Cp-Be*dr*Kr Ae-Be*dv*Kv-L*Ce -Be*cr -Be*cv];
Acl=[Atemp;br*Kr zeros(2,6) ar zeros(2,2);zeros(2,6) bv*Kv zeros(2,2) av];
Btemp=[-Bp*dr*Kr*Nr -Bp*dv*Kv*Nv NN;-Be*dr*Kr*Nr -Be*dv*Kv*Nv zeros(6,2)];
Bcl=[Btemp;br*Kr*Nr zeros(2,6)*Nv zeros(2,2);zeros(2,6)*Nr bv*Kv*Nv zeros(2,2)];
Ccl=[Cp zeros(2,10)];
Dcl=[zeros(2,14)];
eig(Acl);          %USED FOR CHECKING STABILITY OF THE PLANT

%%RUN ITERATION OF THIS PLANT WITH DIFFERENT NOISE INPUTS
continue='y';  %THE ITERATION WILL RUN UNTIL INTERRUPTED
count=1;                    %STARTS THE COUNT AT 1
topcount=100;    %TOTAL NUMBER OF TRIALS TO RUN
falldown=0;                 %RESETS NUMBER OF TIMES 'SUBJECT' FELL

%%%START LOOP
while (continue=='y')
        %%%CREATE UNCORRELATED, WHITE NOISE
        noise=[randn(1000,14)];
        t=linspace(0,30,1000);      %TIME VECTOR
        pole=-10*2*pi;                      %VESTIBULAR FILTERING
        numfilt=[-pole*pole*pole];
        denfilt=poly([pole pole pole]);
        temp1=lsim(numfilt,denfilt,noise(:,7),t);
```

```
        temp2=lsim(numfilt,denfilt,noise(:,8),t);
        temp3=lsim(numfilt,denfilt,noise(:,9),t);
        temp4=lsim(numfilt,denfilt,noise(:,10),t);
        temp5=lsim(numfilt,denfilt,noise(:,11),t);
        temp6=lsim(numfilt,denfilt,noise(:,12),t);
        noise(:,7:12)=[temp1 temp2 temp3 temp4 temp5 temp6];
        %%%DONE CREATING NOISE

        %%%RUN SIMULATED 30 SECONDS OF STANDING
        [Y,X]=lsim(Acl,Bcl,Ccl,Dcl,noise,t);
        x=Y(:,1)*Len*1000;
        y=Y(:,2)*Len*1000;
        %%%FIND RMS
        rmsx(count)=mean(abs(x));
        rmsy(count)=mean(abs(y));
        %%%DO TEMPORAL ANALYSIS OF TRIAL
        skip=200;
        for i=1:skip
        dx2(:,i)=mean((x(1:length(x)-skip+1)-x(i:length(x)-skip+i)).^2);
        dy2(:,i)=mean((y(1:length(y)-skip+1)-y(i:length(y)-skip+i)).^2);
        dr2(:,i)=mean((y(1:length(y)-skip+1)-y(i:length(y)-skip+i)).^2+(x(1:length(x)-skip+1)-
x(i:length(x)-skip+i)).^2);
        end

        %%%PUT TEMPORAL STUFF IN GLOBAL VARIABLES
        Fdr2(:,count)=dr2';
        Fdx2(:,count)=dx2';
        Fdy2(:,count)=dy2';

        %%%CHECK TO SEE IF 'SUBJECT' FELL OVER
        if (max(abs(x))<20) & (max(abs(y))<40)
                count=count+1;                          %%%THE PERSON DIDN'T FALL OVER
        else
                falldown=falldown+1;      %%%THE PERSON DID FALL OVER
        end
        %%%CHECK TO SEE IF LIMIT OF TRIAL # HAS BEEN REACHED
        if (count==topcount+1)
        continue='n';  %%STOP RUNNING TRIALS
        end

end  %%%REPEAT SEQUENCE


%%%THE REST OF THIS PROGRAM DOES EXACTLY WHAT
%%%posture_analyze_2.m DOES

dr2=mean(Fdr2');
dx2=mean(Fdx2');
dy2=mean(Fdy2');



%%% PLOT DATA AND DETERMINE OPEN AND CLOSED LOOPS
%%% THIS DETERMINES THE SHORT AND LONG TERM PERIODS OF TEMPORAL DATA
clg
plot(dr2)
hold on
plot(dx2);
```

```
plot(dy2);
%axis([0 length(dr2) 0 100])
title('Subject XXX Trial # 1')
xlabel('Time (sec)')
ylabel('<Δ r ^2>  (mm ^2)')
text(1,90,'Click on one point on the first line (steep slope)')
s1=2;
plot([s1 s1],[0 100],':g');
s2=ginput(1);
s2=ceil(s2(1));
plot([s2 s2],[0 100],':g');

clg
plot(dr2)
hold on
plot(dx2);
plot(dy2);
%axis([0 length(dr2) 0 100])
title('Subject XXX Trial # 1')
xlabel('Time (sec)')
ylabel('<Δ r ^2>  (mm ^2)')
plot([s1 s1],[0 100],':g');
plot([s2 s2],[0 100],':g');
text(1,90,'Click on two points on the second line (shallow slope)')
l1=ginput(1);
l1=ceil(l1(1));
plot([l1 l1],[0 100],':g');
l2=ginput(1);
l2=ceil(l2(1));
plot([l2 l2],[0 100],':g');

%%% DEFINE t, dr, dx, AND dy FOR THE RANGES INPUTTED ABOVE
%%% THESE VARIABLES ARE USED FOR DETERMINING Ds AND Dl
sdr=dr2(s1:s2);
sdx=dx2(s1:s2);
sdy=dy2(s1:s2);
st=t(s1:s2);
ldr=dr2(l1:l2);
ldx=dx2(l1:l2);
ldy=dy2(l1:l2);
lt=t(l1:l2);

%%% DEFINE VARIABLES FOR LOG/LOG PLOTS
%%% THESE VARIABLES ARE USED FOR DETERMINING Hs AND Hl
logsdr=log10(sdr);
logsdx=log10(sdx);
logsdy=log10(sdy);
logst=log10(st);
logldr=log10(ldr);
logldx=log10(ldx);
logldy=log10(ldy);
loglt=log10(lt);

%%% REGRESS LINES
%%% THIS DETERMINES THE SLOPE OF EACH LINE
Ds=(sdr/[st])/2
Dxs=(sdx/[st])/2
Dys=(sdy/[st])/2
```

```
Dl=(ldr/[lt;ones(size(ldr))])/2
Dxl=(ldx/[lt;ones(size(ldr))])/2
Dyl=(ldy/[lt;ones(size(ldr))])/2

%%% REGRESS LOG/LOG LINES
%%%   THIS DETERMINES THE CORRELATION COEFFICIENT OF EACH LINE
Hs=(logsdr/[logst;ones(size(logsdr))])/2
Hxs=(logsdx/[logst;ones(size(logsdr))])/2
Hys=(logsdy/[logst;ones(size(logsdr))])/2
Hl=(logldr/[loglt;ones(size(logldr))])/2
Hxl=(logldx/[loglt;ones(size(logldr))])/2
Hyl=(logldy/[loglt;ones(size(logldr))])/2

%%%   PLOT THE RESULTS
clg
plot(t,dr2);
hold on
st=[0 2];
lt=[0 10];
plot(st,st*2*Ds(1),':r')
plot(lt,lt*2*Dl(1)+2*Dl(2),':r')
axis([0 time 0 100])
title('Subject XXX Trial # 1')
xlabel('Time (sec)')
ylabel('<Δ r ^2>  (mm ^2)')

%%%%FIGURE OUT WHERE THE CRITICAL POINT IS
lowtime=linspace(0,3,1000);
shortline=lowtime*2*Ds;
longline=lowtime*2*Dl(1)+2*Dl(2);
diff=longline-shortline;
[dummy,index]=min(abs(diff));
criticaltime=lowtime(index);
criticaldistance=(shortline(index)+longline(index))/2;
```

APPENDIX E

STABILOGRAM-DIFFUSION PLOT DIFFUSION COEFFICIENT AND CORRELATION COEFFICIENT SUMMARY TABLES

This section summarizes the results of the temporal analysis carried out on the posture data from this experiment. Each Pre-exposure block of data represents the mean temporal characteristics of 8 posture trials while each of the other clocks is the sum of 6 trials of 30 seconds each.

Recall that the diffusion coefficient D represents the relative amount of stochastic activity during that period. Table E1 and E2 clearly show that more stochastic activity was present during the short term than during the long term period. Tables E3 and E4 present the correlation coefficient H for each trial. This data represents the characteristics of the log-log plot of square distance versus time interval. Notice that the coefficients were much higher in the short term than the long term, revealing that persistent behavior was exhibited short term, but anti-persistent behavior was exhibited long term. A more in depth summary of this data is presented in Section 5.2.4, Posture Data.

Diffusion Coefficient D

Pre-Exposure			No Exercise		
Ds	Dxs	Dys	Ds	Dxs	Dys
11.1722	7.9628	3.2095	10.6810	7.7036	2.9774
5.2074	3.7737	1.4337	8.0401	5.8662	2.1739
9.0561	6.4954	2.5607	7.9143	5.8366	2.0776
10.2068	6.7453	3.4615	9.7540	5.4379	4.3161
7.8841	5.0030	2.8811	7.9203	5.0374	2.8828
5.7295	3.1607	2.5688	6.5126	4.4461	2.0666
3.7196	2.5860	1.1336	2.8735	2.2929	0.5806
3.9684	2.7025	1.2659	4.9968	3.9616	1.0352
3.2750	2.1476	1.1274	3.4027	2.6226	0.7801
6.9860	4.7544	2.2316	6.5891	4.8040	1.7850
Knee Bends			Broad Jumps		
Ds	Dxs	Dys	Ds	Dxs	Dys
8.9568	6.7791	2.1777	9.4955	6.9130	2.5825
4.5736	3.3594	1.2142	6.7265	4.9366	1.7899
6.7214	5.0060	1.7154	7.6582	6.0757	1.5824
8.8215	5.4564	3.3652	11.2136	6.1357	5.0779
8.6668	6.0066	2.6602	10.4275	6.8142	3.6132
6.3062	3.7608	2.5455	5.3593	3.6303	1.7290
2.3145	1.9310	0.3835	2.1553	1.5633	0.5920
5.1408	4.1188	1.0220	4.6506	3.6612	0.9894
4.4559	3.3591	1.0968	3.7452	2.8329	0.9123
6.4701	4.4144	2.0556	5.6101	4.3459	1.2642

Pre-Exposure			No Exercise		
Dl	Dxl	Dyl	Dl	Dxl	Dyl
2.1199	2.0272	0.0927	1.9091	1.7987	0.1104
1.4494	1.3127	0.1367	2.3480	2.2679	0.0801
0.5907	0.4554	0.1353	1.4010	1.0656	0.3353
0.7702	0.5924	0.1778	1.0592	0.9996	0.0596
3.0051	2.6606	0.3445	2.6827	2.3579	0.3248
1.0817	1.0605	0.0212	3.5695	3.2244	0.3451
0.7390	0.6255	0.1136	0.8572	0.5626	0.2946
1.4039	1.1077	0.2963	1.3416	0.8411	0.5005
0.4810	0.4774	0.0036	1.1296	1.0199	0.1097
1.3004	1.0602	0.2402	1.7503	0.9055	0.8448
Knee Bends			Broad Jumps		
Dl	Dxl	Dyl	Dl	Dxl	Dyl
1.4382	1.3415	0.0967	1.9674	1.9351	0.0323
0.9217	0.8031	0.1186	1.0652	0.9873	0.0780
1.1686	1.0347	0.1338	1.2454	1.1529	0.0925
0.6733	0.5238	0.1495	1.1715	1.0786	0.0929
2.9473	2.4414	0.5059	2.2167	1.7649	0.4518
2.9697	2.0925	0.8772	2.0141	1.9188	0.0953
0.8428	0.5844	0.2584	0.9177	0.6978	0.2200
1.6427	1.3174	0.3253	1.7988	1.2315	0.5673
1.5271	1.4690	0.0581	1.4301	1.1709	0.2591
1.5435	1.0409	0.5026	0.5624	0.3999	0.1625

Correlation Coefficient H

Pre-Exposure			No Exercise		
Hs	Hxs	Hys	Hs	Hxs	Hys
0.5539†	0.5638	0.4769	0.5524†	0.5638	0.5258
0.5005†	0.6659	0.4163	0.6199†	0.6659	0.5245
0.5407†	0.5020	0.4603	0.4428†	0.5020	0.3173
0.4410†	0.5141	0.3838	0.5150†	0.5141	0.5165
0.8071	0.7758	0.8069	0.7670	0.7758	0.7520
0.7280	0.7269	0.7720	0.7376	0.7269	0.7621
0.7969	0.7316	0.8178	0.7265	0.7316	0.7075
0.7229	0.7300	0.6876	0.7261	0.7300	0.7119
0.8242	0.7673	0.8284	0.7582	0.7673	0.7294
0.7011	0.7212	0.7854	0.7386	0.7212	0.7903
Knee Bends			Broad Jumps		
Hs	Hxs	Hys	Hs	Hxs	Hys
0.5056†	0.5459	0.4055	0.5121†	0.5359	0.4576
0.4737†	0.5264	0.3616	0.4861†	0.5429	0.3678
0.507†	0.5731	0.3757	0.4633†	0.5047	0.3462
0.4976†	0.5323	0.4500	0.4700†	0.4665	0.4743
0.7434	0.7364	0.7599	0.7806	0.7748	0.7916
0.7590	0.7412	0.7871	0.7328	0.7084	0.7905
0.7254	0.7229	0.7397	0.7241	0.7133	0.7543
0.7894	0.8033	0.7387	0.7725	0.7745	0.7658
0.8182	0.8256	0.7966	0.8068	0.8087	0.8012
0.6954	0.6683	0.7616	0.6707	0.6650	0.6908

†Data Point Not Used In Analysis Due to Signal Noise Problem

Pre-Exposure			No Exercise		
Hl	Hxl	Hyl	Hl	Hxl	Hyl
0.3158	0.3505	0.1110	0.2708	0.3129	0.0925
0.2897	0.3077	0.1893	0.3004	0.3261	0.1035
0.1166	0.1116	0.1507	0.2422	0.2410	0.2457
0.1715	0.1944	0.1218	0.2229	0.2955	0.0419
0.3642	0.4122	0.1982	0.3110	0.3620	0.1604
0.1819	0.2586	0.0111	0.3794	0.4704	0.1453
0.3120	0.3282	0.2462	0.3213	0.2934	0.3986
0.3919	0.3974	0.3737	0.2826	0.2248	0.5153
0.1459	0.1836	0.0015	0.3423	0.3490	0.2904
0.2724	0.3096	0.1767	0.3459	0.3107	0.3975
Knee Bends			Broad Jumps		
Hl	Hxl	Hyl	Hl	Hxl	Hyl
0.2269	0.2685	0.0665	0.2602	0.3313	0.0219
0.2857	0.2909	0.2561	0.1958	0.2014	0.1484
0.2331	0.2398	0.1974	0.2386	0.2628	0.1095
0.1646	0.1896	0.1133	0.2148	0.2922	0.0509
0.3823	0.4256	0.2641	0.3139	0.3493	0.2325
0.3766	0.4178	0.3066	0.3218	0.4371	0.0901
0.3454	0.3280	0.3916	0.3425	0.3463	0.3312
0.3415	0.3341	0.3808	0.3414	0.3124	0.4347
0.3572	0.3752	0.1678	0.2705	0.2597	0.3343
0.3072	0.3342	0.2641	0.1967	0.1990	0.1913